UNIVERSITY OF TECHNOLOGY SYDNEY

Modelling rainfall erosivity for dynamic hillslope erosion estimation in events of wildland fires, snowmelt, and extreme rainfall

Submitted by

Qinggaozi Zhu

A thesis submitted in fulfilment of the requirements for the degree of

Doctor of Philosophy

School of Life Sciences, Faculty of Science,

University of Technology Sydney

Australia

October 2018

Certificate of original authorship

I certify that the work in this thesis has not previously been submitted for a degree nor has it been submitted as part of requirements for a degree except as fully acknowledged within the text.

I also certify that the thesis has been written by me. Any help that I have received in my research work and the preparation of the thesis itself has been acknowledged. In addition, I certify that all information sources and literature used are indicated in the thesis. This research is supported by the Australian Government Research Training Program.

Production Note:
Signature of student: Signature removed prior to publication.

Date: 15th Oct 2018

Acknowledgements

I am deeply grateful for the guidance and support from my principal supervisor Professor Qiang Yu. It was him who encouraged me to study in University of Technology Sydney (UTS) and suggested me to study at New South Wales (NSW) Government Office of Environment and Heritage (OEH). I would like to thank him for holding me to a high research standard; this work would not be possible without his patient supervision, insightful criticisms and expert guidance.

I would like to express my special appreciation and thank to my co-supervisor, Dr Xihua Yang, who provided me the chance to working with many OEH scientists and involved me into the Warrumbungle and Alpine projects. I would like to thank him, who is always willing to supervise me in various ways throughout the whole period. I need to extend a very grateful thank to my co-supervisor, Distinguished Professor Alfredo Huete, who inspired and encouraged me to focusing on soil erosion modelling, and always willing to help and talk.

This work would not have been successful without the unconditional support and invaluable advice of several people. I would like to thank Dr Alan Seed from Bureau of Meteorology, who kindly provided advice to weather radar data although he didn't know me before. I'd like to thank Professor Peter Kinnell for assisting with rainfall erosivity modelling and technical review. I thank the Climate Change Research Centre of the University of New South Wales, particularly Professor Jason Evans, Dr Fei Ji and Dr Alejandro Di Luca, for providing the NARCliM rainfall and snow projections. Dr Thomas Chubb from Snowy Hydro Ltd for providing the field measurements of snow

depth and water content. I am deep grateful to Dr Rachael Nolan, an expert in bushfire and hydrology, who helped me a lot for my draft manuscript and thesis.

Additionally, I would like to express my special appreciation and thank to these professional and research scientists in NSW OEH. Dr Mitch Tulau, who trained me well and helped me with the rain gauges equipment in the field, also gave me lots of valuable comments for my draft report and manuscript. Dr Senani Karunaratne, Robin McAlpine and Sally McInnes-Clarke, we always had good company on field trips down to Warrumbungle National Park, although it took long hours driving and some freezing winter nights without the heater. Many OEH scientists and visitors assisted with fieldwork on groundcover and remote sensing measurements. All these are greatly appreciated. Thanks to the Craig Wall from National Park and Wildlife Services (NPWS) at Coonabarabran Office, who allowed me visit and collect weather and soil data into Warrumbungle National Park.

I have to thank staffs in IT support, administrative staff members of the School of Life Sciences, Graduate Research School and Faculty of Science. I really appreciate your help for these years. My friends at UTS had made these years study life quite enjoyable. I'd like to thank my friends, Dr Zunyi Xie, Dr Xueling Li, Tran Nguyen Ngoc, Paras Sidiqui, Dr Rolanda Lam and Dr Buddhi Dayananda, who are always willing to help in ways. I couldn't complete the thesis without your encouragement.

Most importantly, I would like to thank my family for their love, encouragement and understanding. I must deeply thanks to my parents, who supported my PhD study and always encourage and help me out of difficulties. I'm the only child to my parents, it's been hard to them when I decided to study overseas four years ago, but they still supported me without a word of complaints. This PhD research is impossible unless the

unfailing support and courage given by my partner Dr Zheyuan Du. I feel very lucky to have him around me.

This research was funded and supported by NSW OEH and UTS top-up scholarship, as part of the project on OEH Climate Change Impacts on NSW's Alpine Region Biodiversity. I am grateful to the University of Technology Sydney and NSW Office of Environment and Heritage provides facilities for conducting this work.

Contents

List of figures

List of tables

Summary

Rainfall erosivity and hillslope erosion are being significantly affected by frequent extreme weather events and ongoing climate change. Projected warmer climate in Australia will comprehensively change the erosion rates through more intensive storm events, more severe and frequent wildfire and less snowmelt. Moreover, Australian rainfall is dominated by high seasonal and interannual variability for current and also future climate, which was believed to increase the hillslope erosion and accelerate the land degradation through the high variation of rainfall erosivity. Changes in rainfall amount that have significant effects on rainfall erosivity and hillslope erosion in Australia have been well-studied, however, the impacts from extreme weather events, such as wildfire, storm events and snowmelt are not well quantified and rarely monitored. To estimate the near real-time rainfall erosivity and erosion change, it is essential to link extreme weather events with hillslope erosion model in response to the needs of effective ecosystem and environment management. The output of this research will assist with government decision-making of soil and land management, and more importantly, in adapting to changing climate and extreme weather.

In my research, I selected two case study areas in southeast Australia to assess the effect of extreme weather events on hillslope erosion through the dynamic rainfall erosivity factor. I chose Warrumbungle National Park (WNP) for the case study of near real-time estimation of rainfall erosivity because of an intensive storm event after a catastrophic wildfire in 2013. I chose New South Wales (NSW) and Australian Capital Territory (ACT) Alpine region, covering the Snowy Mountains, to project and assess the impacts of extreme rainfall and snowmelt on rainfall erosivity and the spatial and temporal changes.

Wildfire removes the soil cover and results in in insufficient cover to protect soils, which potentially opens a window for an extreme erosive event (e.g. storm). Hence, understanding the spatial distribution and temporal variation of wildfires and erosive rainfall events are highly important. I used the radar rainfall data (1km, 10-min), calibrated by rain gauges rainfall, to estimate the near real-time rainfall erosivity on a daily basis. I used the latest satellite-derived fractional vegetation cover (500m, Version 3.1.0), LiDAR DEM (5m and 10m) data and soil digital mapping along with radar-based rainfall erosivity to model the post-erosion by using Revised Universal Soil Loss Equation (RUSLE). I found that there was a positive correlation between radar-based and gauged rainfall (R^2 = 0.75, E_c = 0.66). The highest rainfall erosivity was estimated as 826.76 MJ mm ha^{-1} hr^{-1} for a single storm event. The modelled average annual rate of hillslope erosion since May 2014 was 1.35 t ha^{-1} yr^{-1}; and appears to be declining due to the vegetation recovery after the wildfire. There is strong seasonal and spatial variation of post-fire erosion, which is mostly driven by rainfall erosivity and the fire severity.

Six extreme rainfall indices (ERIs) derived from the NSW and ACT Regional Climate Modelling (NARCliM) Project (Evans et al., 2016) were selected to assess the extreme rainfall impact on rainfall erosivity for the baseline (1990-2009), near future (2020-2039) and far future (2060-2079). I used twelve ensembles (four Global Climate Models and three Regional Climate Models) and bias-correction rainfall data from NARCliM to estimate the future rainfall erosivity. I found that there was a strong positive correlation between the maximum 5-day accumulated precipitation (Rx5day) and the rainfall erosivity estimated from the NARCliM projections. In comparison with the result from Australia Bureau of Meteorology (BoM) in the baseline period, it is possible to estimate the approximately erosivity value (R^2 = 0.813, E_c = 0.74) from ERIs (e.g. Rx5day) especially to where without radar or gauged rainfall data.

Snow and temperature projections for the 60 years derived from NARCliM were applied to adjust the snowmelt runoff (Bormann et al., 2014) and rainfall erosivity model during the melting season (September, October and November) across the NSW and ACT Alpine region. Weekly measurements of snow depth and snow water equivalent at three filed sites in the Snowy Mountains were obtained from Snowy Hydro Ltd to assess the snowmelt-adjusted rainfall erosivity model. In addition, the NSW soil property projections were obtained from OEH (Gray et al., 2017) and used to calculate soil erodibility based on Yang et al. (2017). Other input data, such as a 30 m DEM, and the latest satellite-derived fractional vegetation cover (500m, Version 3.1.0) at a monthly time-step since 2000 (Guerschman et al., 2009) were used along with the snowmelt-adjusted rainfall erosivity to model the hillslope erosion by using RUSLE in the Alpine region. I found that the snowmelt in spring is estimated to increase the rainfall erosivity by about 12.95% in the baseline period compared to the results without snowmelt adjustment. However, the snow impact is projected to be 24.84% for the near future and then less (1.63%) for the far future due to the projected higher temperatures and less snow depth, using NARCliM simulations. The highest erosion risk area within the study area is projected to be 19.95 t ha^{-1} yr^{-1} in South East and Tablelands (SET). ACT has the highest average erosion rate (0.37 t ha^{-1} yr^{-1}). Despite higher rainfall erosivity in the NSW and ACT Alpine region, the corresponding hillslope erosion is projected to be less than in the ACT since the soil erodibility and groundcover factor area relatively low.

This research assessed the impact of extreme weather events on rainfall erosivity and hillslope erosion in selected study areas in southeast Australia. The erosion amount and changes under climate change do not simply result from a single factor, but are comprehensively derived from various factors, including rainfall erosivity, groundcover,

slope length and steepness and soil erodibility. These factors always combine and interact to influence and accelerate the mechanism of the erosion process under more frequent and more extreme weather events. The current outcomes would effectively enhance the capability of policy marker, and provide adaptation and mitigation strategies in responding to wildland fires and a changing climate. Automated Geographic Information System (GIS) scripts have been developed to calculate the time-series rainfall erosivity and hillslope erosion, so that the processes of large quantity data are realistic, repeatable and portable.

The proposed outline for this thesis is as follows:

Chapter 1: Introduction

Chapter 2: Estimation of storm event-based rainfall erosivity from weather radar data in burnt area

Chapter 3: Modelling and monitoring post-fire erosion across Warrumbungle National Park

Chapter 4: Extreme rainfall indices and its impact on rainfall erosivity under climate change

Chapter 5: Rainfall erosivity, hillslope erosion and the spatial-temporal variability across Australian Alpine region

Chapter 6: Final conclusion and future direction

Chapter 1: Introduction

1.1 Soil erosion processes and types

Soil performs a series of vital functions in the ecosystem, which includes supporting food production, storing water and nutrients, and providing habitat for various organisms (Morgan, 2009). Degradation in the quality of soil through erosion can cause massive damage to the local environment, such as threatening and reducing soil productivity, fertility and nutrients (Lal, 1998), and potentially contaminating water supplies because of the increased flux of sediment and nutrients (Smith et al., 2011).

Soil erosion is a natural process, defined as the physical process by which soil particles are detached and removed from the ground surface due to the wind, falling raindrops, water flowing, tillage or irrigation, gravity and other forces (Segura et al., 2014, Lal, 1994, Brady and Weil, 2010, Hillel and Hatfield, 2005). For example, irrigation-induced erosion can damage productive soils which may have a very slow recovery (Lehrsch et al., 2005). Erosion by wind occurs when strong winds blow on dry and bare soils, causing on-site and off-site problems and reducing soil productivity (Zobeck and Van Pelt, 2005). Water erosion can diminish the yields of agricultural and forest products because of the detachment and transport of soil by rainfall, runoff, melting snow or ice (Gilley, 2005). Water erosion can be divided into five separate categories comprising: rill erosion, interrill erosion, gully erosion, ephemeral gully erosion and stream channel erosion (Gilley, 2005, Hudson, 2015). Similarly, Broz et al. (2003) and Morgan (2009) have defined soil erosion categories as splash, sheet, rill and gully erosion (Figure. 1-1).

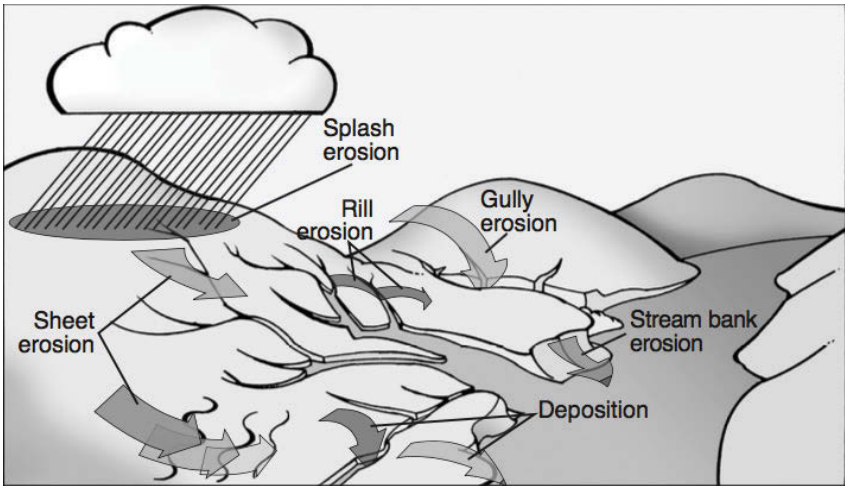

Figure 1-1 Types of soil erosion by water (Broz et al., 2003)

Most of Australia's soils are geologically very old, and because of few tectonic activity, there is little new soil formation. Thus, soil erosion is a really important environmental problem. As agents of erosion, rainfall and runoff are supplied to the Australian landscape in a highly variable manner (Hairsine et al., 2009). Hairsine et al. (2009) stated that hillslope erosion (sheet and rill erosion) is the major form of water-induced erosion in the Australian landscape.

The process of water erosion generically occurs within three steps: detachment, transport and deposition (Figure. 1-2). Soil particles firstly detach because of the impact of raindrops, flowing water, or freezing and thawing of the topsoil, they are then transported by floating, rolling, dragging or splashing and finally are deposited at some place lower in elevation (Toy et al., 2002).

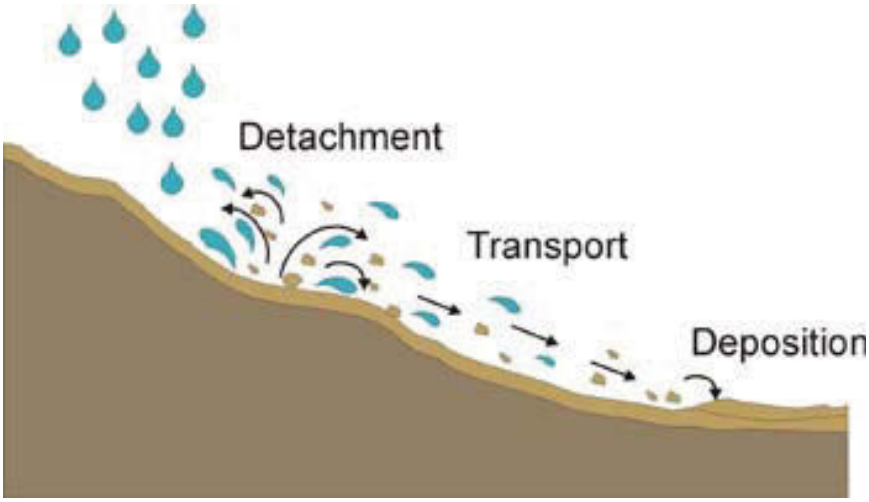

Figure 1-2 Soil erosion process by water (Yang and Yu, 2014)

In Australia, an important feature of the erosion process is that erosive episodes are frequently linked to preceding prolonged dry periods (Hairsine et al., 2009). At these times, soils are likely to be exposed to erosive events where the ground cover is sparse and protection is limited. What is worse, it potentially brings more soil loss when the extreme erosive events occur together with a catastrophic bushfire in the same area. Bushfire usually occur following these prolonged dry periods (Bradstock, 2010). For example, massive hillslope erosion occurred in a severely burnt area after a storm event in Warrumbungle National Park in southeast Australia on 1st Feb 2013, which opened a window for extreme erosive events because of the lack of vegetative soil cover protection. Hence, high spatio-temporal data such as radar weather data are required to assist management efforts and make adaptive strategies to control post-fire erosion.

1.2 Modelling hillslope erosion

Erosion is influenced by various factors including climate (rainfall characteristics), soil properties, topography and land use (Hudson, 2015). Soil erosion models are applied to estimate the erosion rates through impact factors and predict the potential effects for different land uses (Lal, 1994, Gilley, 2005). No matter what model is adopted to quantify soil erosion by water, there are four independent variables that

cannot be neglected: rainfall characteristics, slope, soil properties, and protective cover (Toy et al., 2002, Morgan and Nearing, 2016).

The Universal Soil Loss Equation (USLE) was proposed by Wischmeier and Smith (1965) to predict average annual gross soil loss. This empirical model was developed by analysing more than 10,000 plot-years of experiments in the USA and was widely applied to many non-agriculture areas (Wischmeier and Smith, 1978). USLE emphasized the effect of rainfall on soil erosion, where contained a rainfall erosivity factor (rainfall energy and intensity) into the formula. The modified version (MUSLE) has been an attempt to compute soil loss from individual storm events (Williams, 1975, Williams and Berndt, 1977), where the rainfall energy is replaced by the runoff factor (Aksoy and Kavvas, 2005, Zhang et al., 2009, Kinnell, 2005). Later on, MUSLE was updated, and is widely known as the Revised Universal Soil Loss Equation (RUSLE) (Renard et al., 1997), where the mathematical form of the model remained the same but the approaches of calculation for some factors were changed. For instance, the rainfall characteristics from the revised USLE include both rainfall and runoff erosivity factors (includeing snow melt where such runoff is significant) (Lal, 2001).

In order to adapt to erosion process, the Water Erosion Prediction Project (WEPP) was developed from USDA in 1985 as a continuous simulation computer model (Nearing et al., 1989, Foster and Lane, 1987). This process-based model includes runoff as a factor and has its strength in predicting soil loss and deposition rather than modelling average long-term erosion in USLE/RUSLE (Tiwari et al., 2000). However, WEPP is extremely sensitive to parameter estimation and requires additional validation and often fails to predict the correct erosion and sediment area, especially for single storm events (Van Oost et al., 2005, Favis-Mortlock et al., 2001). The latest water erosion model from the USLE family is the Revised Universal Soil Loss Equation

version 2 (RUSLE2) (Foster, 2005). It has the capability to accommodate daily precipitation data and is commonly used today for estimating rill and interrill soil erosion caused by rainfall.

Admittedly, USLE/RUSLE requires minimal parameters (Zhang et al., 2009) and was not designed to estimate event soil loss, however, some process-based models (e.g. WEPP) require considerable effort to calibrate parameters to run them (Kinnell, 2010). Also, their failure to estimate better results than achieved by applying the USLE/RUSLE model has encouraged the use of USLE family models for which it was not designed (Tiwari et al., 2000, Kinnell, 2010). USLE and its revision (RUSLE and RUSLE2) were the most frequently used models (Kinnell, 2017) for providing soil loss data in the world including Australia (Lu et al., 2003, Rosewell, 1996).

In this study, RUSLE and RUSLE2 were applied to estimate rainfall erosivity and soil loss at single event, daily, monthly and annual (R factor) scale (in Warrumbungle National Park). Rainfall and runoff erosivity were calculated by 10-min radar-derived rainfall data in a burnt area (Warrumbungle National Park in New South Wales) and calibrated by adding snowmelt impacts (e.g. Australian Alps Region in New South Wales) in southeast Australia.

Some dynamic distributed erosion and sediment models estimate soil loss that accounts for the hydrological impact. For instance, the European Soil Erosion Model (EROSEM) (Morgan et al., 1998) is able to simulate interill and rill process involved in runoff for a small catchment. The Agricultural Nonpoint Source model (AGNPS) is event-based that predicts sediment, runoff and nutrient transport from agricultural watersheds (Young et al., 1989, Young et al., 1995). The Soil and Water Assessment (SWAT) model is a continuous-time, semi-distributed, process-based river basin model (Arnold et al., 2012) that potentially models the erosion caused by runoff.

1.3 Principal hillslope erosion factors

Rainfall and runoff erosivity (R-factor), along with crop and crop management (C-factor), topographic (LS-factor) factors including slope steepness (S) and slope length (L), soil erodibility (K-factor) and the soil conservation factor (P-factor) are defined as the main elements that affect hillslope erosion modelling from the Universal Soil Loss Equation family (Renard et al., 1997, Kinnell, 2010).

Rainfall erosivity, as well as groundcover (crop management factor) are the most dynamic factors due to their great seasonal and annual variation. More rainfall erosivity in wet seasons is caused by high erosive rain events resulting in a greater amount of soil loss when the other factors remain constant. For the groundcover factor, there is generally more erosion on a bare ground surface where there is no vegetation protection when the other factors are kept constant. In terms of the LS factor, steeper and longer slopes increase discharge and peakflow and thus substantially increase the likelihood of erosion. Though soil erodibility and the LS factors are relatively more stable compared to the R-factor and C-factor, Shakesby and Doerr (2006)'s review of post-fire effects found that the heating of soils usually reduces soil aggregate stability and destroys the soil water repellency, thus enhancing soil erodibility. P-factor is critical for soil and water conservation, as well as the adaption to climate change of erosion.

However, greater erosion and the risk of soil degradation are not only derived from the individual factors, but usually from the combined effect of several factors especially when extreme weather occurs. For example, a severe wildfire causes effectively greater rainfall erosivity and runoff due to the reduction of vegetation within the burnt area. Furthermore, the fire possibly changed the landscape, as well as chemical and physical characteristics of burnt soil, reduceing the aggregate stability for months, or even years.

It is predicted that severe wildfire can trigger dramatic increases in erosion one year after burning (Robichaud et al., 2000). The soil loss level returns to its undisturbed values in 3-4 years after a wildfire (Benavides‐Solorio and MacDonald, 2001, de Dios Benavides-Solorio and MacDonald, 2005), as the vegetation recovers and soil begins to return to a pre-fire state (Shakesby and Doerr, 2006, Gordon et al., 2017). The impact of an extreme storm event on post-fire erosion will be presented in Chapters 2 & 3.

The process of erosion derived from snowmelt runoff is more complicated. When snow cover thaws in the winter and spring season, the soil remains wet and makes it more erodible and permeable due to the repeated freezing and thawing (Renard et al., 1997). Snowmelt runoff further causes more erosion as it usually occurs in late winter or spring, when the ground has less vegetative protection (Meusburger et al., 2014). Compared to unfrozen soil, snowmelt runoff in spring and rain or snow effectively causes more erosivity and erosion because the permeability of the surface soil increases during freezing and thawing (Edwards et al., 2007). The erosivity impact of snowmelt runoff on soil erosion is given in Chapter 5.

1.4 Rainfall erosivity estimation

The definition of rainfall erosivity (unit: MJ mm ha^{-1} hr^{-1} yr^{-1}) started from the development of USLE (Wischmeier and Smith, 1978), where it was defined as the sum of unit rainfall energy (E) and the maximum consecutive 30-min intensity (I_{30}, mm hr^{-1}) for a one-year period. The rainfall erosivity in annual, seasonal and monthly periods are calculated by adding the values of the $E \times I_{30}$ for a single storm over the different time intervals. Wischmeier and Smith (1958) found that a maximum 30-min intensity is statistically superior based on the soil plots data when compared to the maximum continuous 5-min, 15-min, or 60-min intensities. Based on recent research from soil

plots in northwest China, Zheng and Chen (2015) found that maximum rainfall intensities in 10-min or 20-min periods worked as well as the 30-min time-period. Further, Panagos et al. (2016b) noted that the calculated rainfall erosivity values decreased as the rainfall measurement interval increased from studies in Europe. Yin et al. (2007) suggested that there is a linear function between time resolution of rain data and conversion factors from the study in China, while Panagos et al. (2016b) examined it as an exponential relationship.

Erosive storm events are defined as rain events greater than 12.7 mm or maximum rainfall intensity of more than 12.7 mm hr^{-1} in Wischmeier (1959) and later revisions of USLE (Renard et al., 1997). This threshold is able to be adjusted under the area of consideration, for example, erosive rain was adjusted to as low as 10 mm and 10 mm hr^{-1} when applied in Germany (Rogler and Schwertmann, 1981).

1.4.1 KE-I relationships

The E factor is calculated from rainfall kinetic energy-intensity (KE-I) relationships that have been derived from a disdrometer to collect raindrop size data at certain geographic locations over some period of time (Kinnell, 2010).

Compared to USLE, the only revision in RUSLE is the kinetic energy equation for rainfall erosivity (Renard et al., 1997). The rainfall energy (KE, MJ ha^{-1}) and intensity (i, mm hr^{-1}) (KE-I) formula was proposed by Brown and Foster (1987). The equation as below is the general form (Kinnell, 1981) for the relationship between rainfall kinetic energy and rainfall intensity

$$KE = e_{max}\,[1 - a\,exp(-b\,i)] \quad (1)$$

where e_{max} represents the maximum unit energy as intensity becomes larger, i is the rainfall intensity (mm hr^{-1}), parameters a and b are coefficients that model the form of the curve (Angulo-Martínez et al., 2016).

Based on the work of Rosewell (1986), the value of e_{max} was set as 0.29. The value of coefficient a as 0.72 (McGregor and Mutchler, 1976), and the value of coefficient b as 0.05 (Brown and Foster, 1987). Thus, the KE-I relationship is recommended as below for RUSLE (Renard et al., 1997).

$$KE = 0.29\,[1 - 0.72\,exp(-0.05\,i)] \quad (2)$$

McGregor et al. (1995) compared the unit rainfall energy calculation from USLE and RUSLE. Foster et al. (2003) changed the coefficient b from 0.05 to 0.082 for the erosivity calculation for RUSLE2 to adjust the KE-I relation based on the work of McGregor and Mutchler (1976) as below.

$$KE = 0.29\,[1 - 0.72\,exp(-0.082\,i)] \quad (3)$$

It is believed that Eq. (2) (RUSLE), proposed by Brown and Foster (1987), underestimated the erosivity by approximately 9% than that from USLE when rainfall intensity was below 35 mm hr^{-1} (Figure. 1-3). Comparing to the work from Foster et al. (2003) (Eq. 3), there is no large difference (less than 2%) between RUSLE and RUSLE2 when rainfall intensity is more than 80 mm hr^{-1} (Figure. 1-3). Unit rainfall energy tends close to 0.30 MJ^{-1} mm^{-1} ha^{-1} when rainfall intensity is greater than 80 mm hr^{-1}. The results from USLE are slightly more than those from the RUSLE and RUSLE2 estimations when rainfall intensities are less than12 mm hr^{-1}, and when above 12 mm hr^{-1}, they are less than those from the RUSLE2 calculation but more than RULSE values.

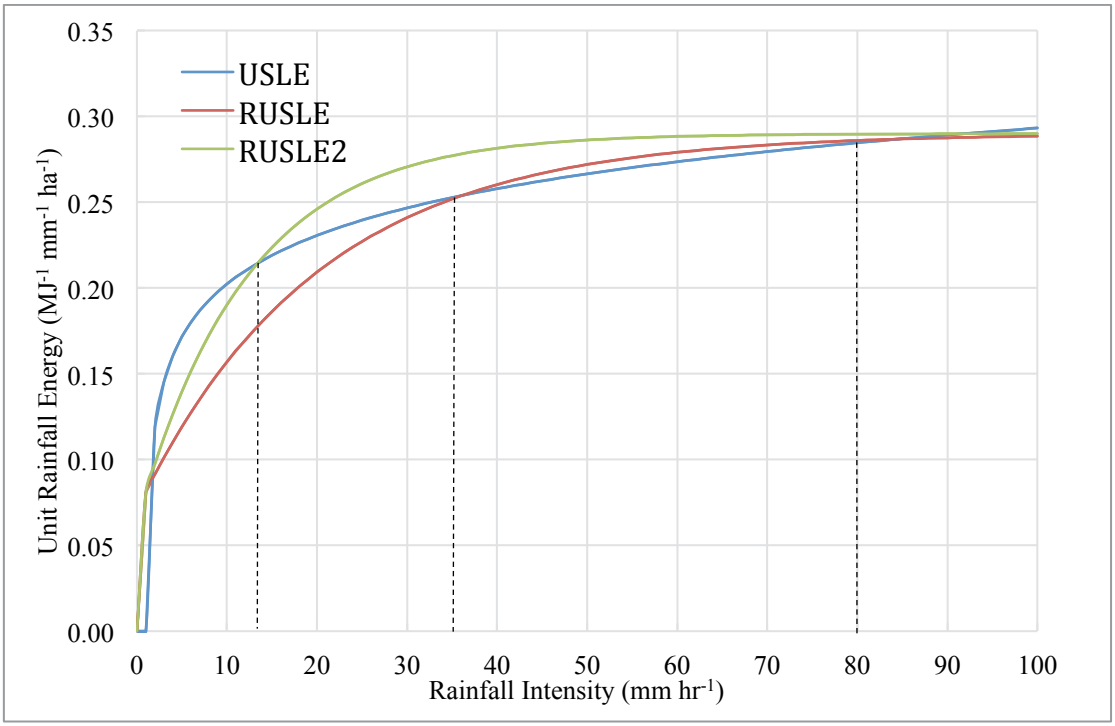

Figure 1-3 Unit rainfall energy calculated by rainfall intensity from USLE, RUSLE and RUSLE2

Numerous rainfall kinetic energy-intensity (KE-I) relationships have been developed, some have been applied in the US (Brown and Foster, 1987, Kinnell, 1981), Europe (Petan et al., 2010, Cerro et al., 1998), Korea (Lim et al., 2015) and universally (Van Dijk et al., 2002) from previous studies (Table 1-1). Rosewell (1986) calibrated a KE-I relation for New South Wales (NSW), Australia. Despite the evaluation from different erosivity methods, the rainfall energy from individual storm events is difficult to accurately predict from rainfall intensity due to natural variability in rainfall characteristics (Van Dijk et al., 2002).

Moreover, some local conditions could significantly influence the rainfall energy estimation, such as air pressure and elevation. The velocities of raindrops are greater as at higher elevations. Geographic elements, for example, latitude and longitude, coastal or inland, also have impacts on the erosivity calculation. Based on rain collection in local stations, Van Dijk et al. (2002) found that there is more than expected energy at similar rainfall intensity at semi-arid to sub-humid locations.

Table 1-1 Some reported kinetic energy (KE, MJ m^{-2} mm^{-1}) and rainfall intensity (I, mm hr^{-1}) relations.

Study	**Location**	**KE-I relation**	**Rain range (mm hr^{-1}) / Elevation (m)**
1. Brown and Foster (1987)	Mississippi, United States	$0.29\ (1-0.72\ e^{-0.05i})$ (RUSLE)	0-161 / 180
2. Cerro et al. (1998)	Barcelona, Spain	$0.384\ (1-0.54\ e^{-0.029i})$	1-150 / 25
3. Foster et al. (2003)	United States	$0.29\ (1-0.72\ e^{-0.082i})$ (RUSLE2)	0-161 / 180
4. Kinnell (1981)	Miami, Florida, United States	$0.293\ (1-0.28\ e^{-0.018i})$	2-309 / 3
5. Kinnell (1981)	Zimbabwe	$0.292\ (1-0.89\ e^{-0.048i})$	19-229 / 1230
6. Lim et al. (2015)	Daejeon, central Korea	$0.258\ (1-0.54\ e^{-0.05i})$	0.1-142 / 58
7. Petan et al. (2010)	Koseze and Kozjane, SW Slovenia	$0.298\ (1-0.60\ e^{-0.07i})$ $0.319\ (1-0.60\ e^{-0.055i})$	0.1-288 / 405-595
8. Rosewell (1986)	Gunnedah and Brisbane, Australia	$0.29\ (1-0.60\ e^{-0.040i})$ $0.264\ (1-0.67\ e^{-0.035i})$	1-161 / 25-305
9. Sanchez-Moreno et al. (2012)	Santiago Island, Cape Verde	$0.35\ (1-0.79\ e^{-0.03i})$	0-157 / 321
10. Van Dijk et al. (2002)	Universal	$0.283\ (1-0.52\ e^{-0.042i})$	-
11.Wischmeier and Smith (1978)	United States	$0.119 + 0.0873\log_{10} i$ (USLE)	0-161 / 180

Hence, the applications of various erosivity methods have to be carefully determined by calibration from local weather stations, although the difference from KE-I relationships is not significantly large. The comparison of two different KE-I relationships will be presented in Chapter 2. Another method for daily rainfall erosivity prediction has been developed depending on the corresponding coordinate and elevation of each site and applied in NSW Alpine Region in Chapter 5.

Rainfall erosivity (R-factor) is highly influenced by the rainfall intensity and duration. Higher EI_{30} values mean an intensive rainfall or moderate rainfall with a short duration. However, it is difficult to determine whether erosivity comes from the intensive rainfall or short rain duration. The R-factor has been updated in RUSLE2 as the product of rainfall amount and rainfall density (Foster et al., 2003).

Erosivity density, introduced from RUSLE2, is defined as the ratio of the monthly erosivity to monthly precipitation (Foster et al., 2003, Kinnell, 2010), with a unit of MJ ha^{-1} hr^{-1}. Erosivity density is regarded as a preferred method for erosivity inputs, determined from analysis of modern weather data as a part of the RUSLE2 development (Foster et al., 2003). It is generally expressed as the spatial and temporal patterns of the relationship between the R-factor and the precipitation on a monthly basis (Panagos et al., 2016a). As the monthly erosivity density is directly proportional to the average monthly 30-min rainfall intensity, Dabney et al. (2011) found that erosivity density reflected the seasonal variation in rainfall intensity at a location. The distribution of high erosivity density areas may contribute to identifying high-risk locations for particular months and seasons (Panagos et al., 2015).

Erosivity density and precipitation datasets were combined to classify erosivity risk area in Europe (Panagos et al., 2015). Rainfall erosivity is not solely dependent on the rainfall amount; if the erosivity density value is more than 1 MJ ha^{-1} $month^{-1}$, it represents erosive rainfall occurring in a relatively dry area over a dry month. In contrast, a large monthly average precipitation does not bring high erosive storm events where the erosivity density is less than 0.5 MJ ha^{-1} $month^{-1}$. Panagos et al. (2015) has identified the highest risk area as that where there is low annual average precipitation but high erosivity. It usually causes great damage and is connected to a very high flood risk, when highly erosive rainfall hits dry soils (Diodato et al., 2011).

1.4.2 Snowmelt runoff erosivity

Rainfall intensity and its duration are two basic factors for erosivity, nevertheless, the associated surface runoff factor must be considered as well (Renard et al., 1997). Snowfall is not erosive, whereas high-intensity and short duration rainfall is very erosive (Toy et al., 2002). Snowfall or rainfall on frozen soil does not bring erosion, whereas the snowmelt runoff during spring and rainfall on thawing soils, known as rain-on-snow can bring very high erosion (Ollesch et al., 2005). Moreover, these soils remain wet and more erodible during the freeze-thaw cycles.

The generation of runoff makes the snowmelt-derived erosion a complex, dynamic (Sui and Koehler, 2001) and quite different process from regular erosion, and thus requires temporal variation of snow water equivalent and spatial distribution of snow cover. From observations on cropland in the Northwestern Wheat and Range Region, United States, rill erosion is the primary mechanism of soil loss when topsoil thawing and snowmelt or rain occurs (Austin, 1972).

Although most soil erosion models estimate rainfall erosivity, snowmelt and its potential runoff that cause erosivity in spring were not normally include in these models. For instance, RUSLE does have a rainfall and runoff erosivity factor (R factor), but from the Agriculture Handbook 703 (Renard et al., 1997), the erosive forces of runoff from snowmelt into the was not considered into the index. According to the Agriculture Handbook 537 (Wischmeier and Smith, 1978), to find the rainfall erosivity, it is suggested to adjust the snowmelt erosivity calculation by multiplying local December to March precipitation (measured as inches of water) by 1.5 and then adding the product to the kinetic energy multiplying maximum 30-min intensity (EI_{30}). Hayhoe et al. (1995) has adjusted the snowmelt erosion calculation from USLE in Canada. The results demonstrated that the snowmelt erosion is highly correlated with winter runoff caused

by snowmelt rather than annual or winter rainfall depth. This adaption does not consider redistribution of snow by drifting, sublimation and reduced sediment concentrations in snowmelt (Meusburger et al., 2014).

RUSLE2 has been improved by adding the impact of non-erodible cover from snow. Foster et al. (2003) suggested switching off the RUSLE2 model during the winter period involving snow cover and turning it on after the snowmelt has ended the top frozen soils; although RUSLE2 is not designed for snowmelt-derived erosion. The empirical value of considering erosivity caused by snowmelt can be added to the standard monthly erosivity values to calculate effective monthly erosivity values especially for the melt period during spring months.

Snowmelt and runoff erosion has been simulated by coupling a hydrological model with a sediment load model in Russia (Sukhanovski et al., 2005) and with a soil erosion model in Germany (Ollesch et al., 2006). In addition, the European Soil Erosion Model (EROSEM) (Morgan et al., 1998) and SWAT (Arnold et al., 2012) have been applied in snowmelt erosion prediction, which linked an erosion model to a continuous hydrological model (Kliment et al., 2008). In this study, the snowmelt runoff factor was considered in daily erosivity modelling (Yang and Yu, 2014) in the NSW and ACT Alpine region.

1.5 Extreme weather events impacts on soil erosion

In recent decades, changes in climate extremes have attracted many attentions around the world because extreme climate events often result in more impacts on natural and human systems than that from their mean values. Fu et al. (2010) revealed the trend of extreme events in the last 50-100 years depending on the observed date. Rainfall extremes have been studied on regional, national and global scales (Nearing et

al., 2004; Alexander et al., 2007; Evans et al., 2016; Almagro et al., 2017). Australia will expect that extreme rainfall events across the nation are likely to become more intense, even where annual-average rainfall is projected to decline. Australian temperatures are projected to continue increasing with more extremely hot days and fewer extremely cool days (CSIRO and Bureau of Meteorology, 2016). These studies found some significant changes in percentiles and frequency of extreme events, and the magnitude and the sign of the changes vary with the season and the region (Alexander et al., 2007; CSIRO and Bureau of Meteorology, 2015).

Climate change can alter rainfall erosivity due to alteration of rainfall patterns. The increase in global mean temperature generates an increase in the moisture retention capacity of the atmosphere that is in the order of 7% per degree Celsius. In warm climates, such as in Brazil and Australia, temperature and extreme rainfall events will increase more significantly than in many other regions around the world (Almagro et al., 2017). Increases in both the mean and the variability can exacerbate the increase or decrease in probability of either hot or cold extreme temperatures (Figure.1-4, Houghton et al., 2001). However, few studies have comprehensively assessed extreme events in Australian daily rainfall since an update to the high quality Bureau of Meteorology dataset in the mid-1990s (Gallant et al., 2007).

More frequent intensive rainfalls might be accompanied by a clustering of dry periods, which represents a dangerous combination with regard to water erosion (Sauerborn et al., 1999). The soil particles can be easily carried away because of the increased surface runoff after storm events. However, rainfall erosivity is the most important parameter that has the direct effect of climate change on water erosion (Nearing et al., 2004). More importantly, hillslope erosion occurs mostly during a few severe storm or extreme events. Large and erosive storms are even more variable than

annual rainfall totals. Trends and changes in erosive storms or rainfall extremes are therefore much more important but also difficult to detect in comparison with rainfall totals.

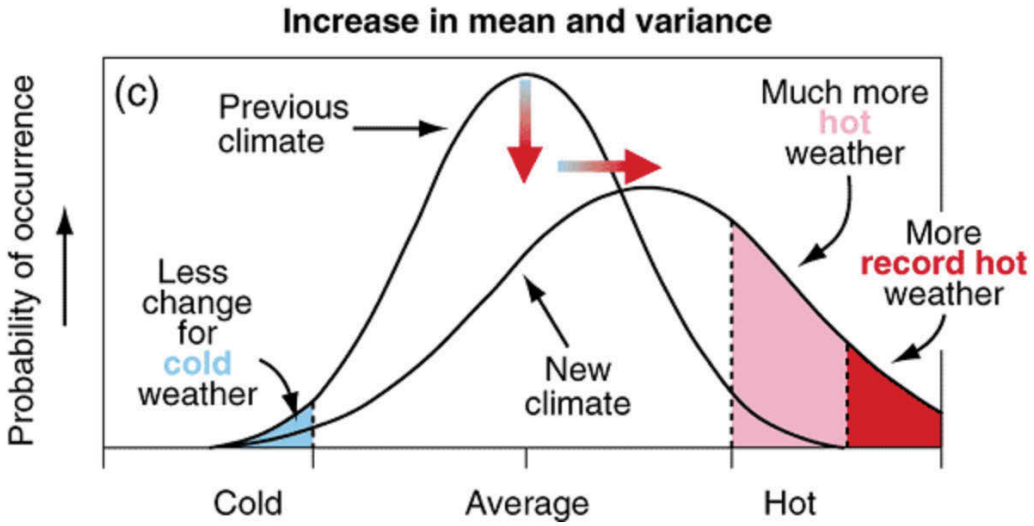

Figure 1-4 Schematic showing the effect on extreme climates when both the mean and variance increase for a normal distribution of climate (Houghton et al., 2001)

1.5.1 Extreme rainfall (rainfall extreme indices)

Extreme climate events such as storms, floods, heat waves and wildfire have significant impacts on society (Haylock and Nicholls, 2000). Various extreme climate indices have been defined to examine whether such extreme events have changed over time, for instance, the number of days per year with the longest dry spell, or with daily rainfall intensity larger than fixed thresholds (e.g. 10 mm d^{-1}, Table 1-2).

Table 1-2 Different rainfall extreme indices and their definitions

Abbreviation	Description	Unit
CDD	Duration of the longest dry spell in a year. Count the largest number of consecutive days where: $RR_{ij} < 1mm$*	days
CWD	Maximum length of wet spell in a year. Count the largest number of consecutive days where: $RR_{ij} \geq 1mm$	days
R10mm	Annual counts of days with rainfall greater than 10mm. Count the days where: $RR_{ij} \geq 10$ mm	days
R20mm	Annual counts of days with rainfall greater than 20mm. Count the days where: $RR_{ij} \geq 20$ mm	days
Rnnmm	Days with rainfall greater than 25mm. Count the days where: $RR_{ij} \geq 25$ mm.	days
Rx1day (monthly and annually)	Daily maximum precipitation. $Rx1day_j = \max(RR_{ij})$ (monthly) $Rx1day_j = \max(RR_{ij})$ (annually)	mm
Rx5day (monthly and annually)	Maximum 5-day accumulated precipitation (annual and month). Let RR_{kj} be the precipitation amount for the 5-day interval ending k, period j. $Rx5day_j = \max(RR_{kj})$.	mm
R95p	Accumulated precipitation from events above the 95th percentile. Let RR_{wj} be the daily precipitation amount on a wet day w ($RR \geq 1.0mm$) in period i and let $RR_{wn}95$ be the 95th percentile of precipitation on wet days in the period. If W represents the number of wet days in the period, then $R95p_j = \sum_{w=1}^{W} RR_{wj}$ where $RR_{wj} > RR_{wn}95$	mm
R99p	Accumulated precipitation from events above the 99th percentile. Let RR_{wj} be the daily precipitation amount on a wet day w ($RR \geq 1.0mm$) in period i and let $RR_{wn}99$ be the 99th percentile of precipitation on wet days in the period. If W represents the number of wet days in the period, then $R99p_j = \sum_{w=1}^{W} RR_{wj}$ where $RR_{wj} > RR_{wn}99$	mm

Table 1-2 contains the 11 climate extreme indices to precipitation complied from the World Meteorology Organization (WMO) in this thesis. I present seasonal and annual extreme rainfall indices and use 1990–2009 as the baseline period. Rx1day and Rx5day are defined on a monthly basis, while all the other indices are only defined on an annual basis. The extreme indices are based on the working of the NARCliM (New South Wales/Australian Capital Territory Regional Climate Modelling) project (Evans et al., 2014). The impact of extreme rainfall indices on changes to soil erosion is given in Chapter 4.

1.5.2 Wildfire

Weather (hot and dry), wind speed and fuel amount (e.g. litter) are recognised as the main factors that cause wildfire (Bradstock, 2010, Brown, 1972, Shakesby and Doerr, 2006, Nyman et al., 2011). The climate characteristics of southeast Australia (hot dry summers) make it prone to wildfire (Bradstock, 2010) occurrence and post-fire erosion (Bradstock et al., 2002, Luke and McArthur, 1978, Shakesby, 2011). Wildfire plays an important role in determining erosion risk, whether it is a rare, severe fire that removes the top soil over large areas or a regular, low severity one (Cawson et al., 2012, Tulau, 2015, Arkle and Pilliod, 2010, de Dios Benavides-Solorio and MacDonald, 2005).

Severe wildfires have a highly important impact on soil erosion and sediment (Tulau, 2015). For rainfall erosivity, such severe wildfires result in canopy loss and bring effectively greater erosivity as the burnt soil is exposed to the erosive rain. In terms of the groundcover, a high severe fire burns vegetation protection, removes the soil cover and accelerates the soil loss rates (Shakesby et al., 2007) until the vegetation recovers (Gordon et al., 2017, Shakesby, 2011). Furthermore, severe wildfire increases

water repellency, reduces the soil aggregate stability due to the physio-chemical change and increases slope length (Nyman et al., 2011) because of the combustion of obstacles. By examining wildfire severity, Cawson et al. (2012) found that the high severity burnt areas delivered approximately 13 % more sediment than those from low severity areas. Compared to the more severe wildfire, low fire severity areas resulted in less soil erosion due to a shorter vegetation recovery period (Raison et al., 1986).

It is predicted that an increasing number of fire weather days is likely to be experienced in south-eastern Australia each year from current climate change projections (Pitman et al., 2007). Warmer and drier conditions and higher frequency of extreme weather in the meantime is trending which accelerates the risk of wildfire (Nyman et al., 2011, Hennessy et al., 2005). High severe wildfire, similar to crop harvest on arable land, removes the topsoil and opens a window for extreme erosion events (Shakesby et al., 2007, Van Oost et al., 2005). Hence, the prediction of high spatio-temporal resolution of EI_{30} is highly important in particular to this region under climate change (Alexander et al., 2007).

1.6 Research Questions and Aims

This research will assess the impact of extreme rainfall and wildfire on rainfall erosivity by using high spatio-temporal resolution radar data in Warrumbungle National Park, and modelling the climate change (e.g. extreme rainfall indices, snowmelt) impact on hillslope erosion over NSW and ACT Alpine regions. This research will provide answers to the following important questions:

1) How does rainfall erosivitiy and soil loss change over time since fire?

2) How will soil erosion rates respond to climate change (e.g. highly frequent occurrence of extreme climate events) in the future?

The specific aims of this research are to:

i) Calibrate weather radar rainfall data against gauge measurements and estimate rainfall erosivity after a single storm event.

ii) Monitoring post-fire hillslope erosion.

iii) Modelling previous, present and future rainfall erosivity by considering snowmelt in spring (September, October and November).

iv) Examine the impact of rainfall extreme indices on rainfall erosivity.

v) Predict the soil loss along with effects of each factor (groundcover, topographic and soil erodibility factor) under climate change.

1.7 Significance

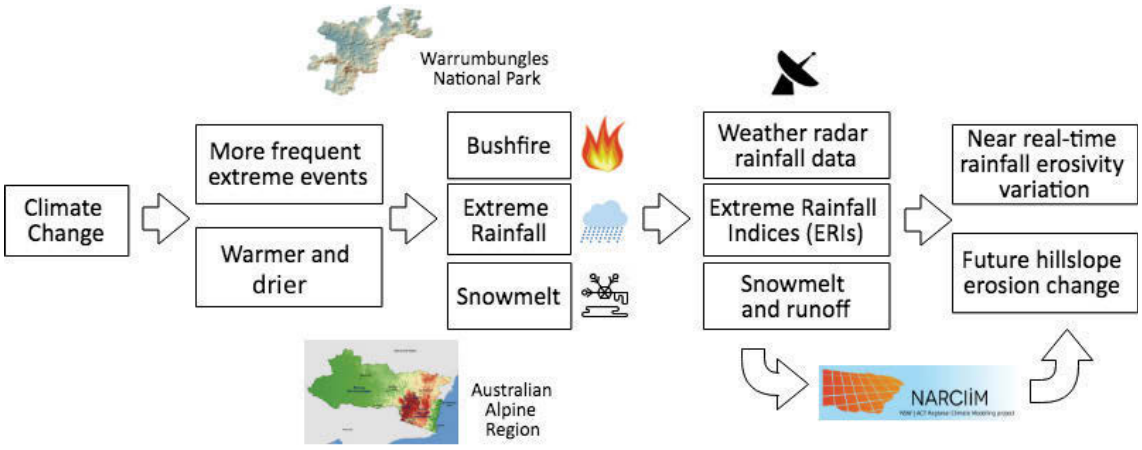

Figure 1-5 Flow chart for this research

Projected warmer and wetter climate in Australia will comprehensively change the erosion rates through more intensive storm events, more severe and frequent wildfire and less snowmelt. Australia's adaptation strategies to climate change play a significant role in the world, since its high seasonal and interannual climate variability. Thus, It is essential to link the extreme weather events and hillslope erosion model to provide effective ecosystem and environment management. The modelled results of this research will provide the baseline of the adaptation planning to the policy-maker to the

world. The output of this research would effectively enhance the capability of government to manage land and soil, and provide adaptation and mitigation strategies in responding to a changing climate. Automated GIS scripts have been developed to calculate the time-series rainfall erosivity and hillslope erosion, so that the processes of modelling are able to applied to elsewhere data is available.

1.8 Study area background and data source

The study area is located in southeast Australia, including two case study areas. One is Warrumbungle National Park, approximately 25 km west of Coonabarabran, another is the NSW and ACT Alpine region, located in southeast Australia.

Warrumbungle National Park (WNP) is 233.11 km^2 in size and ranges from 381m to 1205m. The climate is hot and humid in summer and mild to cool in winter, with a summer-dominate precipitation. A catastrophic wildfire ravaged WNP on 12 January 2013 and burnt about 90% of the park area. A storm event followed by several (18, 19 January) other storms occurred on 1 February 2013 with 100-150mm rain falling into the burnt area.

I used the radar rainfall data (1km, 10-min), calibrated by rain gauges rainfall, to estimate the near real-time rainfall erosivity on a daily basis. The latest satellite-derived fractional vegetation cover (500m, Version 3.1.0), LiDAR DEM (5m and 10m) data and soil digital mapping were used along with radar-based rainfall erosivity to model the post-erosion by using RUSLE. More information of the datasets is listed into Chapter 2 and 3 (Section 2.2 and Section 3.3.1).

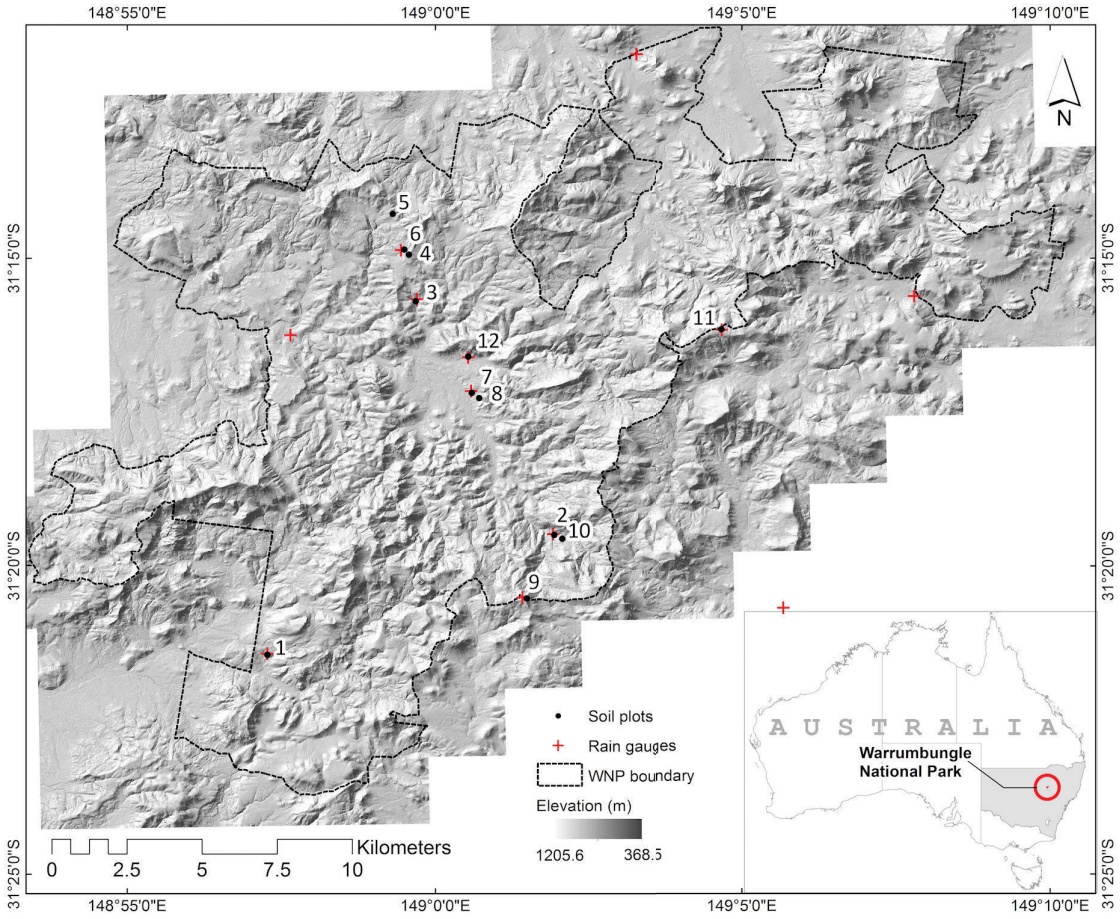

Figure 1-6 Warrumbungle National Park

NSW and ACT Alpine region covers the Kosciuszko National Park in NSW and southwest Australian Capital Territory (ACT). This region contains the highest range (2,228 m above sea level) and the only skiing areas of mainland Australia, where it is important for rainfall and runoff conservation especially under the shadow of climate change (Hennessy et al., 2005).

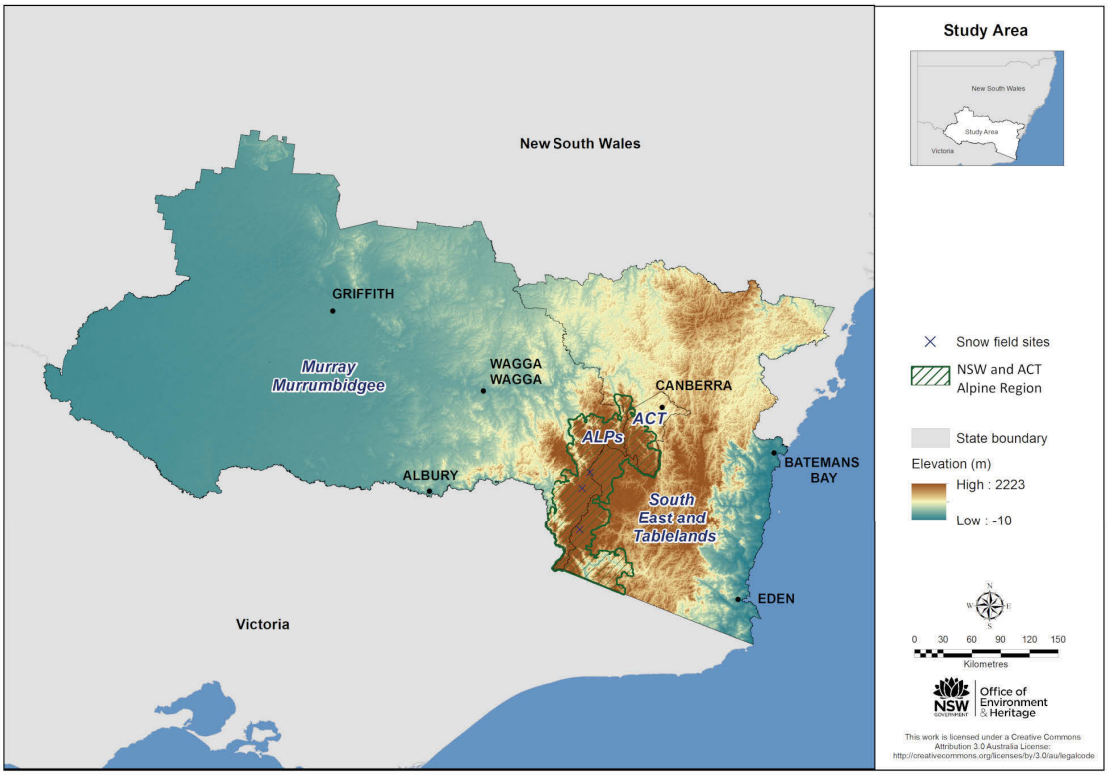

Figure 1-7 NSW and ACT Alpine region and surronding state planning regions

The data used in the study are derived from the New South Wales and Australia Capital Territory Regional Climate Model (NARCliM) project (Evans et. al. 2014). Simulations from four selected global climate models (GCMs) were used in NARCliM to drive three selected regional climate models (RCMs) to form a 12-member GCM/RCM ensemble. Six extreme rainfall indices (ERIs) derived from NARCliM Project (Evans et al., 2016) were selected (R95p, R99p, R20mm, Rnnmm, Rx1day and Rx5day) to assess the extreme rainfall impact on rainfall erosivity for the baseline (1990-2009), near future (2020-2039) and far future (2060-2079).

Snow and temperature projections for the 60 years derived from NARCliM were applied to adjust the snowmelt runoff (Bormann et al., 2014) and rainfall erosivity model in spring (September, October and November) across the NSW and ACT Alpine region. Weekly measurements of snow depth and snow water equivalent at three filed sites in the Snowy Mountains were obtained from Snowy Hydro Ltd to assess the

snowmelt-adjusted rainfall erosivity model. In addition, the NSW soil property projections were obtained from OEH (Gray et al., 2017) and used to calculate soil erodibility based on Yang et al. (2017). Other input data, such as the 30 m DEM, the latest satellite-derived fractional vegetation cover (500m, Version 3.1.0) on monthly basis since 2000 (Guerschman et al., 2009) were used along with the snowmelt-adjusted rainfall erosivity to model the hillslope erosion by using RUSLE in Alpine region. More information of the datasets is listed into Chapter 4 and 5 (Section 4.2.2 and Section 5.2.2).

1.9 References

Almagro, A., Oliveira, T.P.S., Nearing, M.A. & Hagemann. S. 2017. Projected climate change impacts in rainfall erosivity over Brazil. *Scientific Reports.* 7: 8130 .

Aksoy, H. & Kavvas, M. L. 2005. A review of hillslope and watershed scale erosion and sediment transport models. *Catena,* 64**,** 247-271.

Alexander, L. V., Hope, P., Collins, D., Trewin, B., Lynch, A. & Nicholls, N. 2007. Trends in Australia's climate means and extremes: a global context. *Australian Meteorological Magazine,* 56**,** 1-18.

Angulo-Martínez, M., Beguería, S. & Kyselý, J. 2016. Use of disdrometer data to evaluate the relationship of rainfall kinetic energy and intensity (KE-I). *Science of the Total Environment,* 568**,** 83-94.

Arkle, R. S. & Pilliod, D. S. 2010. Prescribed fires as ecological surrogates for wildfires: a stream and riparian perspective. *Forest Ecology and Management,* 259**,** 893-903.

Arnold, J. G., Moriasi, D. N., Gassman, P. W., Abbaspour, K. C., White, M. J., Srinivasan, R., Santhi, C., Harmel, R., Van Griensven, A. & Van Liew, M. W. 2012. SWAT: Model use, calibration, and validation. *Transactions of the ASABE,* 55**,** 1491-1508.

Austin, M. E. 1972. Land resource regions and major land resource areas of the United States (exclusive of Alaska and Hawaii). *Agriculture handbook.* Department of Agriculture.

Benavides-Solorio, J. & Macdonald, L. H. 2001. Post-fire runoff and erosion from simulated rainfall on small plots, Colorado Front Range. *Hydrological Processes,* 15**,** 2931-2952.

Bradstock, R. A., Williams, J. E. & Gill, A. M. 2002. *Flammable Australia: the fire regimes and biodiversity of a continent*, Cambridge University Press.

Bradstock, R.A., 2010. A biogeographic model of fire regimes in Australia: current and future implications. *Global Ecology. Biogeogr*. 19, 145-158.

Brady, N. C. & Weil, R. R. 2010. Elements of the nature and properties of soils. Pearson Prentice Hall Upper Saddle River, NJ, USA.

Brown, J. A. H. 1972. Hydrologic effects of a bushfire in a catchment in south-eastern New South Wales. *Journal of Hydrology,* 15**,** 77-96.

Brown, L. & Foster, G. 1987. Storm erosivity using idealized intensity distributions. *Transactions of the ASAE,* 30**,** 379-0386.

Broz, B., Pfost, D. L. & Thompson, A. L. 2003. Controlling runoff and erosion at urban construction sites. *Extension publications (MU)*.

Cawson, J. G., Sheridan, G., Smith, H. G. & Lane, P. N. 2012. Surface runoff and erosion after prescribed burning and the effect of different fire regimes in forests and shrublands: a review. *International Journal of Wildland Fire,* 21**,** 857-872.

Cerro, C., Bech, J., Codina, B. & Lorente, J. 1998. Modeling rain erosivity using disdrometric techniques. *Soil Science Society of America Journal,* 62**,** 731-735.

CSIRO and Bureau of Meteorology 2015, State of the climate 2016. Commonwealth of Australia, http://www.bom.gov.au/state-of-the-climate/State-of-the-Climate-2016.pdf, accessed June 20, 2018.

Dabney, S. M., Yoder, D. C., Vieira, D. A. & Bingner, R. L. 2011. Enhancing RUSLE to include runoff-driven phenomena. *Hydrological Processes,* 25**,** 1373-1390.

De Dios Benavides-Solorio, J. & Macdonald, L. H. 2005. Measurement and prediction of post-fire erosion at the hillslope scale, Colorado Front Range. *International Journal of Wildland Fire,* 14**,** 457-474.

Edwards, A. C., Scalenghe, R. & Freppaz, M. 2007. Changes in the seasonal snow cover of alpine regions and its effect on soil processes: a review. *Quaternary international,* 162**,** 172-181.

Evans, J., Argüeso, D., Olson, R. & Di Luca, A. 2014. NARCliM extreme precipitation indices report. NARCliM Technical Note 6. Sydney, Australia: Report to the NSW Office of Environment and Heritage.

Evans, J. P., Argueso, D., Olson, R., & Di Luca, A. 2016. Bias-corrected regional climate projections of extreme rainfall in south-east Australia. *Theoretical and Applied Climatology*, 1-14.

Favis-Mortlock, D., Boardman, J. & Macmillan, V. 2001. The limits of erosion modeling. *Landscape erosion and evolution modeling.* Springer.

Foster, G. 2005. Science documentation: Revised universal soil loss equation, Version 2 (RUSLE 2). *USDA-Agricultural Research Service, Washington, DC*.

Foster, G., Yoder, D., Weesies, G., Mccool, D., Mcgregor, K. & Bingner, R. 2003. RUSLE 2.0 user's guide. *USDA-Agricultural Research Service, Washington, DC*.

Foster, G. R. & Lane, L. J. 1987. User requirements: USDA, water erosion prediction project (WEPP) Draft 6.3. *NSERL report (USA)*.

Fu, G., Viney, N. R., Charles, S. P., & Liu, J. 2010. Long-term temporal variation of extreme rainfall events in Australia: 1910–2006. *Journal of Hydrometeorology*, 11(4), 950-965.

Gilley, J. E. 2005. Erosion: water-induced. *In:* HILLEL, D. (ed.) *Encyclopedia of Soils in the Environment.* Amsterdam: Elsevier.

Gordon, C. E., Price, O. F., Tasker, E. M. & Denham, A. J. 2017. Acacia shrubs respond positively to high severity wildfire: Implications for conservation and fuel hazard management. *Science of the Total Environment,* 575**,** 858-868.

Hairsine, P. B., Barson, M., Randall, L. & Wilkinson, S. N. 2009. Identification of areas in Australia where soil loss from hillslope erosion could be reduced. *CSIRO Land and Water Science Report,* 45**,** 1.

Hayhoe, H., Pelletier, R. & Coote, D. 1995. Estimating snowmelt runoff erosion indices for Canada. *Journal of soil and water conservation,* 50**,** 174-179.

Haylock, M. & Nicholls, N. 2000. Trends in extreme rainfall indices for an updated high quality data set for Australia, 1910-1998. *International Journal of Climatology,* 20**,** 1533-1541.

Hennessy, K., Lucas, C., Nicholls, N., Bathols, J., Suppiah, R. & Ricketts, J. 2005. Climate change impacts on fire-weather in south-east Australia. *Climate Impacts Group, CSIRO Atmospheric Research and the Australian Government Bureau of Meteorology, Aspendale*.

Hillel, D. & Hatfield, J. L. 2005. *Encyclopedia of Soils in the Environment*, Elsevier Amsterdam.

Houghton, J. T., Ding, Y., Griggs, D. J., Noguer, M., Van Der Linden, P. J., Dai, X., Maskell, K. & Johnson, C. 2001. *Climate change 2001: the scientific basis*, The Press Syndicate of the University of Cambridge.

Hudson, N. 2015. *Soil conservation: fully revised and updated*, New India Publishing Agency.

Kinnell, P. 1981. Rainfall intensity-kinetic energy relationships for soil loss prediction. *Soil Science Society of America Journal,* 45**,** 153-155.

Kinnell, P. 2005. Why the universal soil loss equation and the revised version of it do not predict event erosion well. *Hydrological Processes,* 19**,** 851-854.

Kinnell, P. 2010. Event soil loss, runoff and the Universal Soil Loss Equation family of models: A review. *Journal of Hydrology,* 385**,** 384-397.

Kinnell, P. 2017. A comparison of the abilities of the USLE-M, RUSLE2 and WEPP to model event erosion from bare fallow areas. *Science of the Total Environment,* 596**,** 32-42.

Kliment, Z., Kadlec, J. & Langhammer, J. 2008. Evaluation of suspended load changes using AnnAGNPS and SWAT semi-empirical erosion models. *Catena,* 73**,** 286-299.

Lal, R. 1994. *Soil erosion research methods*, CRC Press.

Lal, R. 1998. Soil erosion impact on agronomic productivity and environment quality. *Critical reviews in plant sciences,* 17**,** 319-464.

Lal, R. 2001. Soil degradation by erosion. *Land degradation & development,* 12**,** 519-539.

Lehrsch, G., Bjorneberg, D. & Sojka, R. 2005. Erosion: Irrigation-Induced. *In:* Hillel, D. (ed.) *Encyclopedia of Soils in the Environment.* Amsterdam: Elsevier.

Lim, Y. S., Kim, J. K., Kim, J. W., Park, B. I. & Kim, M. S. 2015. Analysis of the relationship between the kinetic energy and intensity of rainfall in Daejeon, Korea. *Quaternary International,* 384**,** 107-117.

Lu, H., Prosser, I. P., Moran, C. J., Gallant, J. C., Priestley, G. & Stevenson, J. G. 2003. Predicting sheetwash and rill erosion over the Australian continent. *Soil Research,* 41**,** 1037-1062.

Luke, R. H. & Mcarthur, A. G. 1978. Bush fires in Australia. *Bush Fires in Australia.*

Mcgregor, K., Bingner, R., Bowie, A. & Foster, G. 1995. Erosivity index values for northern Mississippi. *Transactions of the ASAE,* 38**,** 1039-1047.

Mcgregor, K. & Mutchler, C. 1976. Status of the R factor in northern Mississippi. *Soil Erosion: Prediction and Control, Soil Conservation Soc. Amer***,** 135-142.

Meusburger, K., Leitinger, G., Mabit, L., Mueller, M., Walter, A. & Alewell, C. 2014. Soil erosion by snow gliding–a first quantification attempt in a subalpine area in Switzerland. *Hydrology and earth system sciences,* 18**,** 3763-3775.

Morgan, R., Quinton, J., Smith, R., Govers, G., Poesen, J., Auerswald, K., Chisci, G., Torri, D. & Styczen, M. 1998. The European Soil Erosion Model (EUROSEM):

a dynamic approach for predicting sediment transport from fields and small catchments. *Earth surface processes and landforms,* 23**,** 527-544.
Morgan, R. P. C. 2009. *Soil erosion and conservation*, John Wiley & Sons.
Morgan, R. P. C. & Nearing, M. 2016. *Handbook of erosion modelling*, John Wiley & Sons.
Nearing, M., Foster, G., Lane, L. & Finkner, S. 1989. A process-based soil erosion model for USDA-Water Erosion Prediction Project technology. *Transactions of the ASAE,* 32**,** 1587-1593.
Nearing, M., Pruski, F. & O'Nea M.R. 2004. Expected climate change impacts on hillslope erosion rates: A review. *Journal of Soil and Water Conservation.* 59(1): 43-50.
Nyman, P., Sheridan, G. J., Smith, H. G. & Lane, P. N. 2011. Evidence of debris flow occurrence after wildfire in upland catchments of south-east Australia. *Geomorphology,* 125**,** 383-401.
Ollesch, G., Kistner, I., Meissner, R. & Lindenschmidt, K.-E. 2006. Modelling of snowmelt erosion and sediment yield in a small low-mountain catchment In Germany. *Catena,* 68**,** 161-176.
Ollesch, G., Sukhanovski, Y., Kistner, I., Rode, M. & Meissner, R. 2005. Characterization and modelling of the spatial heterogeneity of snowmelt erosion. *Earth Surface Processes and Landforms,* 30**,** 197-211.
Panagos, P., Ballabio, C., Borrelli, P. & Meusburger, K. 2016a. Spatio-temporal analysis of rainfall erosivity and erosivity density in Greece. *Catena,* 137**,** 161-172.
Panagos, P., Ballabio, C., Borrelli, P., Meusburger, K., Klik, A., Rousseva, S., Tadić, M. P., Michaelides, S., Hrabalíková, M. & Olsen, P. 2015. Rainfall erosivity in Europe. *Science of the Total Environment,* 511**,** 801-814.
Panagos, P., Borrelli, P., Spinoni, J., Ballabio, C., Meusburger, K., Beguería, S., Klik, A., Michaelides, S., Petan, S. & Hrabalíková, M. 2016b. Monthly rainfall erosivity: conversion factors for different time resolutions and regional assessments. *Water,* 8**,** 119.
Petan, S., Rusjan, S., Vidmar, A. & Mikoš, M. 2010. The rainfall kinetic energy–intensity relationship for rainfall erosivity estimation in the mediterranean part of Slovenia. *Journal of hydrology,* 391**,** 314-321.
Pitman, A., Narisma, G. & Mcaneney, J. 2007. The impact of climate change on the risk of forest and grassland fires in Australia. *Climatic Change,* 84**,** 383-401.
Raison, R., Woods, P. & Khanna, P. 1986. Decomposition and accumulation of litter after fire in sub-alpine eucalypt forests. *Austral Ecology,* 11**,** 9-19.
Renard, K. G., Foster, G. R., Weesies, G., Mccool, D. & Yoder, D. 1997. *Predicting soil erosion by water: a guide to conservation planning with the Revised Universal Soil Loss Equation (RUSLE)*, US Government Printing Office Washington, DC.
Robichaud, P. R., Beyers, J. L. & Neary, D. G. 2000. *Evaluating the effectiveness of postfire rehabilitation treatments*, US Department of Agriculture, Forest Service, Rocky Mountain Research Station Fort Collins, Colorado.
Rogler, H. V. & Schwertmann, U. 1981. Erosivität der Niederschläge und Isoerodenkarte von Bayern. *Zf Kulturtechnik und Flurbereinigung,* 22**,** 99-112.
Rosewell, C. J. 1986. Rainfall kinetic energy in eastern Australia. *Journal of Climate and Applied Meteorology,* 25**,** 1695-1701.
Rosewell, C. J. Rates of erosion and sediment transport in Australia. Erosion and Sediment Yield: Global and Regional Perspectives: Proceedings of an

International Symposium Held at Exeter, UK, from 15 to 19 July 1996, 1996. IAHS, 139.
Sanchez-Moreno, J. F., Mannaerts, C. M., Jetten, V. & Löffler-Mang, M. 2012. Rainfall kinetic energy–intensity and rainfall momentum–intensity relationships for Cape Verde. *Journal of Hydrology,* 454**,** 131-140.
Sauerborn, P., Klein, A., Botschek, J. & Skowronek, A. 1999. Future rainfall erosivity derived from large-scale climate models—methods and scenarios for a humid region. *Geoderma,* 93**,** 269-276.
Segura, C., Sun, G., Mcnulty, S. & Zhang, Y. 2014. Potential impacts of climate change on soil erosion vulnerability across the conterminous United States. *Journal of Soil and Water Conservation,* 69**,** 171-181.
Shakesby, R. 2011. Post-wildfire soil erosion in the Mediterranean: review and future research directions. *Earth-Science Reviews,* 105**,** 71-100.
Shakesby, R. & Doerr, S. 2006. Wildfire as a hydrological and geomorphological agent. *Earth-Science Reviews,* 74**,** 269-307.
Shakesby, R. A., Wallbrink, P., Doerr, S. H., English, P. M., Chafer, C. J., Humphreys, G., Blake, W. H. & Tomkins, K. M. 2007. Distinctiveness of wildfire effects on soil erosion in south-east Australian eucalypt forests assessed in a global context. *Forest Ecology and Management,* 238**,** 347-364.
Smith, H. G., Sheridan, G. J., Lane, P. N., Nyman, P. & Haydon, S. 2011. Wildfire effects on water quality in forest catchments: a review with implications for water supply. *Journal of Hydrology,* 396**,** 170-192.
Sui, J. & Koehler, G. 2001. Rain-on-snow induced flood events in Southern Germany. *Journal of Hydrology,* 252**,** 205-220.
Sukhanovski, Y. P., Demidov, V. V. & Ollesch, G. 2005. 191. A Model of Rill Erosion by Snowmelt. *Water and Energy Abstracts,* 15**,** 61-62.
Tiwari, A., Risse, L. & Nearing, M. 2000. Evaluation of WEPP and its comparison with USLE and RUSLE. *Transactions of the ASAE,* 43**,** 1129.
Toy, T. J., Foster, G. R. & Renard, K. G. 2002. *Soil erosion: processes, prediction, measurement, and control*, John Wiley & Sons.
Tulau, M. J. 2015. Fire and Soils: A review of the potential impacts of different fire regimes on soil erosion and sedimentation, nutrient and carbon cycling, and impacts on water quantity and quality. Office of Environment and Heritage, Sydney.
Van Dijk, A., Bruijnzeel, L. & Rosewell, C. 2002. Rainfall intensity–kinetic energy relationships: a critical literature appraisal. *Journal of Hydrology,* 261**,** 1-23.
Van Oost, K., Govers, G., Cerdan, O., Thauré, D., Van Rompaey, A., Steegen, A., Nachtergaele, J., Takken, I. & Poesen, J. 2005. Spatially distributed data for erosion model calibration and validation: The Ganspoel and Kinderveld datasets. *Catena,* 61**,** 105-121.
Williams, J. & Berndt, H. 1977. Sediment yield prediction based on watershed hydrology. *Transactions of the ASAE,* 20**,** 1100-1104.
Williams, J. R. 1975. Sediment-yield prediction with universal equation using runoff energy factor.
Wischmeier, W. & Smith, D. 1965. Rainfall-erosion losses from cropland east of the Rocky Mountains, guide for selection of practices for soil and water conservation. *Agriculture Handbook,* 282.
Wischmeier, W. H. 1959. A rainfall erosion index for a universal soil-loss equation1. *Soil Science Society of America Journal,* 23**,** 246-249.

Wischmeier, W. H. & Smith, D. D. 1958. Rainfall energy and its relationship to soil loss. *Eos, Transactions American Geophysical Union,* 39**,** 285-291.
Wischmeier, W. H. & Smith, D. D. 1978. *Predicting rainfall erosion losses-A guide to conservation planning*. Maryland, United States Department of Agriculture.
Yang, X. & Yu, B. 2014. Modelling and mapping rainfall erosivity in New South Wales. *Soil Research*, 53, 178-189.
Yin, S., Xie, Y., Nearing, M. & Wang, C. 2007. Estimation of rainfall erosivity using 5- to 60-minute fixed-interval rainfall data from China. *Catena,* 70, 306-312.
Young, R., Onstad, C., Bosch, D. & Anderson, W. 1989. AGNPS: A nonpoint-source pollution model for evaluating agricultural watersheds. *Journal of soil and water conservation,* 44**,** 168-173.
Young, R. A., Onstad, C., Bosch, D. & Singh, V. AGNPS: An agricultural nonpoint Source Model. Workshop on Computer Applications in Water Management, 1995. 33.
Zhang, Y., Degroote, J., Wolter, C. & Sugumaran, R. 2009. Integration of Modified Universal Soil Loss Equation (MUSLE) into a GIS framework to assess soil erosion risk. *Land Degradation & Development,* 20**,** 84-91.
Zheng, M. & Chen, X. 2015. Statistical determination of rainfall-runoff erosivity indices for single storms in the Chinese Loess Plateau. *PloS one,* 10**,** e0117989.
Zobeck, T. M. & Van Pelt, R. S. 2005. Erosion: wind-induced. *In:* HILLEL, D. (ed.) *Encyclopedia of Soils in the Environment.* Amsterdam: Elsevier.

Chapter 2*: Estimation of storm event-based rainfall erosivity from weather radar data in burnt area

*This chapter has been accepted for publication in Land Degradation and Development, 2018.

Abstract

Rainfall erosivity impacts all stages of hillslope erosion processes, and is an important factor (the 'R factor') in the Revised Universal Soil Loss Equation (RUSLE). It is estimated as the average annual value of the sum of all erosive events (EI_{30}) over a period of many years. For each storm event, the EI_{30} value is the product of storm energy, E in MJ ha^{-1}, and peak 30-min rainfall intensity (I_{30}, mm hr^{-1}). Previous studies often focused on estimation of the R factor for prediction of mean annual or long-term soil losses. However, many applications require EI_{30} values at much higher temporal resolution, such as post-fire soil erosion monitoring, which requires a time step at storm events or on a daily basis. In this study, we explored the use of radar rainfall data to estimate the storm event-based EI_{30} after a severe wildfire in Warrumbungle National Park in southeastern Australia. The radar-derived rainfall data were calibrated against 12 tipping bucket rain gauges across an area of 239 km^2 and subsequent used to produce a time-series of rainfall erosivity maps at daily intervals since the wildfire in January 2013. The radar-derived daily rainfall showed good agreement with the gauge measurements ($R^2 = 0.75$, $E_c = 0.66$). This study reveals great variation in EI_{30} values ranging from near zero to 826.76 MJ mm ha^{-1} hr^{-1} for a single storm event. We conclude that weather radar rainfall data can be used to derive timely EI_{30} and erosion information for fire incident management and erosion control. The methodology developed in this study is generic and thus readily applicable to other areas where weather radar data are available.

Keywords: weather radar, rainfall erosivity, EI_{30}, storm events, post-fire erosion

2.1 Introduction

Hillslope erosion after a wildfire often causes land degradation and adversely impacts the environment and water quality (de Santos Loureiro & de Azevedo Coutinho, 2001; Klik, Haas, Dvorackova, & Fuller, 2015; Mello, Viola, Beskow, & Norton, 2013; Renard & Freimund, 1994). Individual high-intensity rainstorms can account for appreciable quantities of post-fire erosion (Shakesby & Doerr, 2006). For example, in an early study in eucalypt forest near Sydney, Australia, Atkinson (1984) found that one rainfall event of 16.5 mm lasting 45 min caused the equivalent of a year's loss of soil. Leitch, Flinn, and Van de Graaff (1983) estimated a loss of 22 t ha^{-1} after 21 mm of rain on small plots in burnt eucalypt-dominated forest in the Victorian Central Highlands of Australia.

It is therefore critical to monitor, map, and disseminate both average and more extreme erosion risks for catchments, given the predicted increase in climate variability and fire intensity in many parts of the world (Renard, Foster, Weesies, McCool, & Yoder, 1997; Wischmeier & Smith, 1958). Like cropping, (Van Oost, Govers, & Desmet, 2000), wildfire removes the soil cover and results in insufficient cover to protect soils, which are then vulnerable to an extreme erosive event. Hence, understanding the characteristics of the spatiotemporal distribution of wildfires and erosive rainfall events are critical.

Rainfall and runoff erosivity (the 'R factor') as defined in the Revised Universal Soil Loss Equation (Renard, Foster, Weesies, McCool, & Yoder, 1997) is the average annual value of the sum of all erosive events (EI_{30}) over a period of many years. The R factor has been shown to be highly correlated with soil loss at many sites throughout the world (Panagos et al., 2017). For each storm event, the EI_{30} value is the product of storm energy, E in MJ ha^{-1}, and peak 30-min rainfall intensity (I_{30}, mm hr^{-1}) (Renard,

Foster, Weesies, McCool, & Yoder, 1997; Wischmeier & Smith, 1958). Average monthly or annual rainfall erosivity has been assessed in several studies from long-term precipitation records and local rain gauges (de Santos Loureiro & de Azevedo Coutinho, 2001; Klik, Haas, Dvorackova, & Fuller, 2015; Mello, Viola, Beskow, & Norton, 2013; Renard & Freimund, 1994). Some studies have discussed long-term rainfall erosivity impacts on hillslope erosion modeling at large spatial scales in Europe (Petan, Rusjan, Vidmar, & Mikoš, 2010), New Zealand (Klik, Haas, Dvorackova, & Fuller, 2015), Japan (Santosa, Mitani, & Ikemi, 2010) and Africa (Vrieling, Sterk, & de Jong, 2010). Sidman, Guertin, Goodrich, Unkrich, and Burns (2016) have discussed the effect of post-fire rainfall events on high-risk areas of flooding and erosion. Fischer et al. (2016) have estimated rainfall event erosivity by using radar data. However, there are few studies on the spatial and temporal variation of daily EI_{30} during a post-fire recovery period, despite the key role of erosivity in hillslope erosion.

Weather radar is one of the best sources to derive near real-time precipitation with high spatial and temporal resolution (few minutes to sub-hourly) for large areas (Seed, Siriwardena, Sun, Jordan, & Elliott, 2002; Wüest et al., 2010). It has been used to record real-time rainfall since the 1980s (Battan, 1973), and to provide estimation of spatiotemporal variability of erosivity (Fischer et al., 2016). While radar offers high-resolution spatiotemporal rainfall data, its accuracy can be affected by certain weather types and technical limitations (Steiner, Smith, Burges, Alonso, & Darden, 1999). For example, limited visibility during particular weather events such as graupel and hail can affect the radar-received signal (Battan, 1973). Nevertheless, the adjusted radar-derived rainfall estimation can be very close to those obtained from rain gauges (Hossain, Anagnostou, Dinku, & Borga, 2004).

Weather radar measures the reflectivity (Z) and determines the rain rate (R) through a power law relationship of the formula $Z = aR^b$, known as the Z-R relationship (Seed, Siriwardena, Sun, Jordan, & Elliott, 2002; (Steiner, Smith, Burges, Alonso, & Darden, 1999). The Z-R relationship normally varies by season and changes with the raindrop size distribution, the storm type (Chumchean, Seed, & Sharma, 2008) and the native climate (Seed, Siriwardena, Sun, Jordan, & Elliott, 2002); hence, radar rainfall estimation can be significantly affected by these factors, as well as the uncertainty or errors in reflectivity measurements. Alternative calibration methods include rain gauges and disdrometers (Angulo-Martínez, Beguería, & Kyselý, 2016).

Gauge measurements are representative only at the measurement site (Steiner, Smith, Burges, Alonso, & Darden, 1999), whereas radar estimates instantaneous rainfall at some height above the ground (Steiner, Smith, Burges, Alonso, & Darden, 1999). Gauged rainfall measurements over a wider area have been applied to calibrate the Z-R relationship (Hasan, Sharma, Johnson, Mariethoz, & Seed, 2014). For example, Chumchean, Seed, and Sharma (2006) used a Kalman filtering approach to calibrate the radar rainfall bias in real time in Australia, Rendon, Vieux, and Pathak (2012) adapted the adjustment to radar with seasonal variation in the US; Bringi, Rico-Ramirez, and Thurai (2011) compared radar estimates against a gauge network in the UK, and Rozalis, Morin, Yair, and Price (2010) corrected radar by gauge rainfall to hydrological modelling in Europe.

Severe wildfire and subsequent storm events increase erosion rates, change runoff generation, and potentially contaminate water supplies due to the increased flux of sediment, nutrients and other water constituents (Haberlandt, 2007). Severe wildfires have the potential to increase rainfall erosivity due to the loss of canopy (Nanko, Onda, Ito, & Moriwaki, 2008). Therefore, quantitative and timely assessment of rainfall

erosivity and hillslope erosion after wildfires during individual storm events is essential but remains a research challenge (Yin, Xie, Liu, & Nearing, 2015). This is largely due to the lack of quality rainfall data at high spatial and temporal resolutions at large spatial scales; the processing of these large spatial datasets itself is another challenge.

Key literature for the relevant studies are summarized in Table 2-1. This study focuses on the estimation of storm event-based EI_{30} with the first attempt of using weather radar data to predict the near real-time rainfall erosivity in a burnt area after storm events. The specific objectives of this research were to: (i) identify the bias-correction coefficient between radar rainfall and tipping bucket gauge rainfall data; (ii) estimate daily EI_{30} and its spatial and temporal variation; and (iii) assess the impact of event and daily EI_{30} and apply them to near real-time monitoring of hillslope erosion risk. These objectives primarily define the structural sub-headings in the following methods, results and discussion sections.

However, not all papers included soil erosion modelling and post-fire assessment via radar images and these are denoted with a N/A representing ‘not applicable’ in the relevant part of the ‘Key results’ column. In the ‘Key results’ column the abovementioned three components are identified by the code: (1) identify bias correction and radar rainfall variation in the relationship between gauge and radar rainfall; (2) estimate EI_{30} and its temporal and spatial variation; and (3) assess impact of EI_{30} on soil erosion in the burnt area.

Table 2-1 Summary of relevant studies using radar rainfall to estimate event erosivity in the burnt area

Study	Data/ Model used	Location/ Study Size	Key results
1. Leitch et al. (1983)	Sampling and measurement.	Burnt forest near Warburton, Australia/ 0.35 km^2	(1) N/A (2) N/A (3) It was estimated that about 22 t ha^{-1} soil were washed after wildfire and the following intense thunderstorm (21 mm of rain).
2. Steiner et al. (1999)	WSR-88D radar(1 × 1 km^2, 5-min), rain gauge data/ Z-R relationship	Goodwin Creek, Mississippi, United States/ 21.4 km^2	(1) Radar rainfall estimates with a RMSE approximately 10% for the cumulative storm event of 30mm or more. (2) N/A (3) N/A
3. Legates (2000)	WSR-88D weather radar (4 × 4 km^2, 5-min). 674 gauge-radar pairs over two months/fixed Z-R relationship	The southern Great Plains, United States/ approximately 1000 × 1000 km^2	(1) $Z = 73.97 R^{1.409}$. Radar estimates provide the spatial variation to each storm while gauge measurements are applied to improve the accuracy. (2) N/A (3) N/A
4. Chumchean et al. (2006)	7-month radar and rain gauge data/Kalman filter	Sydney, Australia	(1) Kalman filter approach becomes unstable when the size of the gauging network decreases (less than 1 gauge 70 km^2) (2) N/A (3) N/A
5. Cruse et al. (2006)	NEXRAD radar (4 × 4 km^2, 15-min), 25 rain gauges, other data from NRI/WEPP model	Iowa, United States	(1) The correlation coefficient of monthly radar against 12 rain gauges from Iowa City network is around 0.9, RMSE about 0.12. While when compare to 12 rain gauges from Iowa State University Agriculture Network, correlation coefficient is around 0.7 and RMSE about 0.25. (2) Estimate spatial variation (10 × 10 km^2) of average runoff for a given day. (3) Soil erosion (unburnt) ranges from 0 to over 11.2 t ha^{-1}, which also spatially correlated with rainfall amounts.
6. Rozalis et al. (2010)	Radar rainfall (3 × 1 km^2, 5-min), 15 rain gauges, runoff from hydrometric station/ hydrology model (SCS-CN)	Mediterranean watershed (unburnt) in Israel/ 27 km^2	(1) Radar-derived rainfall was calibrated from rain gauges. (2) N/A (3) According to the prediction from model, the flow magnitude was significantly affected by rain intensity distribution within the storm.

Table 2-1 (continued)

Study	Data/ Model used	Location/ Study Size	Key results
7. Vireling et al. (2010)	TMPA daily and monthly rainfall, radar estimates (3h, 0.25°), rain gauges/ modified Fournier Index (MFI)	Africa continent	(1) 3-hour radar-derived rainfall was not sufficient to represent high-intensity erosive events. (2) Monthly product provided spatial estimates of average annual erosivity. (3) N/A
8. Wüest et al. (2010)	72 Rain gauges (10-min), Swiss weather radars (2 × 2 km^2, 5-min)	Swiss Plateau, Switzerland	(1) The error to intensity per hour and frequency were both less than 25%. (2) N/A (3) N/A
9. Nyman et al. (2011)	Radar-derived intensity (0.5 × 0.5 km^2, 10-min), manual rain gauges and debris flow sites from field survey/ RUSLE model	Catchments in eastern Victoria, Australia/ < 5 km^2	(1) Cumulative radar rainfall for debris flow was adjusted from the rainfall measured at field sites. (2) N/A (3) Debris flows triggered by intense storm events in burnt catchments when I_{30} ranged from 35 mm h^{-1} to 59 mm h^{-1}. Post-fire sheet erosion from measurements indicates that hillslope material provides an important source of sediment.
10. Löwe et al. (2014)	Radar (2 × 2 km^2, 10-min), 6 gauges (10-min) from the Danish SVK network and 2.5 months runoff data in summer /Z-R relationship, stochastic grey-box model	Two catchments in the Copenhagen, Denmark/ 13 km^2 and 30 km^2.	(1) $Z = 50\ R^{1.8}$ (2) Correlation between rainfall and runoff forecasting has been estimated from both radar and gauge measurements. (3) N/A
11. Klik et al. (2015)	High-resolution rainfall data from 35 gauging station (10-min) /RUSLE model	New Zealand/ ~269,600 km^2	(1) N/A (2) The high variability of rainfall erosivity is mainly associated with the climatic and topographic differences across New Zealand. The average storm-based erosivity in summer is 2.1 times more than that from winter. The peak erosivities appear mostly in summer (December to February) (3) N/A
12. Yang and Yu (2015)	Gridded daily rainfall from BoM, 124 sites pluviography rainfall data/ RUSLE model	NSW, Australia	(1) N/A (2) In terms of the same rain in the same month, the rainfall erosivity is higher at lower latitude and at lower elevation (3) N/A
13. Fischer et al. (2016)	Radar rainfall (1 × 1 km^2, 5-min) from RADOLAN and 30 rain gauges/USLE and RUSLE2 model	Bavarian Tertiary Hills, Germany/ ~15,000 km^2	(1) Adjust radar rainfall in 60-min interval from 30 rain gauges (mean difference 4%, RMSE is 3mm) (2) The difference of event rainfall erosivity between adjacent cells is up 120 N h^{-1}. Compare to the daily rainfall, the spatio-temporal variation is considerably stronger. (3) N/A

Table 2-1 (continued)

Study	Data/ Model used	Location/ Study Size	Key results
14.Sidman et al. (2016)	USGS stream gauges, DHR radar / KINEROS2, AGWA model	North Creek within Zion National Park, United States/ 243.83 km^2	(1) Rainfall representation by using radar was applied in areas with low-gauge density. (2) N/A (3) The varying rainfall representation has a great impact on the peak flow when modeling runoff after wildfire, while not significantly affected the predictions for hotspot areas.
15. This study	Radar rainfall from BoM (1 × 1 km^2, 10-min, 256× 256), twelve rain gauges from field, / RUSLE model	Warrumbungle National Park, Australia/233 km^2	(1) The radar-derived rainfall indicates strong positive correlation with the gauge measurements (R^2 = 0.75). (2) There is great seasonal variation in spatial and temporal distributions of EI_{30} across the Park. Maximum event EI_{30} was estimated about 827 MJ mm ha^{-1} hr^{-1}. (3) The maximum erosion rate from soil plot measurement is approximately 1.0 t ha^{-1} yr^{-1} on average across the WNP. The time series of daily EI_{30} maps can provide timely information for erosion control and monitoring of fire recovery.

2.2 Study site and datasets

The study area for this research is approximately 450 km northwest of Sydney, centered on an area approximately 25 km west of Coonabarabran, and comprises Warrumbungle National Park (WNP) and the fire footprint (74,000 ha). The park ranges in elevation from 381 m to 1205 m. The climate is characterized by hot, usually humid summers and mild to cool winters. The nearest climate data come from Coonabarabran Airport Automatic Weather Station (AWS) (BoM station no. 064017, -31.29^o S, 149.07^o E, elevation 645 m), and until 2013, from Westmount (BoM station no. 064046, -33.33^o S, 149.27^o E, elevation 860 m) on the eastern boundary of the park, where the mean annual rainfall was 1,034 mm. The rainfall is summer-dominated, with January the wettest month, at 131 mm (Bureau of Meteorology, 2018b). The driest month is generally April, with a mean rainfall of 58 mm (Bureau of Meteorology, 2018b). Mean annual rainfall is much lower in the surrounding slopes and plains, at 670

mm (Bureau of Meteorology, 2018b).

A severe wildfire ignited in WNP, New South Wales (NSW), Australia on 12 January 2013. Under the extreme fire weather, 95% of the park was burnt, with 72% of the area categorized as high to extreme burn severity. Fire severity was estimated from RapidEye images based on normalized burn ratio methods (Battan, 1973) and categorized into four classes (0: unburnt; 1:low severity; 2: high severity; 3: extreme severity) (Storey, 2014). Later, on 1 February 2013, an intense storm event (rainfall intensity > 50 mm h^{-1}) occurred, followed by several other storms where 100-150 mm of rain fell over the burnt area. These events led to extraordinary erosion and long-term landscape changes to this iconic park.

A series of 12 closed plots were established in May 2014 at locations across WNP in order to monitor soil erosion and groundcover. The size of these plots were approximately 9 m^2 as recommended by Riley, Crozier, & Blong (1981). Though smaller than the standard USLE plot (length = 22.1 m, slope = 9%), they were easier to install and maintain and allowed for comparison with previous studies in Australia (e.g. Atkinson, 1984; Atkinson, 2012; Yang et al., 2018). Accumulated sediment was collected during each field visit and sent to Yanco Natural Resources Laboratory, where the material was dried and weighed, and particle size classes and soil texture determined (Table 2-2). From July 2015, each plot site or nearby had both standard rain gauge and tipping bucket rain gauge installed from which rainfall intensity could be measured. Figure 1 shows the locations of the 12 soil plots and the tipping bucket rain gauges, and the basic information of these plots are listed in Table 2-2.

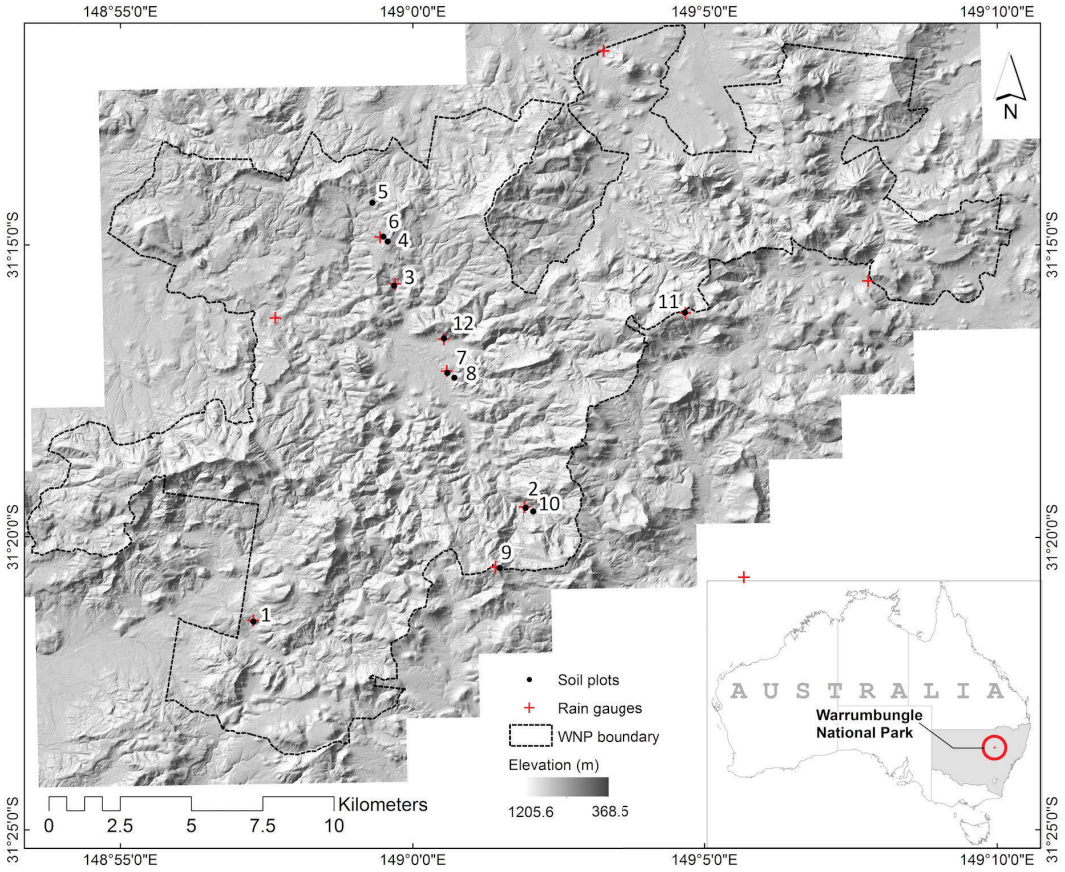

Figure 2-1 The Warrumbungle National Park study area, and the locations of soil plots and tipping bucket gauges

Table 2-2 Basic information of the twelve soil plots within the Warrumbungle National Park

Site	Easting	Northing	Name	Elev (m)	Fire	Geo	Aspect (degree)	Slope (%)	Clay (%)	Silt (%)	Fine Sand (%)	CS (%)
1	148.9546	-31.3575	Gunneemoor oo	595	0	V	240	30	27	13	30	30
2	149.0322	-31.3249	Strathmore lower	608	1	V	330	25	21	27	29	23
3	148.9947	-31.2617	Buckleys West	445	3	S	65	32	11	7	26	56
4	148.9929	-31.2491	Nth fire trail lower	715	2	V	260	22	15	35	24	26
5	148.9885	-31.2380	Nth fire trail upper	692	2	V	180	22	18	26	36	20
6	148.9916	-31.2477	Nth fire trail middle	605	2	V	220	25	13	44	22	21
7	149.0099	-31.2865	Middle valley	447	1	S	135	25	13	9	28	50
8	149.0119	-31.2879	Scabilon hill	519	3	S	250	37	13	33	22	32
9	149.0247	-31.3423	TV Tower	1040	1	V	70	38	8	34	26	32
10	149.0343	-31.3260	Strathmore upper	687	1	V	30	25	22	17	22	39
11	149.0778	-31.2693	Siding Spring	1023	2	V	340	18	19	35	19	27
12	149.0089	-31.2767	Blackman	509	2	S	190	22	14	10	30	46

Elev = Elevation, Geo = Geology, Fire = fire severity (0-3 represent unburnt to severe burnt classes), S = sandstone, V = volcanic, CS = coarse sand

In Australia, weather radar networks have been operated by the Australia Bureau of Meteorology (BoM) since 1948. Nevertheless, the first quantitative rainfall estimation by radar was not published and analyzed until the 1960s (Seed, Siriwardena, Sun, Jordan, & Elliott, 2002). There are 43 full-time weather radar stations across Australia, each one updates images at 10-min intervals with a domain of 256 × 256 km^2 and a spatial resolution of 1 km. For this study, the Namoi (Blackjack Mountain) S-band radar (DWSR 8502S) (-31.0240° S, 150.1915° E) data (10-min, 1 km) were obtained from the BoM. Continuous radar images were obtained for the period from January to March 2013 immediately after fire, and an extended period from January 2014 to June 2017 for on-going monitoring.

2.3 Methods

2.3.1. Radar data processing and bias correction

To calculate the radar-derived rainfall accumulation, the raw radar reflectivity measurements (10-min, 1 km × 1 km) obtained from the Namoi station are firstly corrected by removing the effect of beam blocking. Then rainfall accumulation is converted from the corrected radar reflectivity through a Z-R relationship as below (Bureau of Meteorology, 2018a),

$$Z = 60\,R^{1.7} \tag{2-1}$$

where Z represents the reflectivity and R is the rain rate per pixel. BoM keeps this Z-R relationship constant rather than varying it by season, as there are insufficient gauges to conduct a real-time adjustment within the Namoi coverage area. In this study, daily radar-derived rainfall estimations were adjusted against daily rain gauge observations through linear regression once the radar reflectivity was converted to rainfall

accumulation and daily rainfall depth rate.

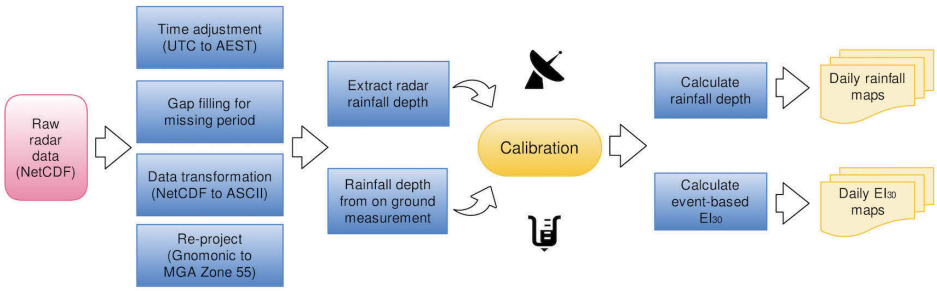

Figure 2-2 Processing steps of radar rainfall

The procedures for the rain gauge adjustment are illustrated in Figure 2-2. Radar-based rainfall accumulations were firstly gap-filled by linear interpolation with data from neighboring time-steps. Matlab scripts were then developed and applied to batch convert the original radar data in NetCDF format to ESRI ASCII grids, which were then input to ArcGIS for extraction of rainfall accumulation and further calculations for EI_{30}. To ensure data consistency, the radar data were re-projected from Gnomonic to MGA Zone 55 so that all datasets were in the same coordinate system. Also, UTC (Coordinate Universal Time) in the radar data was readjusted to local Australian Eastern Standard Time (AEST = UTC + 10:00).

The twelve tipping buckets gauges installed within WNP were used to calibrate the weather radar rainfall data. Where there were data gaps due to rain gauge instrument failure (<15.5%), the missing values were filled from the most appropriate gauge according to linear regression and comparison with all the surrounding RGs.

Bias removal is one of the most important processes in the radar-based rainfall estimation. To adjust the radar rainfall bias, we developed a linear relationship between rainfall measured from rain gauges and from radar. This relationship was based on daily rainfall amounts (July 2015 to June 2017) for reasons that 1) there was too much variation and data gaps in the 10-min rainfall time-series, and 2) the final EI_{30} maps are on a daily basis.

2.3.2. Event-based EI_{30} estimation

The EI_{30} for a single storm event is the value of energy, E in MJ ha^{-1}, multiplied by the peak 30-min rainfall intensity I_{30} (mm hr^{-1}). In this study, E is computed from the 10-min radar-based rainfall in 10-min intervals following Equation 2-2.

$$E = \sum_{r=1}^{N} e_r \Delta V_r \tag{2-2}$$

$$e_r = 0.29[1 - 0.72exp\ (-a\frac{\Delta V_r}{\Delta t_r})] \tag{2-3}$$

where $\Delta V_r/\Delta t_r$ is the rainfall intensity (mm hr^{-1}), while ΔV_r refers to rainfall amount during that particular period, Δt_r, N is the number of 10-minute intervals (e.g. N = 3 for 30-min), e_r (MJ ha^{-1} mm^{-1}) means unit kinetic energy, and *a* is an empirical coefficient. This form of the equation, including empirical coefficients, was based on the work of Kinnell (1981). Equation 2-3 was proposed by Brown and Foster (1987) as a replacement for the original equation presented in the Agriculture Handbook No.537 (Wischmeier & Smith, 1978) and further modified by Foster et al. (2003) as part of RUSLE2. The maximum unit energy was taken as 0.29 based on the work of Rosewell (1986). The difference of these two equations is that the revised exponent value (0.082) is slightly higher than the counterpart value (0.05) of Brown and Foster (1987). It is believed that this kinetic energy and intensity (KE-I) coefficient (Brown & Foster, 1987) underestimates the rainfall erosivity by about 10% (Nearing, Yin, Borrelli, & Polyakov, 2017; Renard & Freimund, 1994). Thus, in this study, we compared daily EI_{30} computed from Brown and Foster (1987) (RUSLE) with its revised version (Foster et al., 2003) (RUSLE2).

The rainfall intensity for 30-min (mm hr^{-1}) intervals, I_{30} is calculated as

$$I_{30} = P_{30} \times 2 \tag{2-4}$$

where P_{30} is the maximum 30-min rainfall depth (mm). It is multiplied by 2 to convert

to an hourly scale. Peak rainfall amounts in 30-min intervals was extracted from radar images at every three 10-min intervals. Renard, Foster, Weesies, McCool, and Yoder (1997) recommended including all storm events in the R-factor calculation. Most literature has defined erosive storm events as cumulative rainfall events greater than 12.7 mm, that is, at least 12.7 mm rain within 30-min, and separated by a break of more than 6 hours. However, the discrepancy in the calculated R factor due to different rainfall thresholds increases as the mean annual rainfall decreases because the relative contribution of small storm events to the R factor increases in dry areas (Yu, 1999). Hence the threshold was set as 5 mm d^{-1} instead of 12.7 mm in this study to ensure that small events that did not produce runoff were not included in the determination of daily erosivity.

2.3.3 Model performance and erosion risk assessment

Once event-based EI_{30} values were computed from the radar data at 10-min intervals, these values were accumulated to total daily, monthly and annual rainfall erosivity (R-factor). Model performance was measured by the coefficient of efficiency, E_c (Nash & Sutcliffe, 1970), which is commonly used to assess model performance in hydrology and soil sciences (Loague & Freeze, 1985; Risse, Nearing, Laflen, & Nicks, 1993):

$$E_c = 1 - \sum_{i=1}^{M}(y_i - \hat{y})^2 / \sum_{i=1}^{M}(y_i - \bar{y})^2 \quad (2\text{-}5)$$

where y_i are observed values while $\hat{y}$ are modelled values, $\bar{y}$ is the average of observed values, and M represented the sample size. Essentially, E_c is an indicator of how close the scatter of predicted versus actual values are to the 1:1 line (Yang, Yu, & Xie, 2015). The common coefficient of determination (R^2), root mean square difference (RSME) and standard error of the mean (SEM) were also applied to assess model performances

by comparing the plot values (e.g. gauged rainfall data) with the simulated values estimated by weather radar and the KE-I relationship.

2.4 Results

2.4.1 Bias correction and radar rainfall variation

Time-series of daily rainfall (>5 mm d^{-1}) from July 2015 to June 2017 (two hydrological years) were compared with different data sources (Figure. 2-3) including 1) pluviograph data from AWS (064017) at every 6-min, and 2) mean rainfall amount from the twelve tipping bucket rain gauges. The comparisons show that there is a good relationship between radar-derived rainfall and the gauge rainfall measurements. The relationship between raw radar and gauged rainfall during two hydrological years when combined is relatively weak (Figure. 2-3c, $R^2 = 0.5$, $E_c = 0.043$) compared to the individual relationships for each hydrological year separately (Figure. 2-3a and 2-3b, $R^2 > 0.7$). The weaker relationship with the pluviograph data ($R^2 = 0.45$) might be due to the location of the pluviograph station (AWS 064017), which is about 30 km away from most of the rain gauges. For this reason, we only used the rain gauge data for the bias correction and the pluviograph data were only used as complementary data sources when gauge data were not available, such as immediately after the wildfire in 2013 (Figure. 3e and 3f), since gauges were not installed in WNP until July 2015.

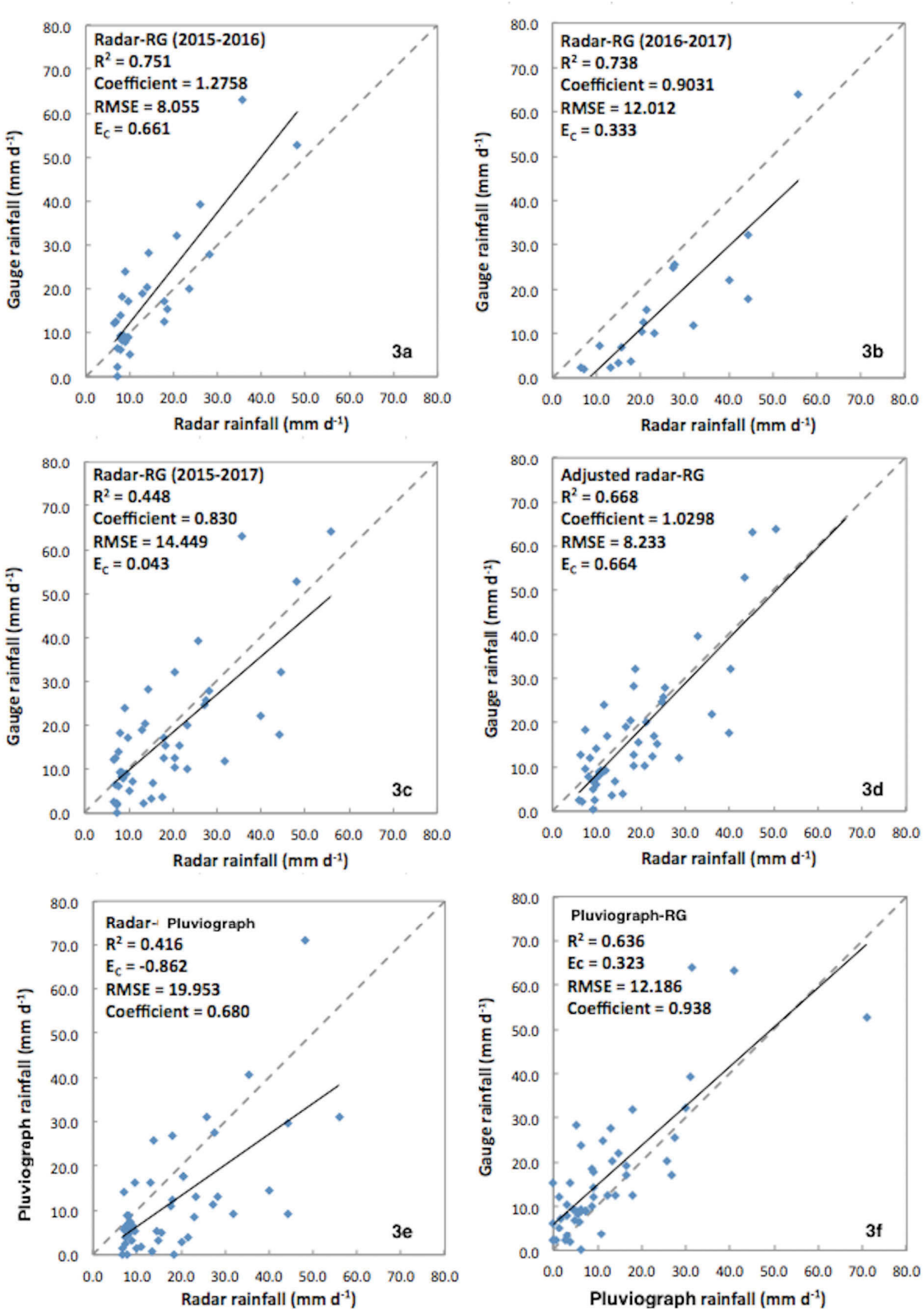

Figure 2-3 Relationship between radar-derived, gauge-measured and pluviograph rainfall

An adjustment factor (AF) was applied to calibrate the radar-based estimates pixel by pixel and for all radar data with 10-min time step:

$$R_{gauge} = AF \times R_{radar} \quad (6)$$

where R_{gauge} is the daily rainfall collected from the tipping bucket rain gauges on the ground, AF is the adjustment factor and R_{radar} is radar-based rainfall extracted from the pixel in which the gauge is located. Two AFs were applied (corresponding to the two hydrological years). For the 2015-2016 hydrological year an AF of 1.28 was applied (Figure. 2-3a), while for the 2016-2017 hydrological year an AF of 0.90 was applied (Figure. 2-3b). For the regressions used to derive both AFs, there was a strong correlation between gauge and radar-derived rainfall (R^2 = 0.74-0.75, RMSE = 8.06-1201, E_c = 0.33-0.66).

After calibration against the gauges in WNP (Figure. 2-3d), time-series rainfall depth maps derived from the radar data were produced at hourly, daily and monthly intervals. Figure 2-4 shows examples of daily rainfall derived from the radar data when the daily average rainfall amount from 12 stations was more than 5 mm. The daily rainfall amounts were accumulations over the previous 24 hours to 9:00 am local time. The peak radar rainfall was estimated to be as high as 61.87 mm hr^{-1} for 2 February 2013. Hotspot areas with large daily rainfall amounts coincided with areas of extreme burn severity (e.g. on 18, 19 Jan, 2, 22 Feb and 5 Mar 2013). These calibrated rainfall data were subsequently used for EI_{30} calculations, and compared with observed soil loss from hillslope plots on a monthly time-step.

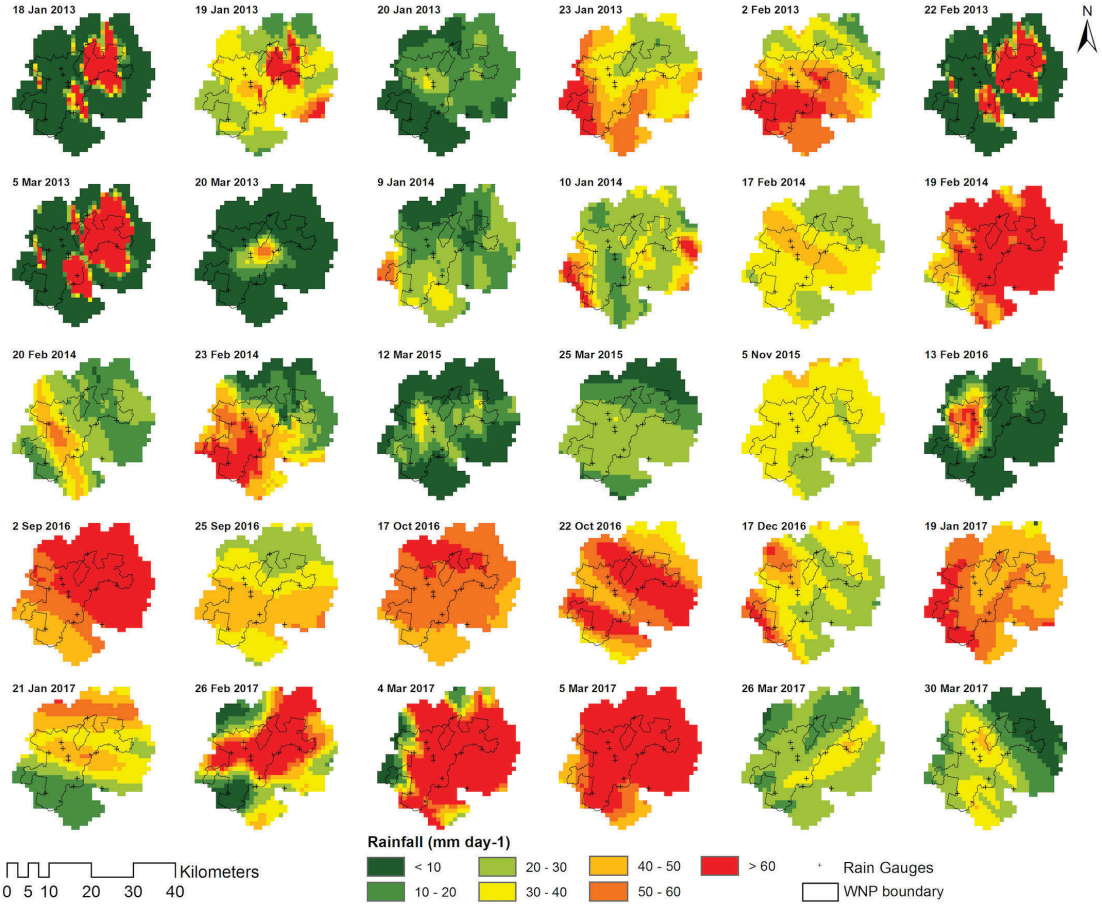

Figure 2-4 Radar-derived daily rainfall after calibration from January 2013 to June 2017. The shape here is actually the fire ground for selected storm events (daily rainfall > 5 mm d^{-1})

2.4.2 EI_{30} and its temporal and spatial variation

The modelled daily EI_{30} over two hydrological years follows a similar trend to rainfall in general, irrespective of which data sources (radar or gauge rainfall) or methods (KE-I relation from RUSLE or RUSLE2) were used (Figure. 2-5a, 2-5b, 2-5c and 2-5d). The results show a strong agreement ($R^2 = 0.80$, $n = 52$) between the radar-based EI_{30} and the gauge-based EI_{30}, although the radar-derived data (empirical coefficient: 0.05) underestimated the daily EI_{30} by approximately 8.20% compared to the daily EI_{30}, when estimated using the 0.082 KE-I coefficient.

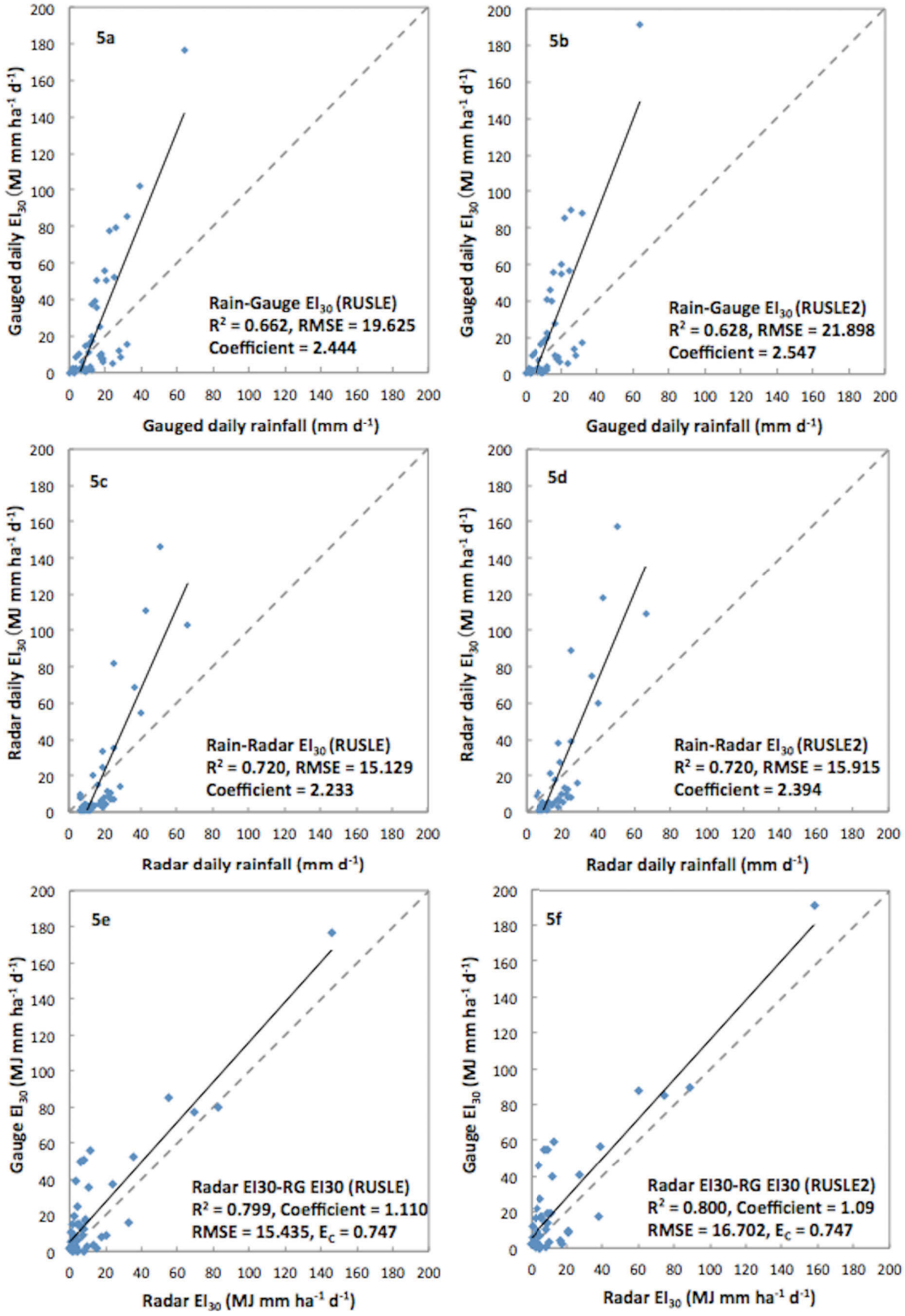

Figure 2-5 (a) Regression of gauge daily rainfall and gauge daily EI_{30} (empirical coefficient: 0.05); (b) Regression of gauge daily rainfall and gauge daily EI_{30} (empirical coefficient: 0.082); (c) Regression of radar daily rainfall and radar- derivde daily EI_{30} (empirical coefficient: 0.05); (d) Regression of radar daily rainfall and radar-derivde daily EI_{30} (empirical coefficient: 0.082); (e) Comparison of daily EI_{30} (empirical

coefficient: 0.05) from radar rainfall gauge measurement; (f) Comparison of daily EI_{30} (empirical coefficient: 0.082) from radar rainfall gauge measurement.

To examine seasonal variation, monthly EI_{30} values were accumulated from daily radar-derived EI_{30} values and compared against the monthly EI_{30} values calculated from the gauge sites and pluviograph data. Table 2-3 shows the similar seasonal variation in EI_{30} from all these different data sources. The higher EI_{30} values appeared in summer (December, January & February), with the EI_{30} values in winter (June, July & August) significantly lower. These variations are reflected in all EI_{30} estimates from radar, gauges and pluviograph measurements.

Table 2-3 Seasonal variation of EI_{30} and storm event assessment on 1 February 2013

Plu = pluviograph rainfall data, RG = rain gauge data.

Seasonal EI_{30} (RUSLE) %	Jul 2015-Jun 2016			Jul 2016-Jun 2017			20130201 12:30-13:30 %	Rain		EI_{30} (RUSLE)		EI_{30} (RUSLE2)	
	RG	Radar	Plu	RG	Radar	Plu		Plu	Radar	Plu	Radar	Plu	Radar
Summer	42.5	31.6	38.1	24.4	29.4	35.9	Daily	91.6	87.0	99.9	88.7	99.9	86.9
Autumn	19.9	23.2	19.0	33.5	28.5	38.5	Monthly	50.5	29.1	80.7	31.2	79.5	31.1
Winter	12.0	21.5	7.2	10.3	11.6	2.0	Seasonal	10.9	8.03	53.8	9.28	56.3	10.2
Spring	25.6	23.8	35.8	31.8	30.5	23.6	Annually	5.9	-	37.6	-	35.2	-
Summer & Autumn	62.4	54.7	57.1	57.9	57.9	74.4	Month/ season	21.7	27.6	66.6	29.7	70.8	32.7
Spring & Summer	68.1	55.3	73.9	56.2	59.9	59.5	Season/ annual	54.0	-	70.0	-	62.6	-

For the storm event on 1 February 2013 between 12:30 pm and 13:30 pm, there were noticeable differences in absolute values between pluviograph and radar-derived event EI_{30}. As shown in Table 2-3, the event radar EI_{30} during the storm accounts for more than 9% of seasonal EI_{30} for the three summer months (December to February). In contrast, for the pluviograph data, the EI_{30} estimated from the same event accounts for more than 50 % of the seasonal EI_{30} for summer months. Event-based EI_{30} was largely consistent with the radar-derived rainfall; each peak EI_{30} value corresponds to the peak rainfall intensity (Figure. 2-4). For any given time-step (e.g. daily, monthly), the predicted rainfall erosivity varied spatially across the park. The EI_{30} fluctuated in response to the radar-derived rainfall estimates.

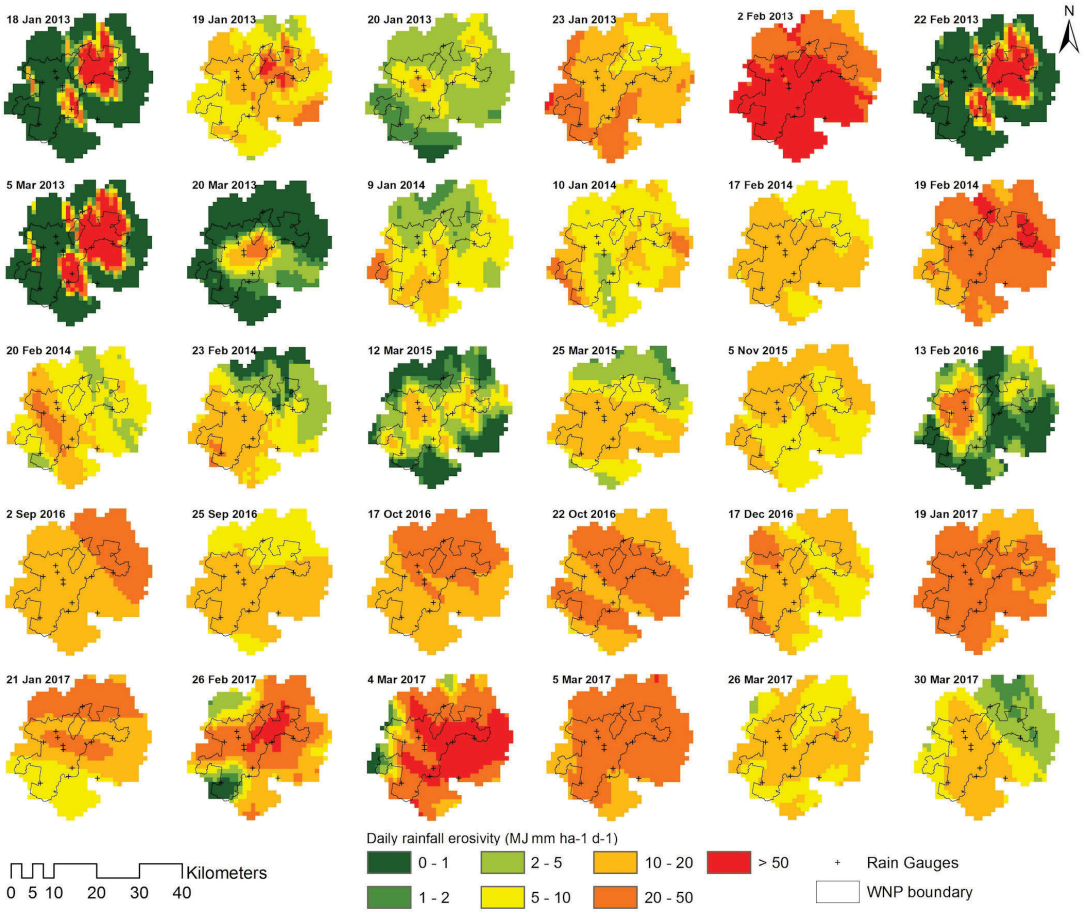

Figure 2-6 Time series EI_{30} maps and the spatial variations in the monitoring period from January 2013 to June 2017.

Figure 2-6 shows the daily EI_{30} of storm events and their spatial variation over the monitoring period (January 2013 to June 2017). These maps can be used to identify potential high erosion risk areas during storm events. For example, the daily EI_{30} variation on 4 March 2017 in Figure 2-6 refers to a daily EI_{30} value as high as 826.76 MJ mm ha^{-1} hr^{-1} for a single event.

2.4.3 Impact of EI_{30} on erosion

The measured erosion during each field visit follows a similar seasonal pattern to the monthly EI_{30} in general (Figure. 2-7a), irrespective of which data source was applied (radar or gauge). Among the soil plots across the park, high erosivity was apparent at

Site 1 and Site 11 as shown on Figure 2-7b. Areas near these sites had experienced stronger storm events and flash flooding than most other soil plots. The higher cumulative EI_{30} values resulted in higher soil losses from the soil plots.

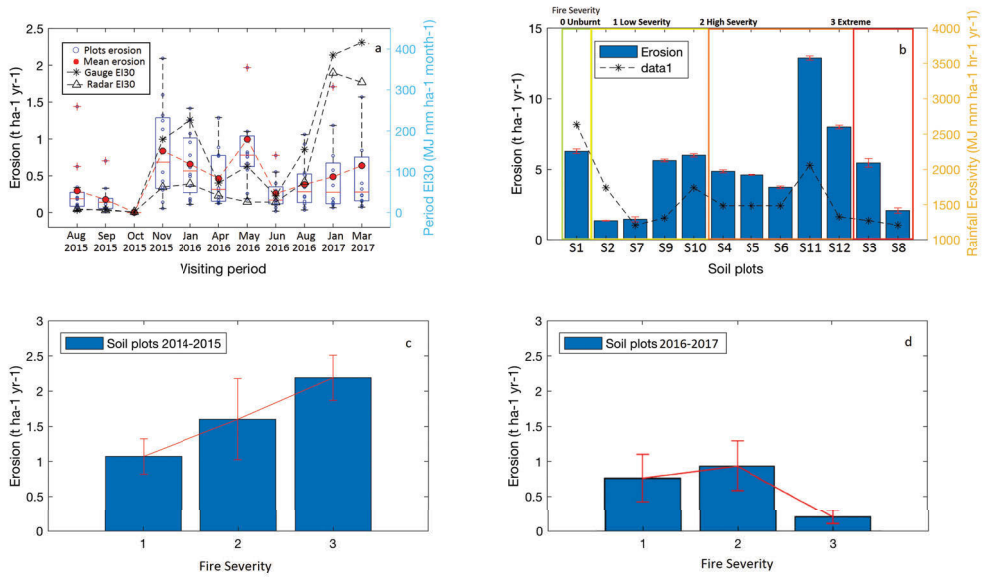

Figure 2-7 (a) Comparison of Monthly EI_{30} and erosion from July 2015 to June 2017; (b) Spatial variation of rainfall erosivity and erosion; (c) The relationship between fire severity and erosion from 2014-2015; (d) The relationship between fire severity and erosion from 2016-2017.

The relationship between the annual sum of EI_{30} and post-fire erosion was compared and assessed at soil plot sites from July 2015 (Figure. 2-7b). Error bars represent the standard error of mean (SEM) of average erosion measurements. The measured soil loss at each plot reflects the influence of EI_{30} but there is an obvious discrepancy between observed soil loss and EI_{30}. values. For example, the highest erosion rates were measured at Site 11; however, the corresponding EI_{30} was not the highest. Heavy rainfall occurred near Site 2, but the measured erosion rates from that soil plot were relatively low.

There exists a good relationship between fire severity and erosion from the twelve measured erosion plots installed in 2014 (Figure. 2-7c). Higher erosion occurred in

extremely burnt area within one year after the wildfire (Figure. 2-7c), but such relationships became weaker in subsequent years (2016-2017, Figure. 2-7d) due to vegetation recovery and erosion control measures.

2.5 Discussion

2.5.1. Bias correction and radar rainfall variation

Radar rainfall can play a significant role in representing rainfall intensity, especially in areas without a high density of gauge networks (Hossain, Anagnostou, Dinku, & Borga, 2004; Sidman, Guertin, Goodrich, Unkrich, & Burns, 2016). Even where rain gauges or pluviograph rainfall stations exist, they are unlikely to replace radar-derived rainfall estimates, due to high spatial and temporal resolution from radar data.

The tipping bucket gauges measured the rainfall depth across the WNP and provided precise calibration and supplementary observation for radar estimation (Legates, 2000). However, the rainfall gauges are sparse and thus unable to identify all the hotspot areas across the park without the assistance of the radar-derived rainfall. This also limited the application of the Kalman filter in calibration of radar rainfall as it requires a much higher density of gauges (about one gauge per 70 km^2) (Chumchean, Seed, & Sharma, 2006).

The pluviographic rainfall data from the Coonabarabran Airport AWS (064017) was available at 6-min intervals from January 2013 to present. In contrast, the twelve rain gauges were installed in the WNP only since July 2015, thus the pluviographic rainfall data is as essential as the radar-derived rainfall for estimating the daily rainfall erosivity immediately after wildfire (since Jan 2013).

The results from this study illustrate that there is a strong positive correlation between radar-derived rainfall and daily EI_{30} (R^2 = 0.72). Higher radar rainfall estimates correspond to greater rainfall erosivity at the same grid cell. The variation of rainfall mirrors the variation of EI_{30} particularly in the severely burnt area. In agreement with Sidman, Guertin, Goodrich, Unkrich, and Burns (2016), the varying rainfall has a great impact on peak rainfall erosivity modeling.

2.5.2. EI_{30} and its temporal and spatial variation

Seasonal variation of rainfall erosivity is apparent due to the large seasonal variation of rainfall amount and intensity. The highest seasonal EI_{30} occurred in summer, with the lowest in winter. This seasonal variation agrees with previous studies using long historical rainfall records which show strong seasonality with the highest rainfall erosivity in summer and lowest in winter (Renard, Foster, Weesies, McCool, & Yoder, 1997).

Compared with daily rainfall, the spatio-temporal variation of rainfall erosivity was considerably larger (Fischer et al., 2016). From our results, the average seasonal EI_{30} in summer is approximately 2-3 times greater than that predicted in winter, based on radar estimation and gauge measurements respectively. In comparison, Yang, Yu, and Xie (2015) reported that the R factor between summer and winter had about 7-fold difference in NSW statewide. Klik, Haas, Dvorackova, and Fuller (2015) found that rainfall erosivity in summer was 2.1 times higher than that from winter in New Zealand, modelled from gauged rainfall.

Spatial distribution is a highly important factor when estimating erosivity and erosion in burnt area as wildfire removes the soil cover and creates a potential window for extreme erosion events (e.g. storm events). Radar EI_{30} revealed that the spatial variation of daily EI_{30} is mostly driven by the spatial variations in rainfall (Figure. 2-5c

and 5d), and explicitly predicted the high-risk areas due to a particular event (Figure. 2-6).

In this study, radar data have been first applied to detect high-risk areas and temporal variation of daily EI_{30} (Figure. 2-6). However, daily EI_{30} estimated using RUSLE was underestimated by 8.20% in comparison to that from RUSLE2 (Figure. 2-5e). This underestimation agrees with Nearing, Yin, Borrelli, and Polyakov (2017) and Foster et al. (2003), who believed that the KE-I relationship from RUSLE underestimates the rainfall erosivity by approximately 10%. Despite changing the coefficient to 0.082 instead of the commonly applied 0.05 in RUSLE2 (Foster et al., 2003), the radar-derived daily EI_{30} was still underestimated by 11% (Figure. 2-5f) compared to the gauge-estimated EI_{30}. Nevertheless, it is worth noting that no matter which coefficient has been used, they were both developed based on experiments and data collected in the US. Furthermore, although an absolute difference exists among different KE-I relations, these slight differences will not significantly affect the estimated results for the WNP study. Thus, we continue to use the KE-I relationship proposed by Brown and Foster (1987) in the following sections. Another possible explanation for the discrepancy might be due to the gap period of the radar estimation, which may miss some rainfall events, while the point-based gauge measurement fills the gap of radar rainfall.

2.5.3 Impact of EI_{30} on post-fire erosion

Similar seasonal variation was apparent from the time-series of erosion measurements and monthly EI_{30} (Figure. 2-7a). More soil loss was observed in summer when heavy rainstorms occurred, while less erosion was measured in the dry winters. In general, higher erosion rates were positively correlated with fire severity, however,

relatively high erosion rates were also evident in some unburnt areas such as Site 1. This discrepancy is probably due to the vegetation recovery of burnt areas and the effects of other RUSLE factors such as soil and topographic factors. For example, the slope steepness factor for Site 1 was measured as high as 0.3 (Table 2-2).

The average erosion from plots in extremely burnt areas decreased by about 94.1% from 2014 (2.19 t ha^{-1} yr^{-1}) to 2017 (0.13 t ha^{-1} yr^{-1}). In comparison, the erosion changes in low (1.07 t ha^{-1} yr^{-1} in 2014 to 0.48 t ha^{-1} yr^{-1} in 2017) and high severity (1.6 t ha^{-1} yr^{-1} in 2014 to 0.6 t ha^{-1} yr^{-1}in 2017) burn areas over three years gradually decreased by 55.0% and 63.1% respectively. One explanation for these differences is that the rapid vegetation recovery in high severity burn areas (Gordon, Price, Tasker, & Denham, 2017) leads to a reduction of post-fire erosion rates (Figure. 2-7c and 2-7d). Thus, mapping the burn severity, and not just the fire footprint, combined with radar-based event EI_{30} provides important information at a high spatio-temporal resolution for erosion process modelling after wildfire.

RUSLE or the revised model (RUSLE2) was originally designed to predict average annual soil loss. Both models have limitations for post-fire erosion modelling, in particular they are unable to account for changes in soil hydrophobicity, which can affect sediment run-off, and often temporarily increases after fire (Sheridan, Lane, & Noske, 2007). As such these models have limitations in predicting hillslope erosion for a particular storm event. However, some alternative process-based models such as WEPP (Nearing, Foster, Lane, & Finkner, 1989) are extremely sensitive to parameter estimations and those predictions are often poor (Van Oost, Govers, & Desmet, 2000) while RUSLE requires low data inputs, is robust and has widely been used across the world. It is possible to estimate daily (or storm event-based) soil loss with time-series EI_{30} at a sub-daily scale as discussed above or the product of the runoff ratio (Q_R) and

EI_{30} index (Kinnell, 2010; Kinnell, 2014) given the fact that soil erodibility and topographic factors are stable while groundcover factor changes seasonally (Yang et al., 2018).

Prediction of event-based EI_{30} will be increasingly important due to the higher likelihood of intense storm events under climate change (Alexander et al., 2007). The current climate change projections predict that the region is trending towards an increased risk of wildfire due to warmer and drier conditions (Hennessy et al., 2005; Pitman, Narisma, & McAneney, 2007) and higher frequencies of extreme weather such as storm events (Alexander et al., 2007; Nyman, Sheridan, Smith, & Lane, 2011).

2.6 Conclusions

In this study, we have assessed various rainfall data types covering various periods, including pluviograph rainfall, tipping bucket rain gauges and radar-derived rainfall estimates for their potential for estimating EI_{30}. It is important to choose the most suitable rainfall data to fill the gaps and simulate the time-series of rainfall erosivity into WNP after the wildfire. Radar-derived rainfall data has its advantage in spatial and temporal resolutions. Thus, the exploration of radar rainfall data in estimating EI_{30} is of great importance when rainfall erosivity and post-fire erosion estimation at a storm event or daily time-step is required.

We have developed a set methodology to estimate EI_{30}, compared to the actual erosion from soil plots at sub-daily temporal resolutions and provided timely information for park management on erosion control. Our study has demonstrated that weather radar underestimated rainfall by a factor of 1.28 (R^2 = 0.75) from July 2015 to Jun 2016 and overestimated rainfall (AF = 0.90, R^2 = 0.74) from July 2016 to Jun 2017, but shows strong correlation with gauged rainfall. EI_{30} for storm events or on a daily

basis can be estimated from the radar-based rainfall time-series at high temporal resolution.

Our results indicate that the highest seasonal EI_{30} appeared in summer while the lowest in winter. Hillslope erosion rates in general follow similar seasonality. The time-series radar-derived EI_{30} demonstrate the potential high-risk erosion areas on each rain day. The change of post-fire erosion to some extent is mostly driven by the fire severity. The measured soil loss rates at soil plots correspond well with the EI_{30} estimates in the same periods. Our results provide evidence to support and promote the use of weather radar technology for estimation of rainfall erosivity for individual storm events. As rainfall erosivity is one of the key factors in causing land degradation at a range of scales, this study reveals the potential in using weather radars for real-time or nearly real-time monitoring and prediction of land degradation around the world. Outcomes from this study have been directly used in hillslope erosion monitoring across the WNP at near-real time (Yang et al., 2018). Our methodology and scripts are general, thus applicable for areas where weather radar data available.

Acknowledgements

We thank the New South Wales Office of Environment and Heritage (OEH) for providing funding and data for the Warrumbungle National Park fire recovery research project and our subproject on Soil and Water. Bureau of Meteorology provided the radar rainfall data. We thank Dr Alan Seed for his patient advice on weather radar data. Many staff in the NSW National Park and Wildlife Services, in particular, Craig Wall, provided assistance for fieldwork and advice. Colleagues in Soil and Water, Fire Behaviour, Vegetation and Fauna teams provided useful discussion and advice to our sub-project. These OEH scientists and visitors assisted with fieldwork on groundcover and remote sensing measurements: Ms. Robin McAlpine, Dr. Senani Karunaratne.

2.7 References

Alexander, L. V., Hope, P., Collins, D., Trewin, B., Lynch, A., & Nicholls, N. (2007). Trends in Australia's climate means and extremes: a global context. *Australian Meteorological Magazine, 56*(1), 1-18. https://doi.org/10.1.1.222.5972&rep=rep1&type=pdf

Angulo-Martínez, M., Beguería, S., & Kyselý, J. (2016). Use of disdrometer data to evaluate the relationship of rainfall kinetic energy and intensity (KE-I). *Science of the Total Environment, 568*, 83-94. https://doi.org/10.1016/j.scitotenv.2016.05.223

Atkinson, G. (1984). Erosion damage following bushfires. *Journal of Soil Conservation New South Wales (Australia)*. http://escholarship.library.usyd.edu.au/journals/index.php/LIN

Atkinson, G. (2012). Soil erosion following wildfire in Royal National Park, NSW. Paper presented at the Proceedings of the Linnean Society of New South Wales 134, B25-B38. http://escholarship.library.usyd.edu.au/journals/index.php/LIN

Battan, L. J. (1973). Radar observation of the atmosphere. https://doi.org/10.1002/qj.49709942229

Bringi, V., Rico-Ramirez, M., & Thurai, M. (2011). Rainfall estimation with an operational polarimetric C-band radar in the United Kingdom: comparison with a gauge network and error analysis. *Journal of Hydrometeorology, 12*(5), 935-954. https://doi.org/10.1175/JHM-D-10-05013.1

Bureau of Meteorology (2018a). How Radar-Derived Rainfall Accumulations Are Calculated. Retrieved from http://www.bom.gov.au/australia/radar/about/calculating_rainfall_accumulations.shtml

Bureau of Meteorology (2018b). Monthly rainfall for Coonabarabran (Westmount). Retrieved from http://www.bom.gov.au/jsp/ncc/cdio/weatherData/av?p_nccObsCode=139&p_display_type=dataFile&p_startYear=&p_c=&p_stn_num=064046

Brown, L., & Foster, G. (1987). Storm erosivity using idealized intensity distributions. *Transactions of the ASAE, 30*(2), 379-0386. https://doi.org/10.13031/2013.31957

Chumchean, S., Seed, A., & Sharma, A. (2006). Correcting of real-time radar rainfall bias using a Kalman filtering approach. *Journal of Hydrology, 317*(1), 123-137. https://doi.org/10.1016/j.jhydrol.2005.05.013

Chumchean, S., Seed, A., & Sharma, A. (2008). An operational approach for classifying storms in real-time radar rainfall estimation. *Journal of Hydrology, 363*(1), 1-17. https://doi.org/10.1016/j.jhydrol.2008.09.005

Cruse, R., Flanagan, D., Frankenberger, J., Gelder, B., Herzmann, D., James, D., . . . Opsomer, J. (2006). Daily estimates of rainfall, water runoff, and soil erosion in Iowa. *Journal of Soil and Water Conservation, 61*(4), 191-199. http://www.jswconline.org/content/61/4/191.short

de Santos Loureiro, N., & de Azevedo Coutinho, M. (2001). A new procedure to estimate the RUSLE EI 30 index, based on monthly rainfall data and applied to the Algarve region, Portugal. *Journal of Hydrology, 250*(1), 12-18. https://doi.org/10.1016/S0022-1694(01)00387-0

Fischer, F., Hauck, J., Brandhuber, R., Weigl, E., Maier, H., & Auerswald, K. (2016). Spatio-temporal variability of erosivity estimated from highly resolved and adjusted radar rain data (RADOLAN). *Agricultural and Forest Meteorology, 223*, 72-80. https://doi.org/10.1016/j.agrformet.2016.03.024

Foster, G., Yoder, D., Weesies, G., McCool, D., McGregor, K., & Bingner, R. (2003). RUSLE 2.0 user's guide. *USDA-Agricultural Research Service, Washington, DC*. https://www.tucson.ars.ag.gov/unit/Publications/PDFfiles/1117.pdf

Gordon, C. E., Price, O. F., Tasker, E. M., & Denham, A. J. (2017). Acacia shrubs respond positively to high severity wildfire: Implications for conservation and fuel hazard management. *Science of the Total Environment, 575*, 858-868. https://doi.org/10.1016/j.scitotenv.2016.09.129

Haberlandt, U. (2007). Geostatistical interpolation of hourly precipitation from rain gauges and radar for a large-scale extreme rainfall event. *Journal of Hydrology, 332*(1), 144-157. https://doi.org/10.1016/j.jhydrol.2006.06.028

Hasan, M. M., Sharma, A., Johnson, F., Mariethoz, G., & Seed, A. (2014). Correcting bias in radar Z–R relationships due to uncertainty in point rain gauge networks. *Journal of Hydrology, 519*, 1668-1676. https://doi.org/10.1016/j.jhydrol.2014.09.060

Hennessy, K., Lucas, C., Nicholls, N., Bathols, J., Suppiah, R., & Ricketts, J. (2005). Climate change impacts on fire-weather in south-east Australia. *Climate Impacts Group, CSIRO Atmospheric Research and the Australian Government Bureau of Meteorology, Aspendale*. http://www.cmar.csiro.au/e-print/open/hennessykj_2005b.pdf

Hossain, F., Anagnostou, E. N., Dinku, T., & Borga, M. (2004). Hydrological model sensitivity to parameter and radar rainfall estimation uncertainty. *Hydrological Processes, 18*(17), 3277-3291. https://doi.org/10.1002/hyp.5659

Kinnell, P. (1981). Rainfall intensity-kinetic energy relationships for soil loss prediction. *Soil Science Society of America Journal, 45*(1), 153-155. https://doi.org/10.2136/sssaj1981.03615995004500010033x

Kinnell, P. (2010). Event soil loss, runoff and the Universal Soil Loss Equation family of models: A review. *Journal of Hydrology, 385*(1), 384-397. https://doi.org/10.1016/j.jhydrol.2010.01.024

Kinnell, P. (2014). Modelling event soil losses using the $Q_R EI_{30}$ index within RUSLE2. *Hydrological Processes, 28*(5), 2761-2771. https://doi.org/10.1002/hyp.9790

Klik, A., Haas, K., Dvorackova, A., & Fuller, I. C. (2015). Spatial and temporal distribution of rainfall erosivity in New Zealand. *Soil Research, 53*(7), 815-825. https://doi.org/10.1071/SR14363

Legates, D. R. (2000). Real-time calibration of radar precipitation estimates. *The Professional Geographer, 52*(2), 235-246. https://doi.org/10.1111/0033-0124.00221

Leitch, C., Flinn, D. W., & Van de Graaff, R. (1983). Erosion and nutrient loss resulting from Ash Wednesday (February 1983) wildfires a case study. *Australian Forestry, 46*(3), 173-180. https://doi.org/10.1080/00049158.1983.10674396

Loague, K. M., & Freeze, R. A. (1985). A comparison of rainfall-runoff modeling techniques on small upland catchments. *Water Resources Research, 21*(2), 229-248. https://doi.org/10.1029/WR021i002p00229

Löwe, R., Thorndahl, S., Mikkelsen, P. S., Rasmussen, M. R., & Madsen, H. (2014). Probabilistic online runoff forecasting for urban catchments using inputs from rain gauges as well as statically and dynamically adjusted weather radar. *Journal of Hydrology, 512*, 397-407. https://doi.org/10.1016/j.jhydrol.2014.03.027

Mello, C. d., Viola, M., Beskow, S., & Norton, L. (2013). Multivariate models for annual rainfall erosivity in Brazil. *Geoderma, 202*, 88-102. https://doi.org/10.1016/j.geoderma.2013.03.009

Nanko, K., Onda, Y., Ito, A., & Moriwaki, H. (2008). Effect of canopy thickness and canopy saturation on the amount and kinetic energy of throughfall: An experimental approach. *Geophysical Research Letters, 35*(5). https://doi.org/10.1029/2007GL033010

Nash, J. E., & Sutcliffe, J. V. (1970). River flow forecasting through conceptual models part I—A discussion of principles. *Journal of Hydrology, 10*(3), 282-290. https://doi.org/10.1016/0022-1694(70)90255-6

Nearing, M., Foster, G., Lane, L., & Finkner, S. (1989). A process-based soil erosion model for USDA-Water Erosion Prediction Project technology. *Transactions of the ASAE, 32*(5), 1587-1593. https://doi.org/10.13031/2013.31195

Nearing, M., Yin, S.-q., Borrelli, P., & Polyakov, V. O. (2017). Rainfall erosivity: An historical review. *Catena, 157*, 357-362. https://doi.org/10.1016/j.catena.2017.06.004

Nyman, P., Sheridan, G. J., Smith, H. G., & Lane, P. N. (2011). Evidence of debris flow occurrence after wildfire in upland catchments of south-east Australia. *Geomorphology, 125*(3), 383-401. https://doi.org/10.1016/j.geomorph.2010.10.016

Panagos, P., Borrelli, P., Meusburger, K., Yu, B., Klik, A., Lim, K. J., . . . Chattopadhyay, N. (2017). Global rainfall erosivity assessment based on high-temporal resolution rainfall records. *Scientific Reports, 7*(1), 4175. https://doi.org/10.1038/s41598-017-04282-8

Petan, S., Rusjan, S., Vidmar, A., & Mikoš, M. (2010). The rainfall kinetic energy–intensity relationship for rainfall erosivity estimation in the mediterranean part of Slovenia. *Journal of Hydrology, 391*(3), 314-321. https://doi.org/10.1016/j.jhydrol.2010.07.031

Pitman, A., Narisma, G., & McAneney, J. (2007). The impact of climate change on the risk of forest and grassland fires in Australia. *Climatic Change, 84*(3-4), 383-401. https://doi.org/10.1007/s10584-007-9243-6

Renard, K. G., Foster, G. R., Weesies, G., McCool, D., & Yoder, D. (1997). *Predicting soil erosion by water: a guide to conservation planning with the Revised Universal Soil Loss Equation (RUSLE)* (Vol. 703): US Government Printing Office Washington, DC. https://naldc.nal.usda.gov/download/11126/PDF

Renard, K. G., & Freimund, J. R. (1994). Using monthly precipitation data to estimate the R-factor in the revised USLE. *Journal of Hydrology, 157*(1), 287-306. https://doi.org/10.1016/0022-1694(94)90110-4

Rendon, S. H., Vieux, B. E., & Pathak, C. S. (2012). Continuous Forecasting and Evaluation of Derived Z-R Relationships in a Sparse Rain Gauge Network Using NEXRAD. *Journal of Hydrologic Engineering, 18*(2), 175-182. https://doi.org/10.1061/(ASCE)HE.1943-5584.0000579

Riley, S., Crozier, P., & Blong, R. (1981). inexpensive and easily installed runoff plot. *Journal of the Soil Conservation Service of New South Wales*. http://agris.fao.org/agris-search/search.do?recordID=US201301992895

Risse, L., Nearing, M., Laflen, J., & Nicks, A. (1993). Error assessment in the universal soil loss equation. *Soil Science society of America journal, 57*(3), 825-833. https://doi.org/10.2136/sssaj1993.03615995005700030032x

Rozalis, S., Morin, E., Yair, Y., & Price, C. (2010). Flash flood prediction using an uncalibrated hydrological model and radar rainfall data in a Mediterranean watershed under changing hydrological conditions. *Journal of Hydrology, 394*(1), 245-255. https://doi.org/10.1016/j.jhydrol.2010.03.021

Santosa, P. B., Mitani, Y., & Ikemi, H. (2010). *Estimation of RUSLE EI 30 based on 10 min interval rainfall data and GIS-based development of rainfall erosivity maps for Hitotsuse basin in Kyushu Japan.* Paper presented at the 2010 18th International Conference on Geoinformatics. https://doi.org/10.1109/GEOINFORMATICS.2010.5568195

Seed, A., Siriwardena, L., Sun, X., Jordan, P., & Elliott, J. (2002). On the calibration of Australian weather radars. *CRC for Catchment Hydrology*. https://ewater.org.au/archive/crcch/archive/pubs/pdfs/technical200207.pdf

Shakesby, R., & Doerr, S. (2006). Wildfire as a hydrological and geomorphological agent. *Earth-Science Reviews, 74*(3), 269-307. https://doi.org/10.1016/j.earscirev.2005.10.006

Sheridan, G. J., Lane, P. N., & Noske, P. J. (2007). Quantification of hillslope runoff and erosion processes before and after wildfire in a wet Eucalyptus forest. *Journal of Hydrology*, 343(1-2), 12-28. https://doi.org/10.1016/j.jhydrol.2007.06.005

Sidman, G., Guertin, D. P., Goodrich, D. C., Unkrich, C. L., & Burns, I. S. (2016). Risk assessment of post-wildfire hydrological response in semiarid basins: the effects of varying rainfall representations in the KINEROS2/AGWA model. *International Journal of Wildland Fire, 25*(3), 268-278. https://doi.org/10.1071/WF14071

Steiner, M., Smith, J. A., Burges, S. J., Alonso, C. V., & Darden, R. W. (1999). Effect of bias adjustment and rain gauge data quality control on radar rainfall estimation. *Water Resources Research, 35*(8), 2487-2503. https://doi.org/10.1029/1999WR900142

Storey, M. (2014). Fire Severity Mapping for the Wambelong 2013 Fire. CERMB, University of Wollongong.

Van Oost, K., Govers, G., & Desmet, P. (2000). Evaluating the effects of changes in landscape structure on soil erosion by water and tillage. *Landscape Ecology, 15*(6), 577-589. https://doi.org/10.1023/A:1008198215674

Vrieling, A., Sterk, G., & de Jong, S. M. (2010). Satellite-based estimation of rainfall erosivity for Africa. *Journal of Hydrology, 395*(3), 235-241. https://doi.org/10.1016/j.jhydrol.2010.10.035

Wischmeier, W. H., & Smith, D. D. (1958). Rainfall energy and its relationship to soil loss. *Eos, Transactions American Geophysical Union, 39*(2), 285-291. https://doi.org/10.1029/TR039i002p00285

Wischmeier, W. H., & Smith, D. D. (1978). *Predicting rainfall erosion losses-A guide to conservation planning*. https://www.cabdirect.org/cabdirect/abstract/19786726437

Wüest, M., Frei, C., Altenhoff, A., Hagen, M., Litschi, M., & Schär, C. (2010). A gridded hourly precipitation dataset for Switzerland using rain-gauge analysis and radar-based disaggregation. *International Journal of Climatology, 30*(12), 1764-1775. https://doi.org/10.1002/joc.2025

Yang, X., & Yu, B. (2014). Modelling and mapping rainfall erosivity in New South Wales. *Soil Research*. https://doi.org/10.1071/SR14188

Yang, X., Yu, B., & Xie, X. (2015). Predicting Changes of Rainfall Erosivity and Hillslope Erosion Risk Across Greater Sydney Region, Australia. *International Journal of Geospatial and Environmental Research, 2*(1), 2. https://dc.uwm.edu/ijger/vol2/iss1/2

Yang, X., Zhu, Q., Tulan, M., McInnes-Clarke, S., Sun, L. & Zhang, X.P. (2018). Near real-time monitoring of post-fire hillslope erosion in a burnt national park after

storm events. *International Journal of Wildland Fire.* https://doi.org/10.1071/WF18011 (Online early)

Yin, S.-q., Xie, Y., Liu, B., & Nearing, M. (2015). Rainfall erosivity estimation based on rainfall data collected over a range of temporal resolutions. *Hydrology and Earth System Sciences, 19*(10), 4113. https://doi.org/10.5194/hess-19-4113-2015

Yu, B. (1999). A comparison of the R-factor in the Universal Soil Loss Equation and revised universal soil loss equation. *Transactions of the ASAE*, 42(6), 1615. https://doi.org/10.13031/2013.133

Chapter 3*: Modelling and monitoring post-fire erosion across Warrumbungle National Park

* This chapter has been published in International Journal of Wildland Fire, 2018.

Abstract

Wildfires in national parks can lead to severe damage to property and infrastructure, and adverse impacts on the environment. This is especially pronounced if wildfires are followed by intense storms, such as the fire in Warrumbungle National Park in New South Wales, Australia, in early 2013. The aims of this study were to develop and validate a methodology to predict erosion risk at near real-time after storm events, and to provide timely information for monitoring of the extent, magnitude and impact of hillslope erosion to assist park management. I integrated weather radar-based estimates of rainfall erosivity with the revised universal soil loss equation (RUSLE) and remote sensing to predict soil loss from individual storm events after the fire. Other RUSLE factors were estimated from high resolution digital elevation models (LS factor), satellite data (C factor) and recent digital soil maps (K factor). The accuracy was assessed against field measurements at twelve soil plots across the Park and regular field survey during the 5-year period after the fire (2013–17). Automated scripts in a geographical information system have been developed to process large quantity spatial data and produce time-series erosion risk maps which show spatial and temporal changes in hillslope erosion and groundcover across the Park at near real time.

Keywords: weather radar, remote sensing, rainfall erosivity, soil loss, geographic information system.

Yang, X., Zhu, Q., Tulau, M., McInnes-Clarke, S., Sun, L. & Zhang, X. 2018. Near real-time monitoring of post-fire erosion after storm events: a case study in Warrumbungle National Park, Australia. *International Journal of Wildland Fire*, 27(6), 413-424.

Chapter 4*: Extreme rainfall indices and its impact on rainfall erosivity under climate change

* This chapter has been peer reviewed and published as a technical report from the New South Wales Government Office of Environment and Heritage (in press).
http://climatechange.environment.nsw.gov.au/Impacts-of-climate-change/Soil/Soil-Erosion

Abstract

The Australian Alpine region is highly vulnerable to extreme climate events such as storms, these events effect rainfall erosivity and accelerate the degradation of land in the region. In this study, six extreme rainfall indices were selected to examine the relationship between extreme rainfall indices and rainfall erosivity across the NSW and ACT Alpine region. Rainfall erosivity was esetimated based on the daily erosivity model. Time series (monthly and annual) rainfall extremes for the study area for all the 60 years periods have been produced and spatially interpolated to a high spatial resolution of 100 m in geographic information system (GIS) using a spline interpolation method. Statistical tests were used to quantify the spatial and temporal changes of rainfall extremes and the impacts on rainfall erosivity based on the study area and its sub-regions. The time series maps for the 60-year periods were used to identify the high erosivity risk areas and more vulnerable seasons across the study area. The study demonstrates that extreme rainfall indices (e.g. Rx5day) were potentially applied as an approximation to estimate rainfall erosivity. The ERI-projected rainfall erosivity was possibly regarded as an alternative value for erosivity and erosion management, especially to where without radar or field rainfall data. To assess the model accuracy, ERI-projected rainfall erosivity was then compared with the results from previous studies and the rainfall erosivity calculated from the Bureau of Meteorology (BoM) gridded rainfall ($R^2 > 0.75$, $E_c > 0.74$). Automated GIS scripts have been developed to calculate the time-series rainfall erosivity so that the processes of large quantity NARCliM data are realistic, repeatable and portable.

Additional keywords: extreme rainfall indices, climate change, rainfall erosivity, remote sensing, GIS.

Highlights

- Six extreme rainfall indices are considered in the climate change impact on rainfall erosivity.
- There exists a good relationship between rainfall extreme indices (e.g. Rx5day) and rainfall erosivity.
- High-risk areas and seasons of rainfall erosivity are identified in summer in southeast tablelands.
- Methodology and automated scripts are applicable to other areas.

4.1 Introduction

Globally climate has become more extreme and variable (Solomon et al., 2007), based on the assessment of the Intergovernmental Panel on Climate Change (IPCC). Karl et al. (1999) reported that climate change generally leads to an increase in the frequency and intensity of climate extreme events such as floods, heatwaves, droughts and storms. Such climate extreme events, are rare and have a high impact on the environment, ecosystem and society (Haylock and Nicholls, 2000). Soil erosion is also potentially affected by the land use change and management which is designed to accommodate new climate regimes caused by global climate change (Zhang et al., 2005).

Tools for monitoring changes in extremes have been developed primarily through the use of indices (Frich et al., 2002). These indicators are useful as they are usually meaningfully across many different climates and perform consistent analysis across countries, regions and continents. Climate indices are more likely to be exchanged amongst scientific researchers than daily datasets, as they are able to be compared with the output from climate models.

The temperature indices describe cold and warm extremes (Karl et al., 1999), while rainfall indices describe wet extremes only (Klein Tank and Können, 2003). Rainfall extreme indices (ERIs) are applied to determine the magnitude of extreme rainfall over a certain period in the extent under climate change.

The trends in indices of temperature and precipitation extremes have been discussed in Europe (Klein Tank and Können, 2003), Australia (Fu et al., 2010, Gallant and Karoly, 2010, Gallant et al., 2014), and across the world (Donat et al., 2013). These results

demonstrated an increase in the extent of hot and wet extremes seasonally and annually in Australia (Gallant and Karoly, 2010).

Sauerborn et al. (1999) suggested that more frequent intensive rainfalls might be accompanied by a clustering of dry periods, which represents a dangerous combination with regard to water erosion. Due to the increased surface runoff, the soil particles can be easily carried away. However, rainfall erosivity is the most important parameter that has the direct effect of climate change on water erosion (Nearing et al., 2004). More importantly, hillslope erosion occurs mostly during a few severe storm or extreme events. Trends and changes in erosive storms or rainfall extremes are therefore much more important but also difficult to detect in comparison with rainfall totals.

Several studies have discussed the climate change impact on soil erosion through rainfall erosivity in the USA (Nearing, 2001, Biasutti and Seager, 2015), Japan (Shiono et al., 2013), China (Zhang et al., 2010), South Korean (Lee et al., 2018), Australia (Yang et al., 2015) and all over the world (Panagos et al., 2017).

A recent study by Lee et al. (2018) revealed the climatic teleconnection between the large scale climate indices and mid-latitude hydrologic variables. Zhang et al. (2005) examined the change of annual precipitation and long-term annual mean rainfall erosivity, which implied more serious soil erosion risk in the future. Yang et al. (2015) found that the hillslope erosion risk is likely to increase 10-60% in the Great Sydney Region (GSR) under climate change, and the the percent changes in rainfall erosivity were greater than percent change in total precipitation. Panagos et al. (2017) reported the distribution of rainfall erosivity in the future from climatic variables across the world.

Australian rainfall is dominated by high interannual variability (Nicholls et al., 1997), some of which can be associated with air-sea interactions such as the El Niño-Southern

Oscillation (Nicholls and Kariko, 1993). High interannual variability of precipitation was believed to increase the potential risk of soil erosion and accelerate land degradation through the high variation of rainfall erosivity (Yang et al., 2003). Many previous studies have discussed the changes in rainfall amount and the impacts on rainfall erosivity and hillslope erosion; however, the magnitude of the impact is not well quantified between rainfall amount, rainfall intensity, extreme rainfall events and rainfall erosivity. The high resolution R-factor maps, in both spatial and temporal contexts, can provide detailed information for climate (rainfall) impact assessment. It is easier to achieve the environmental and ecosystem management targets if the mean and changes of rainfall erosivity risk are well understood with assistance of more accurate maps at a range of temporal and spatial scales.

In this study, I examined the climate change impact on rainfall erosivity through extreme rainfall indices across the study area. The relationships between extreme rainfall indices and rainfall erosivity were identified, and further used as an approximation to estimate rainfall erosivity. The ERI-projected rainfall erosivity was possibly regarded as an alternative value for erosivity and erosion management, especially to where without radar or field rainfall data. The ERI-projected rainfall erosivity was then compared with the results from previous studies (Yang and Yu, 2015; Yang et al., 2016) and the rainfall erosivity calculated from the Bureau of Meteorology (BoM) gridded rainfall.

This chapter mainly aims: i) to identify the trends of rainfall extreme events ; ii) to model the changes of ERIs and the relationships with rainfall erosivity based on the NARCliM projections; and iii) to estimate the areas and seasons with high rainfall erosivity risk across the study area.

4.2 Study area and datasets

4.2.1 Study area

The study area extends across the South East and Tablelands (SET), Australia Capital Territory (ACT) and Murray/Murrumbidgee (MM) catchments, bordering the Victorian border in the south and covering an area of more than 171,000 km^2. The study area of this chapter covers NSW and ACT Alpine region (Figure. 4-1), which includes the highest peak in Australia (Mount Kosciuszko, 2,228 m).

SET is located in the south-east corner of NSW, which includes the coastal, alpine and tableland, and slope landscapes of the nurture unique biodiversity hotspot. MM is the home to a diverse range of wetland ecosystems, plants and animal life. This region includes the largest stand of River Red Gum in the world and a 1700 km stretch of Australia's longest river - The Murray (OEH, 2018). The area falls completely within the temperate climatic zone (BoM, 2016) and has a mean annual temperature of -0.4 °C to 21.1 °C, and an average rainfall span of 313 to 1,828 mm.

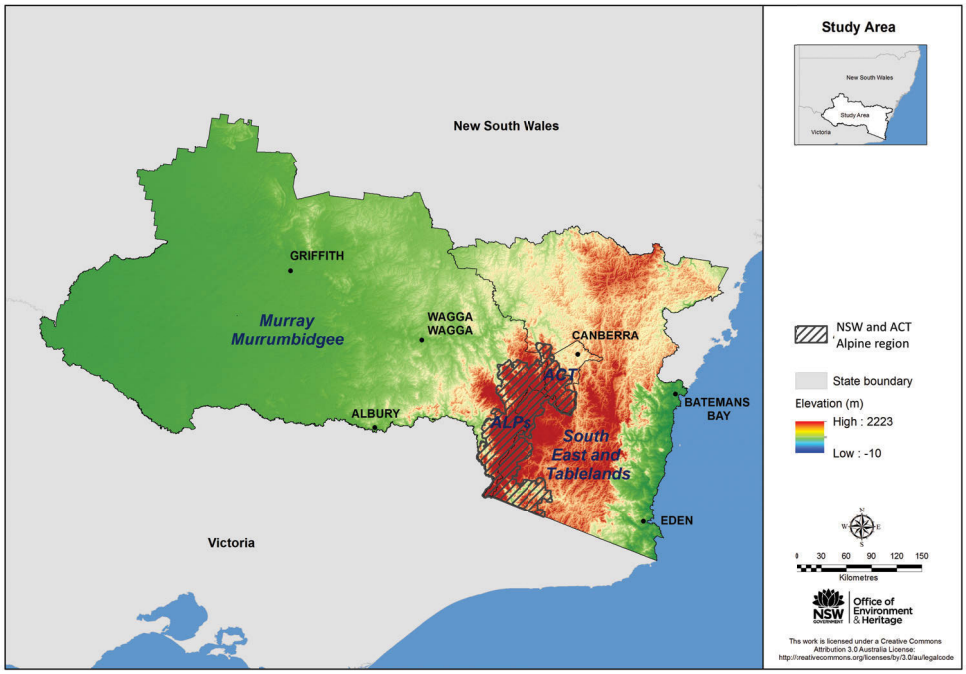

Figure 4-1 Study area

4.2.2 Datasets

The data used in the study are derived from the NARCliM project (Evans *et. al*. 2014a). In NARCliM, simulations from four selected GCMs were used to drive three selected regional climate models (RCMs) to form a 12-member GCM/RCM ensemble. The four GCMs are MIROC3.2, ECHAM5, CCCMA3.1, and CSIRO-MK3.0 from the CMIP3 ensemble, which were selected based on model performance over Australia, independence of errors, and to span the full range of potential future climates over south-eastern Australia (Evans et al., 2014b). The three RCMs correspond to three different physics scheme combinations of the Weather Research Forecasting (WRF) V3.3 model (Skamarock et al., 2008), which were also chosen for adequate skill and error independence, following a comprehensive analysis of 36 different combinations of physics parametrizations over eight significant East Coast Lows (Evans et al., 2014a; Ji et al., 2014). Each RCM-GCM pair has

been run for three 20-year periods: 1990-2009 (baseline), 2020-2039 (near future), and 2060-2079 (far future). Evaluation of NARCliM simulations suggests that the use of the full ensemble provides a measure of robustness such that any result that is common through all models in the ensemble is considered to have higher confidence (Evans et al., 2016).

This study used the bias-corrected rainfall and six extreme rainfall indices for the 60 years with a spatial resolution of 10 km (Bormann et al. 2014; Evans et al., 2016) from NARCliM to estimate the future rainfall erosivity in the NSW and ACT Alpine region. To minimize bias, I used all 12 model ensembles from NARCliM following the recommendation of Evans et al. (2016).

4.3 Methods

4.3.1 Extreme Rainfall Indices (ERIs)

Six extreme rainfall indices (ERIs, Table 4-1) were selected to compare and assess their relationships with rainfall erosivity for each NARCliM ensemble and period (Evans et al., 2014b). These ERIs represent annual accumulated precipitation (e.g. R95p and R99p), count days with extreme rainfall depth (e.g. R20mm and Rnnmm), and illustrate monthly rainfall variation (e.g. Rx1day and Rx5day). The reason to choose these six indices was because they are common and representative in time steps. Note that only Rx1day and Rx5day are defined on monthly basis, whilst all the other indices are defined on an annual basis. Therefore, only Rx1day and Rx5day were applied to examine the seasonal rainfall extremes and their relationships with the seasonal rainfall erosivity and erosion rates.

Table 4-1 The selected six extreme rainfall indices and their definitions.

Abbreviation	Description	Unit
R20mm	Annual counts of days with rainfall larger than 20mm. Count the days where: RR_{ij} ≥20 mm	days
Rnnmm	Days with rainfall larger than 25mm (annual). Count the days where: RR_{ij} ≥25 mm.	days
Rx1day (monthly and annual)	Daily maximum 1-day precipitation. $Rx1day_j = \max(RR_{ij})$	mm
Rx5day (monthly and annually)	Maximum 5-day accumulated precipitation (annual and month). Let RR_{kj} be the precipitation amount for the 5-day interval ending $_k$, period j. $Rx5day_j = \max(RR_{kj})$.	mm
R95p	Accumulated precipitation from events above the 95th percentile. Let RR_{wj} be the daily precipitation amount on a wet day w (RR ≥ 1.0mm) in period i and let $RR_{wn}95$ be the 95th percentile of precipitation on wet days in the period. If W represents the number of wet days in the period, then $R95p_j = \sum_{w=1}^{W} RR_{wj}$ where $RR_{wj} > RR_{wn}95$	mm
R99p	Accumulated precipitation from events above the 99th percentile. Let RR_{wj} be the daily precipitation amount on a wet day w (RR ≥ 1.0mm) in period i and let $RR_{wn}99$ be the 99th percentile of precipitation on wet days in the period. If W represents the number of wet days in the period, then $R99p_j = \sum_{w=1}^{W} RR_{wj}$ where $RR_{wj} > RR_{wn}99$	mm

The calculation dimensions for this study is demonstrated as below,

$$Dimensions = 6\ ERIs \times 4\ GCMs \times 3\ RCMs \times 3\ periods \times 4\ seasons \quad (4\text{-}1)$$

where contains 12 ensembles from NARCliM, three time periods for four seasons and six extreme rainfall indices.

The calculation of rainfall erosivity was developed by Yang and Yu (2014) on a daily basis with significant improvements on parameters. More information about the parameter and model is presented in Yang et al. (2016) and also into Chapter 5.

4.3.2 Model accuracy assessment

Adequate random points were generated in GIS and used to sample raster data values from ERIs and rainfall erosivity for the baseline and future periods. These randomly sampled data were used for statistical analyses and analysis of the relationship between

rainfall extremes and erosivity for all the periods. The randomly sampled ERI-projected erosivity values in the baseline period were used for comparison with results from the BoM gridded rainfall data at 5 km spatial resolution in the same period (Yang and Yu, 2016).

Model performance is measured by the coefficient of efficiency, E_c (Nash and Sutcliffe, 1970) as it is commonly used to assess model performance in hydrology and soil sciences (Yang, 2015).

$$E_c = 1 - \sum_{i=1}^{M}(y_i - \hat{y})^2 / \sum_{i=1}^{M}(y_i - \bar{y})^2 \quad (4\text{-}2)$$

where y_i are observed values while $\hat{y}$ are modelled values; $\bar{y}$ is the average of observed values, and M represented the sample size. Essentially, E_c is an indicator of how close the scatters of projected versus actual values are to the 1:1 line (Nash and Sutcliffe, 1970).

4.4 Results and Discussion

4.4.1 Extreme rainfall indices and their change in the future

This chapter presents the changes of extreme rainfall events and over the 60 years. Note that Rx1day and Rx5day are defined on a monthly basis, while all the other indices are defined on an annual basis. Thus, the seasonal variations and comparisons will be analysed by using Rx1day and Rx5day, while all other indices are applied for annual assessment.

Annual counts of days with rainfall larger than 20mm (R20) were compared from present (1990-2009), near future (2020-2039) and far future (2060-2079). The change of R20 in near future is estimated to increase by approximately 5% in most of the MM area, while both ACT and SET areas are decreasing (Figure. 4-2). The condition in the far future is predicted to be more severe, as most of the study area have more days with rainfall

greater than 20 mm, except the Snowy Mountain and Batemans Bay. Murrumbidgee Valley and Murrumbidgee River are projected to have a significant increase in extreme rainfall (> 20 mm d^{-1}) occurrence in the far futures (> +60% change in annual).

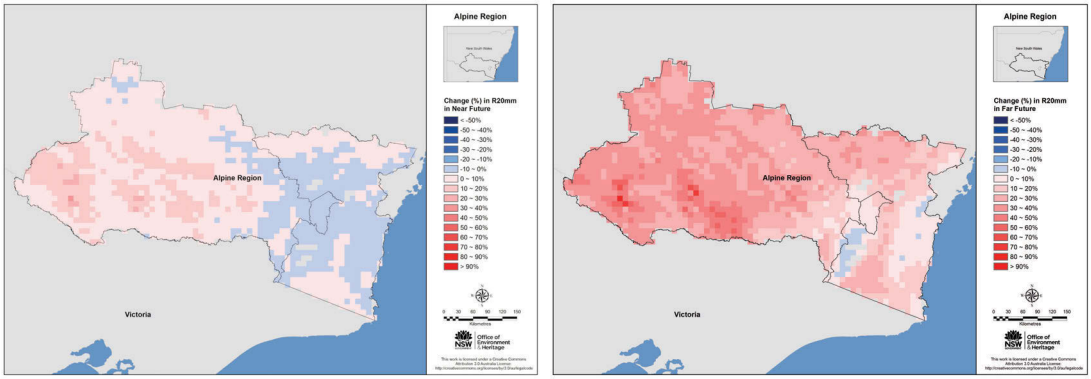

Figure 4-2 Average annual change (%) of R20 compared for near future (2020-2039) and far future (2060-2079).

Rnnmm refers to the days with rainfall over 25 mm in one year. Similar to R20 (Figure. 4-2), the days with rainfall larger than 25 mm during 2020-2039 is predicted to be more than that from present period (1990-2009) for around 85% of the area within MM (Figure. 4-3). However, there are fewer days that experienced rainfall (> 25 mm d^{-1}) for almost all areas in SET (e.g. NSW Great Dividing Range) and across the ACT. Contrastingly, for far future (Figure. 4-3), it is estimated the generally increases across the study area except Kosciuszko National Park in SET side. The spatial variation is significant when comparing far future prediction with present observation, as there is extreme change (> +80%) in southwest of MM but slightly more extreme storm events (< +10% change) in the east coast.

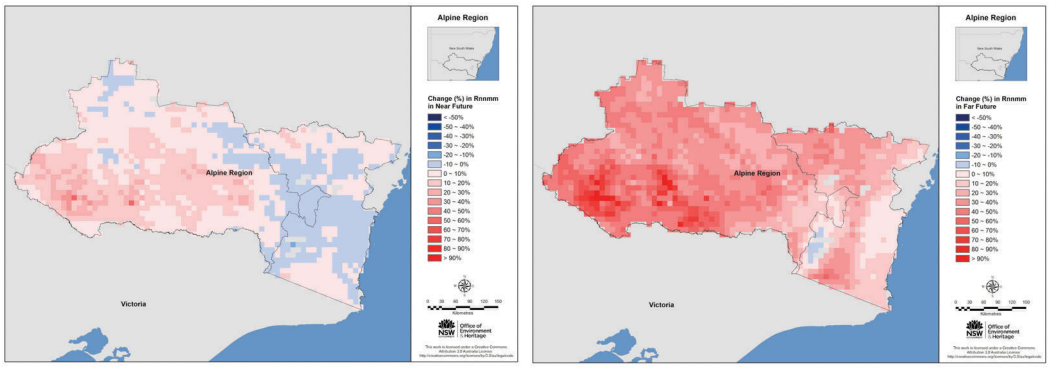

Figure 4-3 Average annual change (%) of Rnnmm compared for near future (2020-2039) and far future (2060-2079).

Rather than count the days with larger precipitation, there are some other percentile-based extreme rainfall indices (Nash and Sutcliffe, 1970) that evaluate the accumulated daily precipitation above a defined precent, such as the 95th percentile (R95) and 99th percentile (R99). These indices reflect the severity of extreme events of a year.

R95 (unit: mm) is the summing-up of the top 5% daily precipitation amount (where > 1.0 mm) on an annual basis. Figure 4-4 shows slight to moderate change of the amount of very wet days between 2020 and 2039 across the study area, with moderate increases in MM and slight decreases within most areas in ACT and SET. In the far future, R95 is projected to generally increase across MM, ACT and SET, and even as large as 50% along the west of MM, though the change could be negligible in near future.

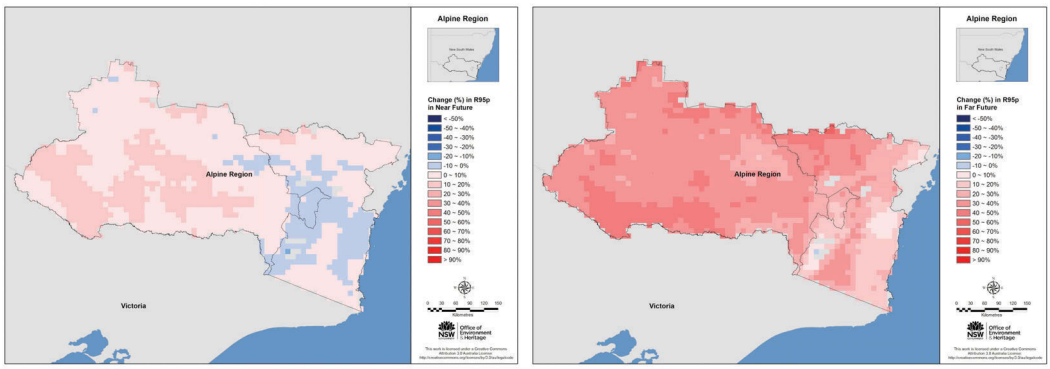

Figure 4-4 Average annual change (%) of R95 compared for near future (2020-2039) and far future (2060-2079).

Similarly, R99 (mm) is the summing-up of the top 1% daily precipitation amount (where > 1.0 mm) on an annual basis. The spatial variation is even greater when considering the top 1% of the total rainfall amount rather than the top 5%, where more than half of the study area is predicted to experience slightly more severe storm events until 2039 (Figure. 4-5). However, extreme wet days are estimated to be much wetter than historically recorded (1990-2009), especially in the tableland area (+40% ~ +50%) and southwest MM (as much as 90%) since 2060 (Figure. 4-5).

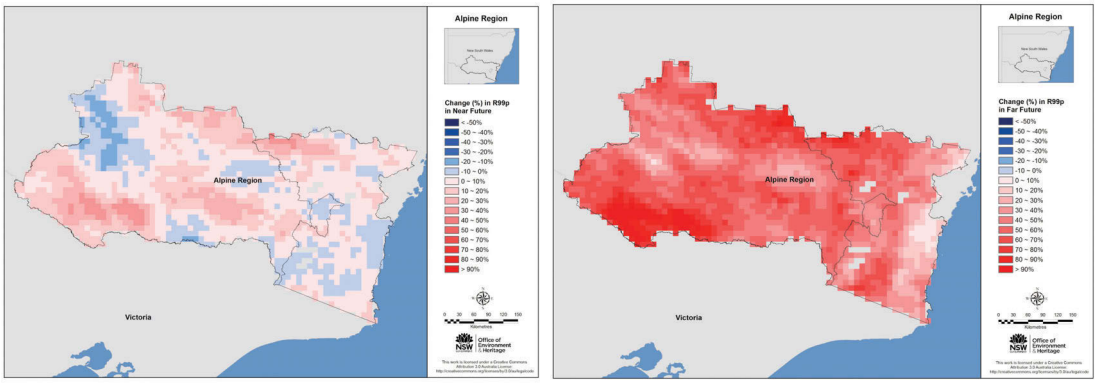

Figure 4-5 Average annual change (%) of R99 compared for near future (2020-2039) and far future (2060-2079).

Rx1day represents the average seasonal and annual daily maximum precipitation. Only Rx1day and Rx5day indices are defined on a monthly basis, which is accessible for the seasonal changes assessment. The annual average change of daily maximum rainfall in the near future is very slight (< ±10%) across MM, ACT and SET, although the Kosciuszko National Park is predicted to be less than before (Figure. 4-6). Furthermore, the trend is generally increasing across the west flat region, Snowy Mountain and southeast tablelands areas, with less than 20% change of annual average Rx1day (Figure. 4-6).

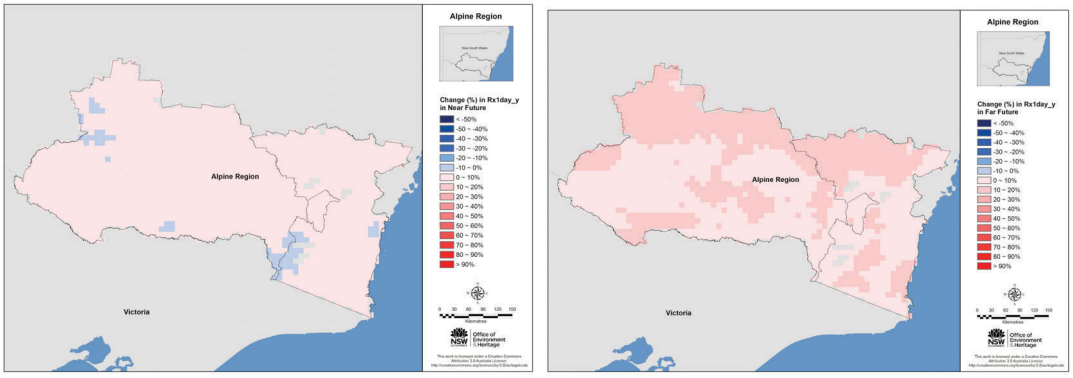

Figure 4-6 Average annual change (%) of Rx1day compared for near future (2020-2039) and far future (2060-2079).

Rx5day represents the average monthly and annual maximum consecutive 5-day precipitation (Evans et al., 2014a). The climate indices that represent extremes of rainfall and rainfall intensity (e.g. Rx1day and Rx5day) (Peterson et al., 2001) are able to examine the seasonal variation from monthly intervals. Rx5day is summing up the consecutive 5-day precipitation that avoid the separation of the extreme storm events (e.g. Rx1day) and undermine the accumulate precipitation and intensity. The average annual change of Rx5day is slight to moderate (−10% ~ +12%) across the study area from 2020 to 2039 (Figure. 4-7), then it is predicted to keep increasing (−5% ~ +25%) in the far future period (Figure. 4-7).

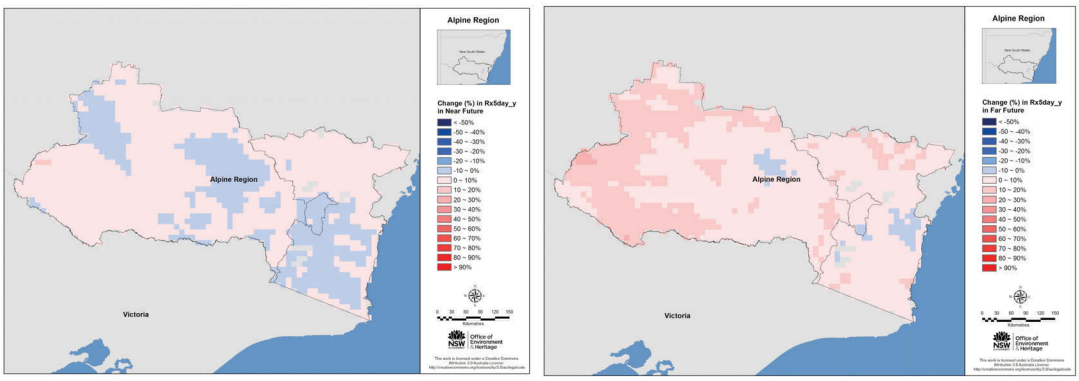

Figure 4-7 Average annual change (%) of Rx5day compared for near future (2020-2039) and far future (2060-2079) periods.

Seasonal changes in the near future is predicted to increase in summer and autumn, while decrease in almost all areas in MM, ACT and SET in winter (−40% ~ +5%) and spring (−20% ~ +5%) (Figure. 4-8). Much larger storm events are predicted in summer than in autumn (−5% ~ +30%), increasing from +0% to +40% from southwest to northeast (east) compared to the baseline. Climate is projected to be drier in winter especially in the south tablelands area (−40% ~ −30%) due to the predicted decreases in rainfall in winter (Araújo and Brito, 2011). The far future has more changes than the near future (Figure. 4-9); where changes are generally increasing for all seasons, with summer and autumn estimated to be wetter (up to 50%), while winter in south tablelands and Kosciuszko National Park in spring is predicted to be drier (up to 25%).

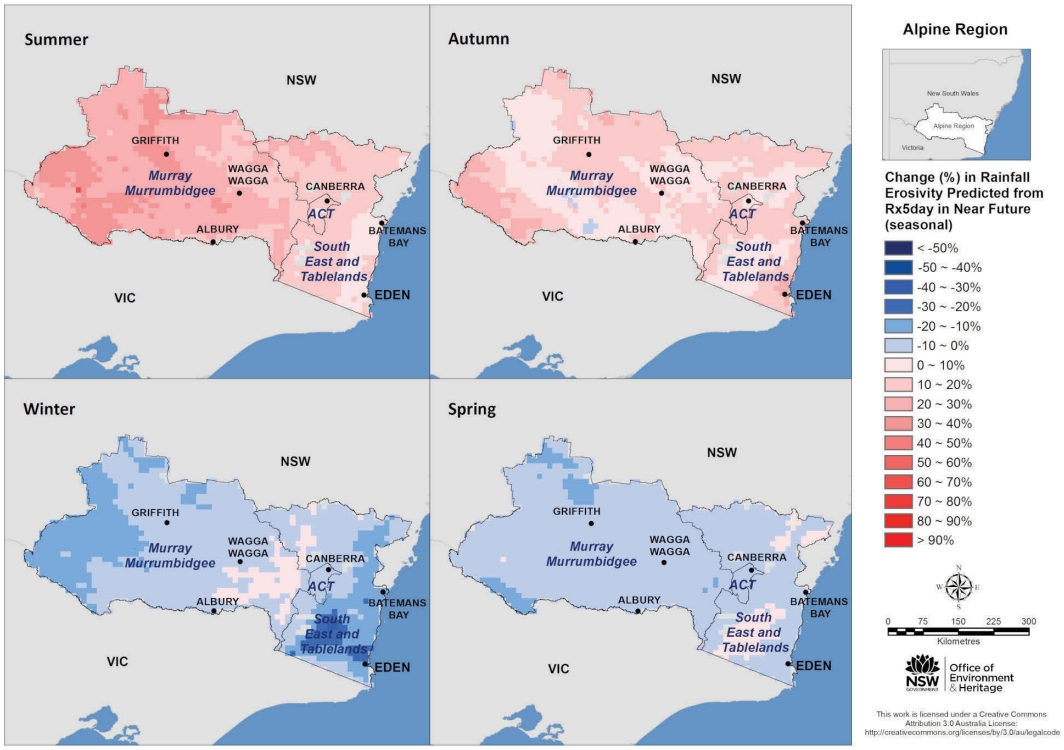

Figure 4-8 Average seasonal change (%) of Rx5day compared near future (2020-2039) to baseline (1990-2009).

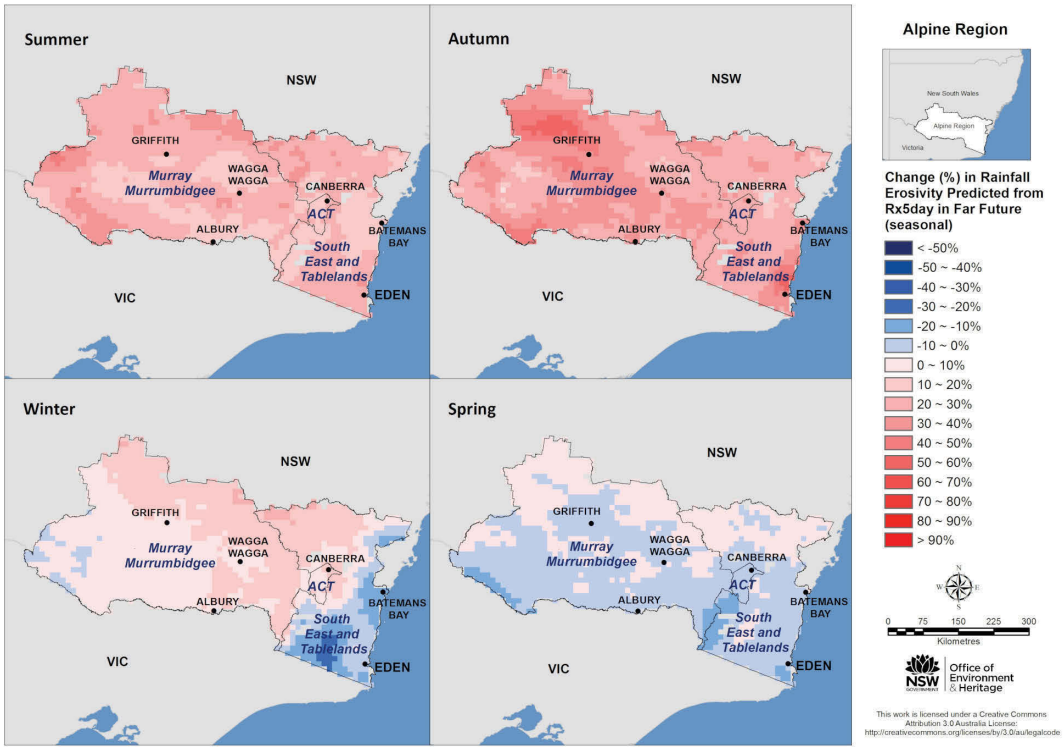

Figure 4-9 Average seasonal change (%) of Rx5day compared far future (2060-2079) to baseline (1990-2009).

The selected six extreme rainfall indices were overall dominated by increasing trends in far future, though less changes in NSW and ACT Alpine region (Kosciuszko National Park) are predicted owing to the projected drier and warmer weather from NARCliM. Rx5day and Rx1day are the only two indices that are capable of showing seasonal variability.

4.4.2 Extreme rainfall indices and their impact on rainfall erosivity

The ERI maps have been prepared for each period for the study area. The relationships between ERIs and rainfall erosivity were assessed and compared using the 5,000 sampling random points within the region generated in ArcGIS.

The relationship between the ERIs and the corresponding rainfall erosivity for each time slice is shown in Figure 4-10. Six ERIs at annual step were compared to examine their correlation with rainfall erosivity (Figure. 4-10a). Rx5day (annual step) is the most effective index that has a stronger correlation with rainfall erosivity for baseline (R^2=0.841), near future (R^2=0.842) and far future (R^2=0.827) periods.

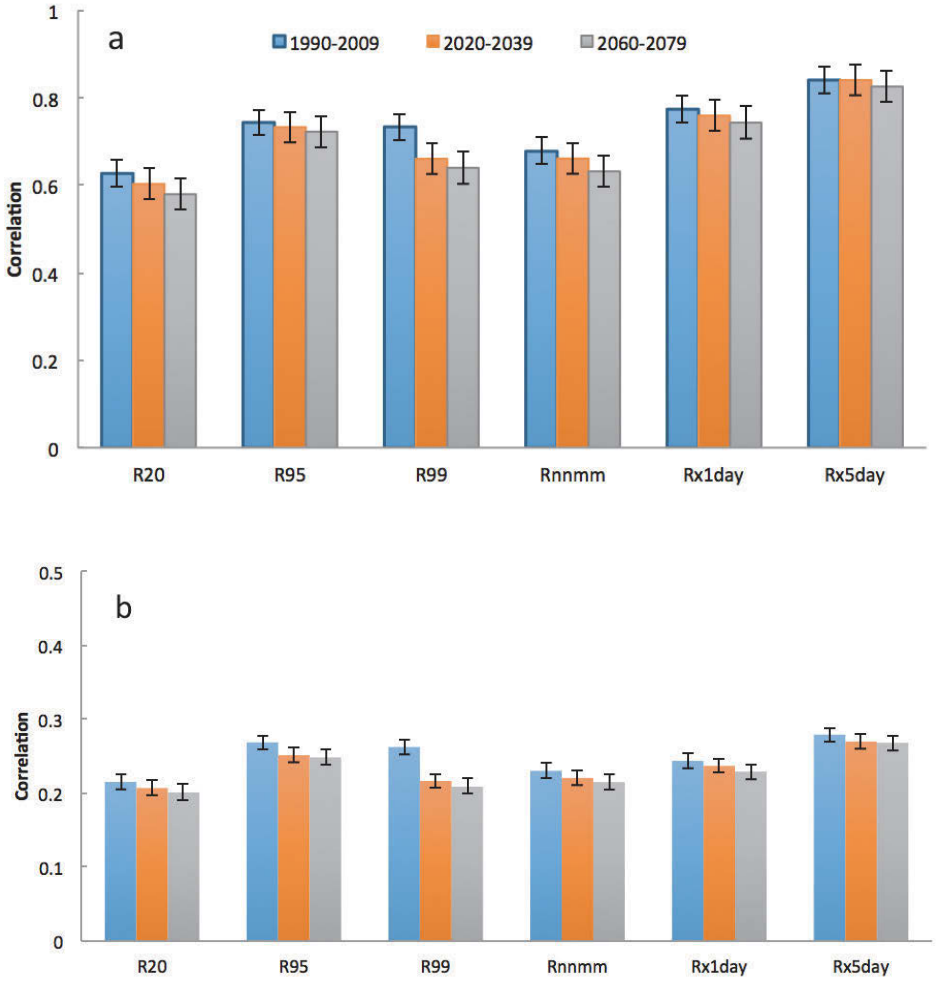

Figure 4-10 The correlation coefficients between different extreme rainfall indices and rainfall erosivity (a) and erosion (b).

As shown in Figure 4-10 (b), the relationships of the corresponding ERIs with hillslope erosion is however much less compared with that of rainfall erosivity (Figure. 4-10a) since hillslope erosion is related to more factors such as groundcover, soil property, slope

steepness and length, but rainfall erosivity is mainly related to rainfall duration and intensity.

The seasonal variations of ERIs (Rx1day, Rx5day) and their relationships with rainfall erosivity are compared in Table 2, It appears that both indices have a higher correlation with rainfall erosivity in summer compared with other seasons. Such a relationship might be due to the greater rainfall amount and higher intensity in summer.

Table 4-2 Comparison between Rx1day and Rx5day and their seasonal correlation with rainfall erosivity.

Correlation	Baseline (1990-2009)		Near Future (2020-2039)		Far Future (2060-2079)	
	Rx1day	Rx5day	Rx1day	Rx5day	Rx1day	Rx5day
Summer	0.790	0.819	0.779	0.798	0.789	0.803
Autumn	0.725	0.766	0.701	0.750	0.672	0.715
Winter	0.790	0.802	0.783	0.801	0.758	0.778
Spring	0.793	0.794	0.778	0.767	0.757	0.764

*Summer (December, January and February), autumn (March, April and May), winter (June, July and August) and spring (September, October and November).

As illustrated above (Table 2), Rx5day has a slightly higher seasonal correlation with erosivity (therefore erosion) than Rx1day in all periods. On an annual basis, the correlation between the mean annual erosivity (from all 12 ensembles) and Rx5day is event stronger (R^2 = 0.813) and higher than any other ERIs. Thus, Rx5day was selected to predict the erosivity and seasonal variation in this study.

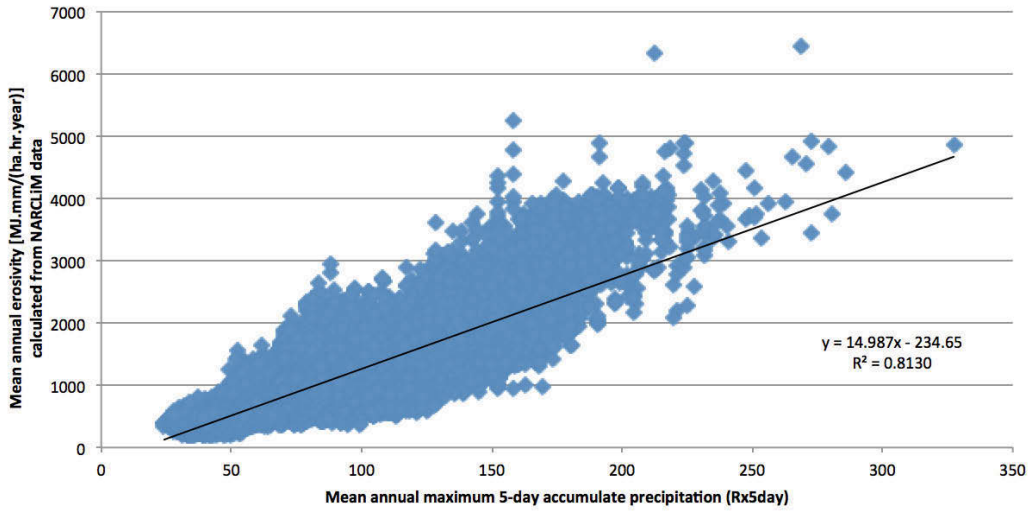

Figure 4-11 The relationship between mean annual erosivity and Rx5day index.

4.4.3 The Rx5day predicted erosivity

The same 5000 sampling points within the study area were used to compare the relationship between Rx5day and seasonal rainfall erosivity. Table 4-3 presents the seasonal relationships between Rx5day and rainfall erosivity from a previous study (Yang et al., 2016).

Table 4-3 The seasonal relationship between Rx5day and rainfall erosivity.

Period	Baseline (1990-2009)		Near Future (2020-2039)		Far Future (2060-2079)	
Regression	slope coefficient	intercept	slope coefficient	intercept	slope coefficient	intercept
Summer	1.684	-50.56	1.732	-52.15	1.860	-58.9
Autumn	1.211	-29.02	1.285	-37.01	1.397	-42.48
Winter	0.586	-9.67	0.588	-10.26	0.627	-11.18
Spring	0.915	-13.81	0.889	-11.13	0.917	-12.5

Based on these relationships, there is greater erosivity in summer than any other seasons across the MM, SET and ACT regions, while winter has the least erosivity in all the three periods (Figure. 4-12). It is predicted that the rainfall erosivity will increase gradually in all seasons from baseline to near future and far future. There is relatively high rainfall erosivity in SET and ACT in all seasons except winter. But in winter most areas across the study area have erosivity less than 100 MJ mm ha^{-1} hr^{-1} $month^{-1}$.

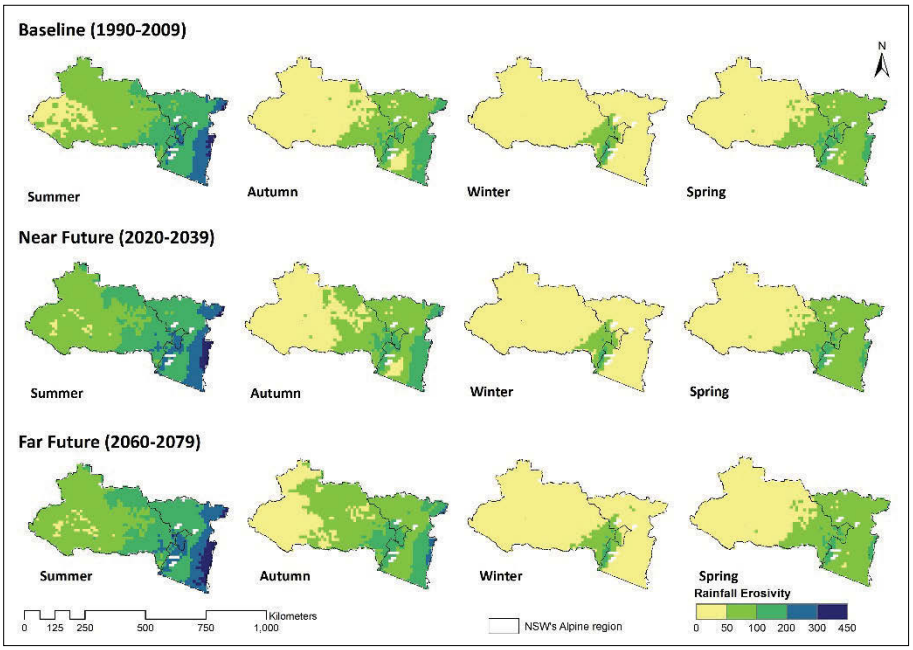

Figure 4-12 Monthly rainfall erosivity (MJ mm ha^{-1} hr^{-1} $month^{-1}$) predicted using Rx5day in baseline (1990-2009), near future (2020-2039) and far future (2060-2079).

The mean annual and seasonal rainfall erosivity from the Rx5day prediction were compared with those estimated from the NARCliM baseline period (1990-2009) and BoM gridded daily rainfall data (5 km) for a 30-year climate normal period (1976-2005). As shown in Table 4-4, there is a strong positive correlation between Rx5day predicted rainfall erosivity and those calculated from NARCliM and BoM data in both annual and seasonal steps. The prediction in summer (DJF) is likely to be more reliable than any other seasons

due to its higher correlation and coefficient of efficiency. In contrast, the winter (JJA) prediction is relatively less accurate (R^2 and E_c both less than 0.4) especially compared to BoM rainfall based erosivity. Meanwhile, there is moderate positive regression relationship from Rx5day predicted erosivity and BoM-based rainfall erosivity in spring (R^2 around 0.7), which is slightly less than those from summer and autumn. One likely reason for the weak correlation in winter/spring might be due to that the previous daily erosivity model did not consider the snow cover in winter and snowmelt runoff in spring (to be presented in Chapter 5). The result illustrated that the variability of rainfall erosivity is more sensitive to variability of rainfall intensity than the variability of precipitation amount.

Table 4-4 Correlation between rainfall erosivity predicted by Rx5day and those calculated from NARCliM and BoM rainfall data (n=4848).

Rainfall Erosivity	NARCliM (1990-2009)			BoM (1990-2009)			BoM (1976-2005)		
	R^2	RMSE	E_c	R^2	RMSE	E_c	R^2	RMSE	E_c
ANN	0.788	61.453	0.786	0.752	66.965	0.739	0.759	65.553	0.748
DJF	0.823	29.036	0.820	0.721	33.074	0.848	0.726	32.893	0.848
MAM	0.763	16.050	0.763	0.715	19.238	0.769	0.721	19.297	0.763
JJA	0.777	8.669	0.776	0.332	30.397	0.365	0.335	29.991	0.370
SON	0.795	11.641	0.794	0.701	17.386	0.872	0.709	16.948	0.877

*ANN is the mean annual rainfall erosivity.

4.5 Conclusions

Understanding rainfall variability, shifts and trends is of primary importance when considering the potential for biophysical, social and economic impacts (Gallant et al., 2007). Extreme rainfall has a significant impact on erosivity and erosion.

In this study, the relationship between extreme rainfall indices and rainfall erosivity across the Alpine region was examined. Time series (monthly and annual) rainfall extremes and erosion risk for the study area for all 60 year periods have been produced and spatially

interpolated 100 m by using a spline interpolation method. The spatial and temporal changes (%) of rainfall extremes and the impacts on rainfall erosivity have been quantified based on the study area and its sub-regions.

The study demonstrates that extreme rainfall indices (e.g. Rx5day) can be used to predict high-risk areas and periods of rainfall erosivity, especially to where there is no radar or field rainfall data. The results showed that the magnitude of rainfall erosivity increased significantly due to climate change or rainfall extremes which agrees to recent studies by Lee et al. (2018).

Acknowledgement

This research was funded through NSW Office of Environment and Heritage (OEH) Climate Change Fund and managed by OEH Climate & Atmospheric Science (CAS). Dr Kathleen Beyer, Larissa Brisbane and Anthony Coward from CAS supported and managed this project. OEH provided a scholarship of $30,000 to support the student at UTS in the conduct of this research project. I thank the Climate Change Research Centre of the University of New South Wales, particularly Professor Jason Evans and Dr Alejandro Di Luca, for providing the NARCliM rainfall and snow projections. I also thank Dr. Thomas Chubb from the Snowy Hydro Ltd for providing the field measurements of snow depth and water content.

4.6 Reference

Araújo, W. D. S. & Brito, J. I. B. D. 2011. Indices of trends of climatic changes for the states of the Bahia and Sergipe by means of daily precipitacion indices and its relation with SST'S of the Pacific and Atlantic. *Revista Brasileira de Meteorologia,* 26**,** 541-554.

Biasutti, M. & Seagher, R. 2015. Projected changes in US rainfall erosivity. *Hydrology and Earth System Sciences,* 19**,** 2945.

BoM (2006), Gridded Koppen classification, *Australian Bureau of Meteorology*, accessed June 2018, http://www.bom.gov.au/climate/averages/climatology/gridded-data-info/metadata/md_koppen_classification.shtml

Donat, M., Alexander, L., Yang, H., Durre, I., Vose, R., Dunn, R., Willett, K., Aguilar, E., Brunet, M. & Caesar, J. 2013. Updated analyses of temperature and precipitation extreme indices since the beginning of the twentieth century: The HadEX2 dataset. *Journal of Geophysical Research: Atmospheres,* 118**,** 2098-2118.

Evans, J., Argueso, D., Olson, R. & Di Luca, A. 2014a. NARCliM extreme precipitation indices report. NARCliM Technical Note 6. Sydney, Australia: Report to the NSW Office of Environment and Heritage.

Evans, J., Ji, F., Lee, C., Smith, P., Argüeso, D., & Fita, L. 2014b. Design of a regional climate modelling projection ensemble experiment–NARCliM. *Geoscientific Model Development, 7*(2), 621-629.

Evans, J., Argueso, D., Olson, R., & Di Luca, A. 2016. Bias-corrected regional climate projections of extreme rainfall in south-east Australia. *Theoretical and Applied Climatology*, 1-14.

Frich, P., Alexander, L. V., Della-Marta, P., Gleason, B., Haylock, M., Tank, A. K. & Peterson, T. 2002. Observed coherent changes in climatic extremes during the second half of the twentieth century. *Climate research,* 19**,** 193-212.

Fu, G., Viney, N. R., Charles, S. P., & Liu, J. 2010. Long-term temporal variation of extreme rainfall events in Australia: 1910–2006. *Journal of Hydrometeorology*, 11(4), 950-965.

Gallant, A. J., Hennesy, K. J. & RISBEY, J. 2007. Trends in rainfall indices for six Australian regions: 1910-2005. *Australian Meteorological Magazine,* 56**,** 223-241.

Gallant, A. J. & Karoly, D. J. 2010. A combined climate extremes index for the Australian region. *Journal of Climate,* 23**,** 6153-6165.

Gallant, A. J., Karoly, D. J. & Gleason, K. L. 2014. Consistent trends in a modified climate extremes index in the United States, Europe, and Australia. *Journal of Climate,* 27**,** 1379-1394.

Haylock, M. & Nicholls, N. 2000. Trends in extreme rainfall indices for an updated high quality data set for Australia, 1910-1998. *International Journal of Climatology,* 20**,** 1533-1541.

Jones, P., Horton, E., Folland, C., Hulme, M., Parker, D. & Basnett, T. 1999. The use of indices to identify changes in climatic extremes. *Climatic Change,* 42**,** 131-149.

Karl, T. R., Nicholls, N. & Ghazi, A. 1999. Clivar/GCOS/WMO workshop on indices and indicators for climate extremes workshop summary. *Weather and Climate Extremes.* Springer.

Klein Tank, A. & Können, G. 2003. Trends in indices of daily temperature and precipitation extremes in Europe, 1946–99. *Journal of climate,* 16**,** 3665-3680.
Lee, J. H., Lee, J.-H. & Julien, P. Y. 2018. Global climate teleconnection with rainfall erosivity in South Korea. *CATENA,* 167**,** 28-43.
Nash, J. E. & Sutcliffe, J. V. 1970. River flow forecasting through conceptual models part I—A discussion of principles. *Journal of hydrology,* 10**,** 282-290.
Nearing, M. 2001. Potential changes in rainfall erosivity in the US with climate change during the 21st century. *Journal of Soil and Water Conservation,* 56**,** 229-232.
Nearing, M., Pruski, F. & O'Neal, M. 2004. Expected climate change impacts on soil erosion rates: a review. *Journal of soil and water conservation,* 59**,** 43-50.
Nicholls, N., Drosdowsky, W. & Lavery, B. 1997. Australian rainfall variability and change. *Weather,* 52**,** 66-72.
Nicholls, N. & Kariko, A. 1993. East Australian rainfall events: Interannual variations, trends, and relationships with the Southern Oscillation. *Journal of Climate,* 6**,** 1141-1152.
OEH (2018),Discover and explore the heritage places and conservation programs in your local area, accessed June 2018, http://www.environment.nsw.gov.au/regions/south-east-and-tablelands
Panagos, P., Borrelli, P., Meusburger, K., Yu, B., Klik, A., Lim, K. J., Yang, J. E., NI, J., Miao, C. & Chattopadhyay, N. 2017. Global rainfall erosivity assessment based on high-temporal resolution rainfall records. *Scientific Reports,* 7**,** 4175.
Peterson, T., Folland, C., Gruza, G., Hogg, W., Moksitt, A. & Plummer, N. 2001. *Report on the activities of the working group on climate change detection and related rapporteurs*, World Meteorological Organization Geneva.
Renard, K. G., Foster, G. R., Weesies, G., McCool, D. & Yoder, D. 1997. *Predicting soil erosion by water: a guide to conservation planning with the Revised Universal Soil Loss Equation (RUSLE)*, US Government Printing Office Washington, DC.
Sauerborn, P., Klein, A., Botschek, J. & Skowronek, A. 1999. Future rainfall erosivity derived from large-scale climate models—methods and scenarios for a humid region. *Geoderma,* 93**,** 269-276.
Shiono, T., Ogawa, S., Miyamoto, T. & Kameyama, K. 2013. Expected impacts of climate change on rainfall erosivity of farmlands in Japan. *Ecological engineering,* 61**,** 678-689.
Solomon, S., Qin, D., Manning, M., Chen, Z., Marquis, M., Averyt, K. B., Tignor, M. & Miller, H. L. 2007. Contribution of working group I to the fourth assessment report of the intergovernmental panel on climate change, 2007. Cambridge University Press, Cambridge.
Yang, D., Kanae, S., Oki, T., K, T. & Musiake, K. 2003. Global potential soil erosion with reference to land use and climate changes. *Hydrological processes,* 17**,** 2913-2928.
Yang, X. 2014. Deriving RUSLE cover factor from time-series fractional vegetation cover for hillslope erosion modelling in New South Wales. *Soil Research,* 52**,** 253-261.
Yang, X. 2015. Digital mapping of RUSLE slope length and steepness factor across New South Wales, Australia. *Soil Research,* 53**,** 216-225.
Yang, X. & Yu, B. 2014. Modelling and mapping rainfall erosivity in New South Wales. *Soil Research*.

Yang, X., YU, B. & Xie, X. 2015. Predicting Changes of Rainfall Erosivity and Hillslope Erosion Risk Across Greater Sydney Region, Australia. *International Journal of Geospatial and Environmental Research,* 2**,** 2.

Zhang, G.-H., Nearing, M. & Liu, B.-Y. 2005. Potential effects of climate change on rainfall erosivity in the Yellow River basin of China. *Transactions of the ASAE,* 48**,** 511-517.

Zhang, Y.-G., Nearing, M., Zhang, X.-C., Xie, Y. & Wei, H. 2010. Projected rainfall erosivity changes under climate change from multimodel and multiscenario projections in Northeast China. *Journal of hydrology,* 384**,** 97-106.

Chapter 5*: Rainfall erosivity, hillslope erosion and the spatial-temporal variability across Australian Alpine region

* This chapter has been peer reviewed and published as a technical report from New South Wales Government Office of Environment and Heritage (in press).
http://climatechange.environment.nsw.gov.au/Impacts-of-climate-change/Soil/Soil-Erosion
This chapter is under revision (minor revision) in International Journal of Climatology.

Abstract

The Australia Alpine region is highly vulnerable to extreme climate events such as extreme rainfall, heat wave and snowfalls, these events would subsequently affect rainfall erosivity and hillslope erosion in the region. In this chapter, we assessed rainfall erosivity, hillslope erosion and their changes in the future periods using the revised universal soil loss equation and the New South Wales (NSW) and Australian Capital Territory (ACT) Regional Climate Modeling (NARCliM) projections. The rainfall erosivity and hillslope erosion in the Alpine study area are projected to increase near 10% and 14% for the near future (2020-2039), further increase to 24% and 30% for the far future (2060-2079) even if the groundcover is maintained at the current condition. The changes in rainfall erosivity and erosion risk have clear temporal variation with the highest erosion risk in summer and about 25% increase in the next 20 to 50 years. The projected changes in autumn range from 12% decrease in Australia Capital Territory (ACT) in the near future to about 69% increase in Murray Murrumbidgee (MM) in the far future. The highest erosion risk area within the study area is predicted to be in South East and Tablelands (SET, maximum rate: 19.95 t ha^{-1} yr^{-1}), but on average ACT has the highest erosion rate, which is 0.37 t ha^{-1} yr^{-1} across the region. In the baseline period, the snowmelt in spring is estimated to increase the rainfall erosivity by about 12.95%, in the NSW and ACT Alpine region compared to the results without snowmelt adjustment. But the snow impact is projected to be 24.84% for the near future and then less (1.63%) for the fat future due to the projected higher temperature and less snow depth in the future.

Additional keywords: rainfall erosivity, soil loss, Alpine, NARCliM.

Highlights

- Daily rainfall erosivity model is used to simulate erosivity risk in the past, present and future.
- Snowmelt in spring increases erosivity by 12-19%.
- High erosion risk occurs in summer in southeast tablelands.
- Methodology and automated scripts are applicable to other areas.

5.1 Introduction

Under future climate conditions, more frequent and higher strength rainfall events will cause more damage to natural system (Haylock and Nicholls, 2000). Rainfall extremes have been studied on regional, national and global scales (Nearing et al., 2004; Alexander et al., 2007; Evans et al., 2016; Almagro et al., 2017). These studies found some significant changes in percentiles and frequency of extreme events, and the magnitude and the sign of the changes vary with the season and the region (Alexander et al., 2007; CSIRO and Bureau of Meteorology, 2015).

Hillslope erosion rates may be expected to change in response to changes in climate for a variety of reasons, the most direct of which is the change in the erosive power of rainfall (e.g. Nearing et al., 2004). More importantly, hillslope erosion occurs mostly during a few severe storm or extreme events. Large and erosive storms are even more variable than annual rainfall totals. Trends and changes in erosive storms or rainfall extremes are therefore much more important but also difficult to detect in comparison with rainfall totals. While changes in rainfall amount and intensity are expected to have significant effects on rainfall erosivity and hillslope erosion; the magnitude of the impact is not well quantified because of the nonlinear nature of the relationship between rainfall amount and rainfall erosivity; and the extreme nature of large erosive events.

The downscaled rainfall and snow projections (snow density) from New South Wales (NSW) and Australian Capital Territory (ACT) Regional Climate Modeling (NARCliM) project (Evans et al., 2014a) have become available for southeast Australia for the baseline (1990-2009 or BA), near future (2020-2039 or NF) and far future (2060-2079 or FF) periods. NARCliM simulations provided relatively high spatial (10 km) and temporal (three

hourly) rainfall and snow, which provide opportunity to investigate changes in extreme rainfall events (Evans et al., 2014b; Evans et al., 2016).

Snowfall in NSW and ACT Alpine region is common in winter and melted in spring but it was neglected in the previous studies in hillslope erosion. It is believed that the exclusion of snowmelt in erosivity and erosion estimation would result in underestimation of soil loss projection in the Alpine and its surrounding areas. Though there are some studies on impact of snowmelt on erosion in other alpine regions in the world, such as estimation of snow gliding processes impact on erosion in Switzerland (Meusburger et al., 2014), improvement of snowmelt runoff indices in Canada (Hayhoe et al., 1995) and development of snowmelt erosion and sediment yield model in Germany (Ollesch et al., 2006), such research has not yet been done in Australia.

Previous work in erosion modeling or assessment in Australia rarely took into consider the impact of snowfall or snow melting as it's not widespread in this continent. The Alpine highland is arguably the only area in Australia has snowfall in every winter. Thus, the impact of snowmelt on erosion in this area cannot be ignored. This research was therefore arguably the first in Australia to consider snow melting in hillslope erosion modeling.

In this study, I examine the relationship between extreme rainfall indices and rainfall erosivity across the Alpine region. I calibrate rainfall erosivity estimation using the snowmelt in spring (September, October and November), and predict hillslope erosion risk and the seasonal and spatial changes. Outcomes from this study include time series (monthly and annual) rainfall extreme indices and erosion risk for the study area for all the 60-year periods being the baseline, near future and far future periods. These time series maps are useful for locating the high erosion risk seasons and areas across the study area

for climate change adaptation, land use planning and development of cost-effective erosion control practices.

This chapter aims to (i) assess the snowmelt impacts on rainfall erosivity across the Alpine region within NSW and ACTs based on the NARCliM projections; and (ii) assess the locations and times with high erosion risk across the study area. Outcomes from this study include (i) time series rainfall erosivity risk within and without snowmelt (ii) hillslope erosion risk maps. These outcomes are to assist the long-term climate change adaptation and regional planning in NSW and ACT Alpine region.

5.2 Study area and data sets

5.2.1 Study area

The Australian Alpine or Alps is the highest mountain range in Australia. The unique NSW section of Australian Alps is found in the southern section of the Great Dividing Range and includes the Snowy Mountains, ACT and the Kosciuszko plateau. The study area covers the NSW and ACT Alpine region and its surrounding areas including Murray Murrumbidgee (MM) and South East and Tablelands (SET), which are two NSW state planning regions, and the ACT (Figure. 5-1). The Snowy Hydro field measurement sites for snow depth and snow water content are also marked as "×" on Figure. 5-1.

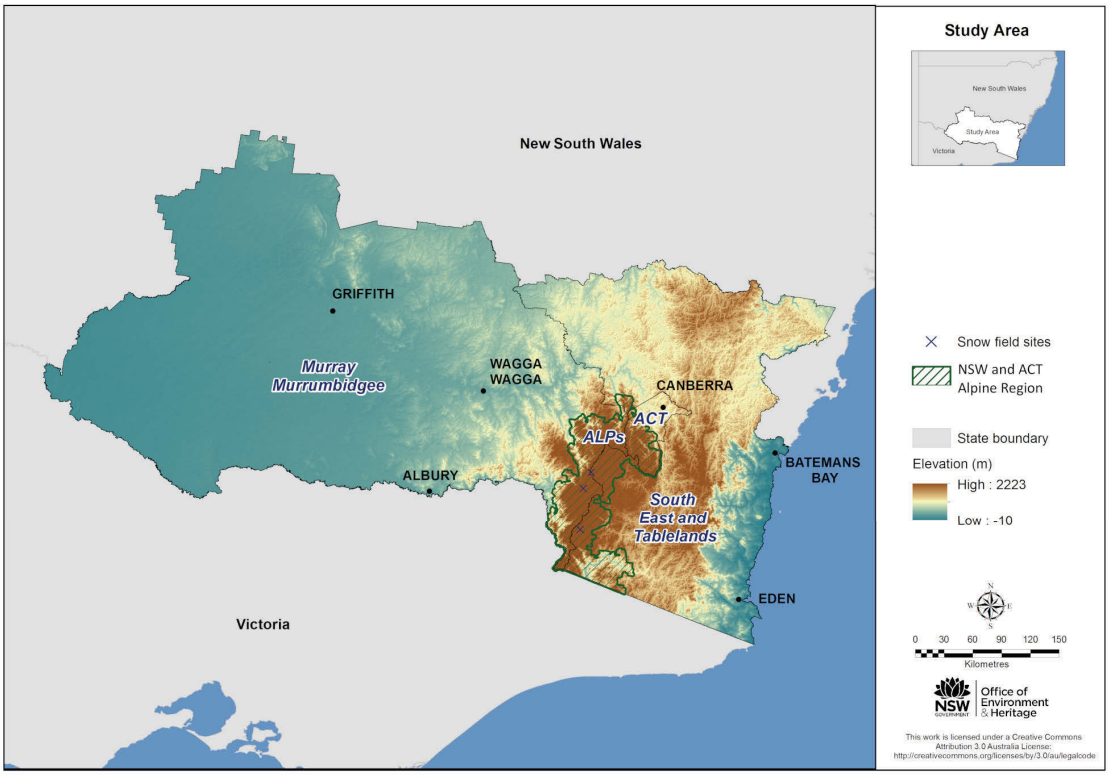

Figure 5-1 Study area.

5.2.2 Data sets

This study used the bias-corrected rainfall, snow and temperature with a spatial resolution of 10 km (Evans et al., 2016) from NARCliM to estimate the future rainfall erosivity in the NSW and ACT Alpine region. Snow depth and density simulation for the 60 years were extracted from the snow projections and used to estimate and adjust the snowmelt runoff (Bormann et al., 2014) and rainfall erosivity during the melting season (spring). To minimize bias, I used all 12 model ensembles (latitude: $-21.67° \sim -40.49°$, longitude: 132.72° to 169.16°) from NARCliM, the combinations of four GCMs

(CCCMA3.1, CSIRO_MK3.0, ECHAM5 and MIROC3.2) and three RCMs (R1, R2 and R3).

I also obtained the weekly measurements of snow depth and snow water equivalent at three filed sites in the snowy mountains (Figure. 5-1) from Snowy Hydro Ltd. The measurements cover the baseline period (1990-2009) and the data were used for calibrating the NARCliM snowpack projections.

In addition, the soil property projections for NSW such as soil organic carbon were obtained from OEH (Gray et al., 2017) and used to calculate soil erodibility based on Yang et al. (2017). Other input data include soil texture from Soil and Landscape Grid of Australia (Grundy et al., 2015) at a spatial resolution of 3 arc second (about 90 m), the 30 m DEM (Shuttle Radar Topography Mission, SRTM), the latest satellite-derived fractional vegetation cover (Version 3.1.0) at a spatial resolution of 500 m and on monthly basis since 2000 (Guerschman et al., 2009).

5.3 Methods

5.3.1 Snowmelt and erosivity estimation

In this study, the snowmelt was considered in simulating and calibrating the rainfall erosivity across the NSW and ACT Alpine region in spring. The daily snowmelt was estimated from the models described in (Bormann et al., 2014) and (Rango and Martinec, 1995):

$$Mp = k \cdot \frac{\rho_s}{\rho_w} \cdot (T_{mean} - T_{ref}) \quad (5\text{-}1)$$

where Mp is potential snowmelt (mm day^{-1}), ρ_s is snow density (g cm^{-3}) simulated based on multiple linear regression (MLR) and climate variables, ρ_w is water density (assumed to be 1 g cm^{-3}), T_{mean} refers to the daily mean temperature and T_{ref} is set to 0 ℃. The calculation of rainfall erosivity was adjusted by adding the snowmelt to the rainfall density using the daily rainfall erosivity model as presented in Yang et al. (2016) and Eq. 1 is re-written as:

$$\hat{E}_j = \alpha[1 + \eta\cos(2\pi fj - \omega)] \sum_{d=1}^{N}(R_d + Mp)^{\beta} \quad (5\text{-}2)$$

The daily rainfall amount R_d was calculated form the bias corrected daily rainfall projections of all the 12 NARCliM ensembles. The snowmelt was predicted at daily scale by using climate change model from NARCliM (four GCMs × three RCMs). The calculation dimensions for this study is demonstrated as below,

$$Dimensions = 4\ GCMs \times 3\ RCMs \times 60\ years \times 90\ days \quad (5\text{-}3)$$

5.3.2 Hillslope erosion estimation

Once the rainfall erosivity is estimated based on the above methods, the hillslope erosion can be calculated using RUSLE (Renard et al., 1997) along with other factors, the slope-steepness factor (LS), groundcover (C) and the soil erodibility (K):

$$A = R \times K \times LS \times C \times P \quad (5\text{-}4)$$

where A is the projected soil loss (t ha^{-1} yr^{-1}), R is rainfall erosivity (MJ mm ha^{-1} hr^{-1} yr^{-1}) as described above, K is the soil erodibility factor (t ha hr ha^{-1} MJ^{-1} mm^{-1}), LS represents the slope and steepness factor (unitless) estimated from Digital Elevation Model (DEM), and C is the cover and management (C) factor (unitless). The erosion control (P) factor (unitless) is not considered in this study.

The K factor was estimated based on Yang et al. (2017) using the recent digital soil maps and soil property projections including soil texture and organic matter (Grundy et al., 2015; Gray et al., 2016; Gray and Bishop, 2017). The LS factor was calculated from the 30 m DEM (Shuttle Radar Topography Mission, SRTM) based on a comprehensive method as described in (Ji et al., 2016). The C factor was estimated on monthly basis and updated from the latest satellite-derived fractional vegetation cover (Version 3.1.0) (Guerschman et al., 2009) based on methods described in Yang (2014). The C factor was adjusted with snow cover in winter months (June, July and August) based on a snow mask prepared from the snow depth projection and a specific value (0.0044) was assigned to the areas covered by snow.

5.3.3 Model accuracy assessment

Adequate random points (> 5000 for the entire study area and 1550 located within NSW and ACT Alpine region) were used to rainfall erosivity and hillslope erosion rates for the baseline (1990-2009), near future (2020-2039) and far future (2060-2079) periods. These randomly sampled data were used for statistical analyses and identification of the relationship between rainfall erosivity with and without snowmelt, and also compared with those calculated from the measured snow depth and snow water content at three Snowy Hydro stations. Model performance is measured by the coefficient of efficiency, E_c (Nash and Sutcliffe, 1970). More information of this method has presented in Section 4.3.2.

The only observed values within the study area are snow depth and snow water content data at the three Snowy Hydro stations which are used to validate that from the NARCliM snowpack projection. However, for the entire Alpine region, the gridded rainfall data and

the derived rainfall erosivity from BoM served as reference values for model comparison and assessment.

5.4 Results and discussion

5.4.1 Impact of snowmelt on erosivity

Adding the snowmelt (mm day^{-1}) as additional rainfall (Loague and Freeze, 1985, Risse et al., 1993) to the daily rainfall erosivity model (Yang and Yu, 2015) resulted in greater variation in rainfall erosivity estimates along the east coast in SET and Kosciuszko National Park (Figure. 5-2) compared with the far western area within MM region for all modelling periods (1990-2009 to 2060-2069). The snowmelt in spring increases the rainfall erosivity in the Alpine area by 13% in the baseline period, 18% in the near future period, but almost nil impact in the far future owing to the projected temperature rise.

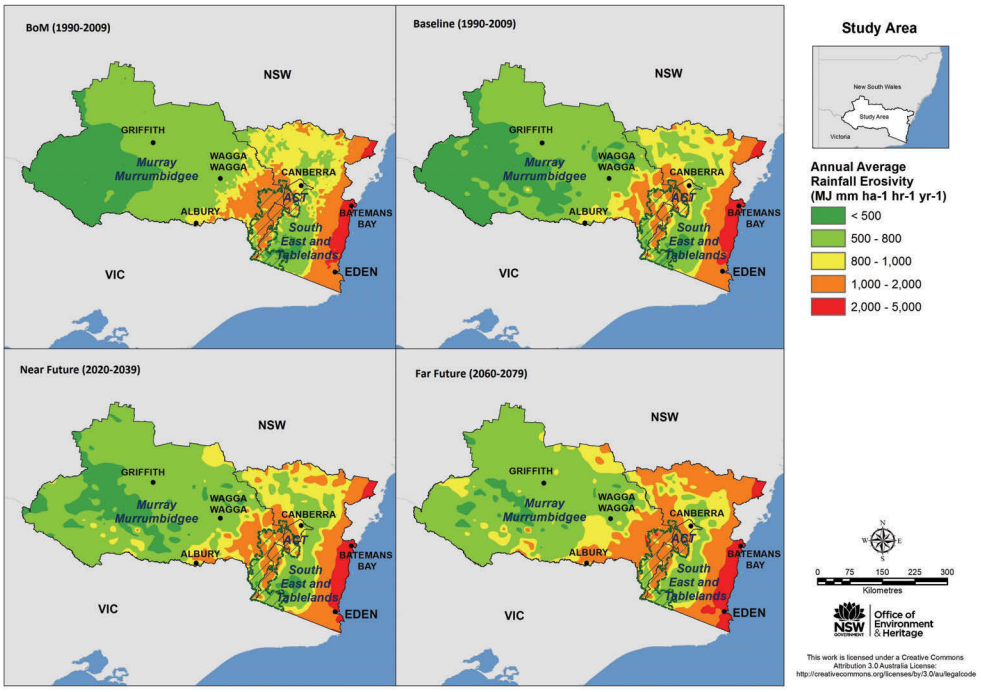

Figure 5-2 Annual mean rainfall erosivity with snowmelt adjustment in baseline (1990-2009), near future (2020-2039) and far future (2060-2079), compared with that calculated from BoM gridded rainfall in baseline (1990-2009) without snowmelt adjustment.

Table 5-1 presents absolute annual and seasonal mean value of rainfall erosivity calculated from snowmelt-erosivity model (Eq. 5-2) for three periods across NSW and ACT Alpine region. There is greater mean annual rainfall erosivity in ACT for in baseline (BA: 1133.38 MJ mm ha^{-1} hr^{-1} yr^{-1}), but it is projected that SET will experience more rainfall erosivity than those from MM and ACT in both near future and far future (NF: 1120.93 MJ mm ha^{-1} hr^{-1} yr^{-1} and FF: 1233.87 MJ mm ha^{-1} hr^{-1} yr^{-1}). SET is estimated to be at higher risk in summer and autumn in the future, and ACT is projected with higher rainfall erosivity in winter and spring although still less than that from NSW and ACT Alpine. Like the Rx5day projected erosivity (Chapter 4), summer is believed to be the season with highest rainfall erosivity whilst winter always has the least across the study area in all the three time periods. Moreover, the risk of rainfall erosivity is generally tending to increase in both mean annual value and seasonal estimation across the study area.

Table 5-1 Mean annual and seasonal rainfall erosivity values (MJ mm ha^{-1} hr^{-1} yr^{-1}) for the three periods across the study area and sub-regions.

Rainfall Erosivity	Baseline (1990-2009)					Near Future (2020-2039)					Far Future (2060-2079)				
	MM	SET	ACT	Region	Alpine	MM	SET	ACT	Region	Alpine	MM	SET	ACT	Region	Alpine
Summer	249.44	504.20	503.17	334.04	326.03	308.03	553.68	514.56	389.09	376.24	289.31	592.79	476.52	388.51	381.72
Autumn	133.77	273.09	252.25	179.76	206.67	125.97	286.88	208.44	178.33	178.77	211.44	332.22	314.60	251.32	271.80
Winter	60.93	83.31	110.81	68.74	170.88	55.14	59.23	99.65	57.06	164.03	74.38	68.49	126.20	73.22	173.88
Spring	143.19	221.54	267.15	169.84	294.80	164.94	223.10	279.61	185.04	295.88	167.45	240.37	257.98	191.91	243.92
ANN	587.33	1082.15	1133.38	752.39	998.38	653.52	1120.93	1108.13	808.60	1014.92	742.58	1233.87	1175.30	904.95	1071.32

To examine the snowmelt impact, rainfall erosivity estimation adjusted by snowmelt rainfall (Eq. 5-2) from the 12 NARCliM emsembles were compared on monthly basis with those calculated from the NARCliM projections without snowmelt (Yang et al., 2016). Estimated rainfall and snowmelt runoff erosivity were assessed and compared with those from observed data (snow water equivalent and snow depth, unit: cm) of three snow sites in Snowy Mountains provided by Snowy Hydro. In terms of the mean annual change, the

rainfall erosivity is estimated to increase (+24.21% on average) in the study area, except some area in ACT (-2.15%). The rainfall erosivity in NSW and ACT Alpine region has 2.22% increase in the near future and further 8.31% increase in the far future.

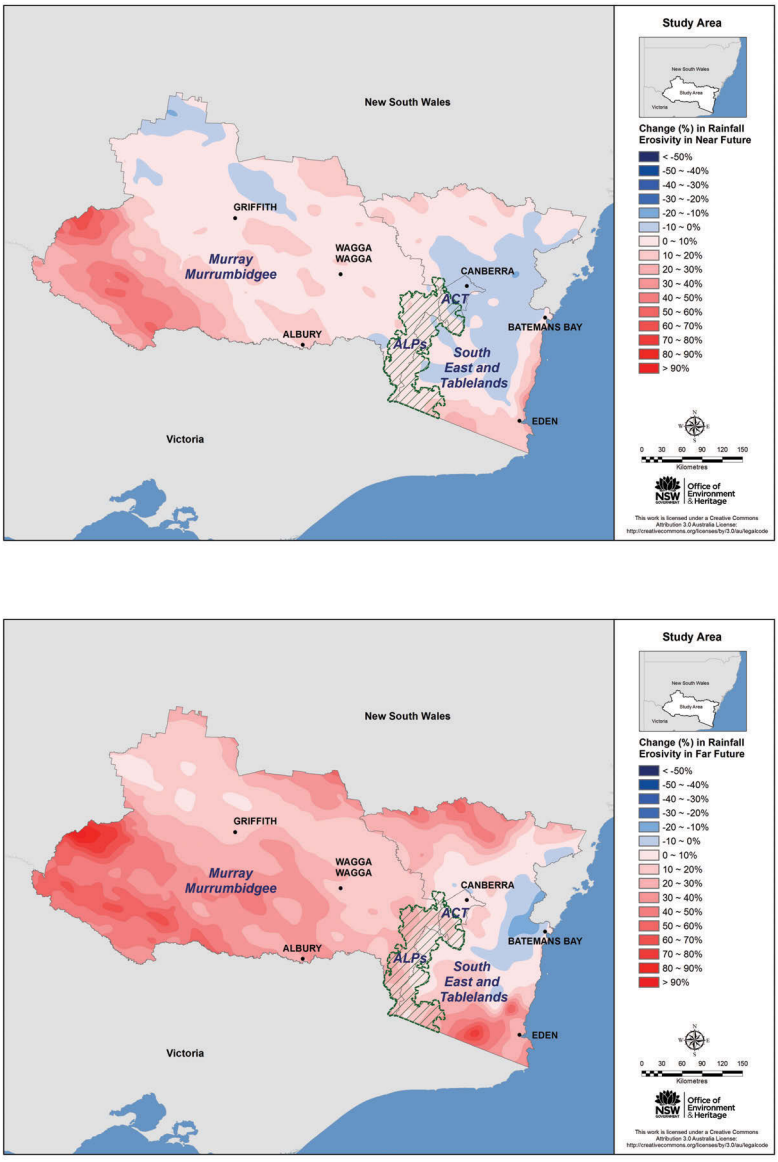

Figure 5-3 Changes of mean annual rainfall erosivity in the near future (2020-2039) and the far future (2060-2079).

The projected average annual and seasonal rainfall erosivity with snowmelt were compared with those stimulated from the previous NARCliM output without considering

the snowmelt (Table 5-2). The effect of snowmelt is highly significant, result in a large increase of rainfall erosivity risk in NSW and ACT Alpine region in spring. The snowmelt adjusted rainfall erosivity during spring season in the baseline period is 12.95% higher than that from the previous NARCliM study without consideration of snowmelt. The change is even doubled in the near future period, reaching 24.84% in 2020-2039. However, the difference is getting much smaller in the far future (only about 1.63%) due to the projected rise in temperature and decrease in snow depth.

Table 5-2 Average annual and seasonal change of rainfall erosivity (MJ mm ha^{-1} $season^{-1}$) with and without snowmelt across the study area.

Season	Erosivity with snowmelt			Erosivity without snowmelt			Change %		
	Baseline	Near future	Far future	Baseline	Near future	Far future	Baseline	Near future	Far future
Summer	326	376	382	345	345	402	-5.50%	9.06%	-5.04%
Autumn	207	179	272	189	210	225	9.35%	-14.87%	20.80%
Winter	171	164	174	192	189	207	-11.00%	-13.21%	-16.0%
Spring	295	296	244	261	237	240	12.95%	24.84%	1.63%
ANN	998	1015	1071	987	981	1074	1.15%	3.46%	-0.25%

5.4.2 Rainfall erosivity variation and change in the future

The relative seasonal changes in rainfall erosivity range from 28.89% decrease in winter in SET in the near future to about 64% increase in autumn in MM in the far future when comparing to the baseline period.

Table 5-3 demonstrates the change (%) of rainfall erosivity within snowmelt from the baseline (1990-2009) to the near future (2020-2039) and the far future (2060-2079). Green cells represent decreasing in the rainfall erosivity while the rest represent increasing. Rainfall erosivity risk is projected to decrease to all three regions (MM, SET and ACT) in

autumn and winter in the near future (Figure. 5-4) but expected to increase in the far future (Figure. 5-5).

Table 5-3 Mean annual and seasonal changes (%) of rainfall erosivity in near future (2020-2039) and far future (2060-2079).

Rainfall Erosivity Change	Change in Near Future					Change in Far Future				
	MM	SET	ACT	Study Area	Alpine	MM	SET	ACT	Study Area	Alpine
Summer	26.04	10.57	2.45	20.79	18.43	18.22	18.16	-4.90	17.89	21.47
Autumn	-3.35	-2.39	-16.82	-3.23	-12.65	64.27	26.63	23.99	51.73	32.71
Winter	-11.37	-28.89	-9.12	-16.91	-6.27	30.23	-13.78	14.67	16.01	-0.07
Spring	16.72	3.55	6.05	12.38	1.53	19.44	10.39	-1.72	16.26	-15.27
ANN	13.00	3.22	-2.15	9.68	**2.22**	28.63	15.83	3.73	24.21	**8.31**

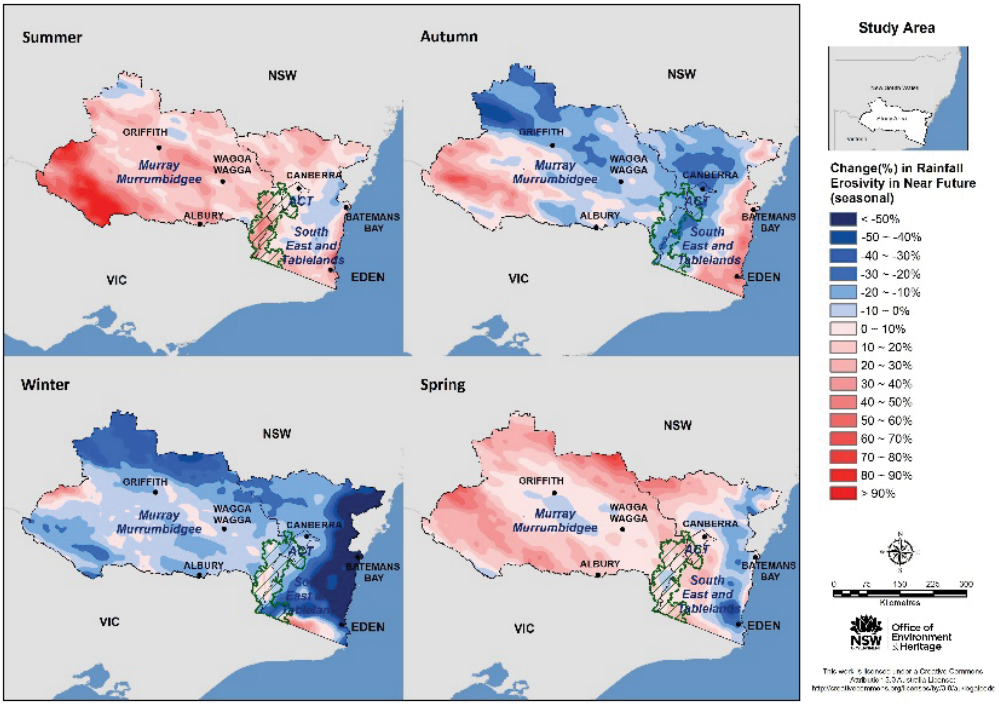

Figure 5-4 Seasonal mean change of rainfall erosivity within snowmelt in the near future (2020-2039)

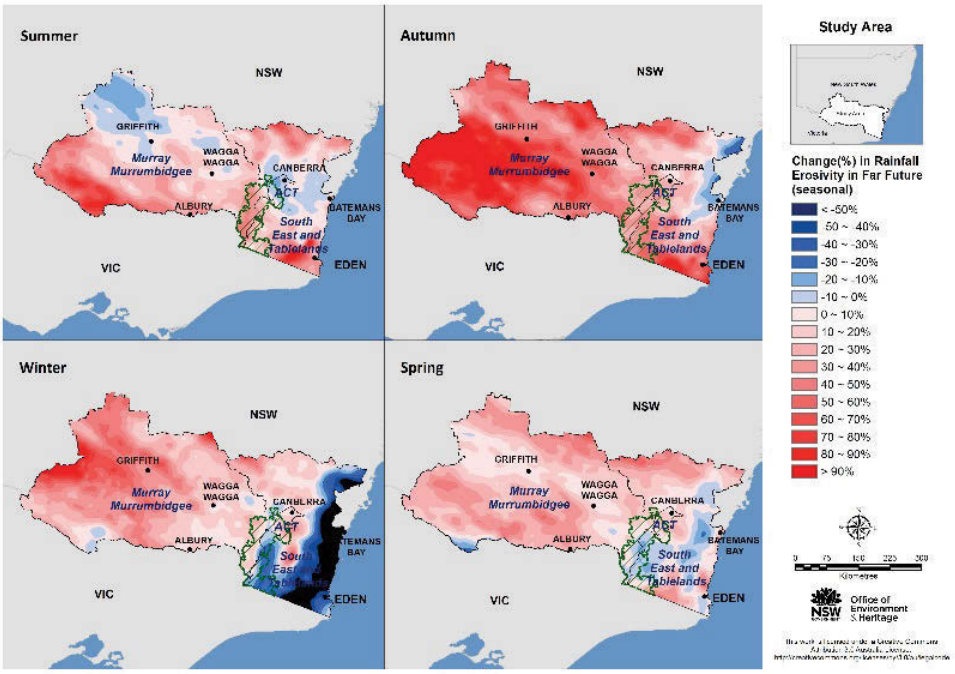

Figure 5-5 Seasonal mean change of rainfall erosivity within snowmelt in the far future (2060-2079)

Turning to the seasonal change, as much as 20.79% increase occurs in summer while about 17% decrease across the study area in winter in the near future. The largest change occurs in autumn (+51.73%) rather than summer (+17.89%) in the far future period. The Tablelands area has greater seasonal variation in near future (+10.57% in summer and -28.89% in winter) but Murray Murrumbidgee is projected has much more deviation to far future (+64.27% in autumn and +19.44% in spring).

Rainfall erosivity calculated from the 12 NARCliM member ensembles vary significantly. Compared with the results from the gridded daily rainfall data (Bureau of Meteorology 2009) for the baseline period (1990-2009), the percent change of mean rainfall erosivity values from the 12 member ensembles range from about -8% to about 8%, with an overall change about 2% (2.26%). All 12 member ensembles, except CCCMA3.1_R1 and MIROC3.2_R1, resulted in an overestimate of the mean annual

rainfall erosivity, while results from MIROC3.2_R1 have less than 1% variation compared to the BoM mean value. CCCMA3.1_R3 and MIROC3.2_R3 have less than 2% variation compared to the result from BoM data. The overall overestimate of rainfall erosivity is due to the 1.65% overall increase in the NARCliM projected mean annual rainfall (525 mm year^{-1}) compared with the BoM rainfall (519 mm year^{-1}) in the same period (1990–2009).

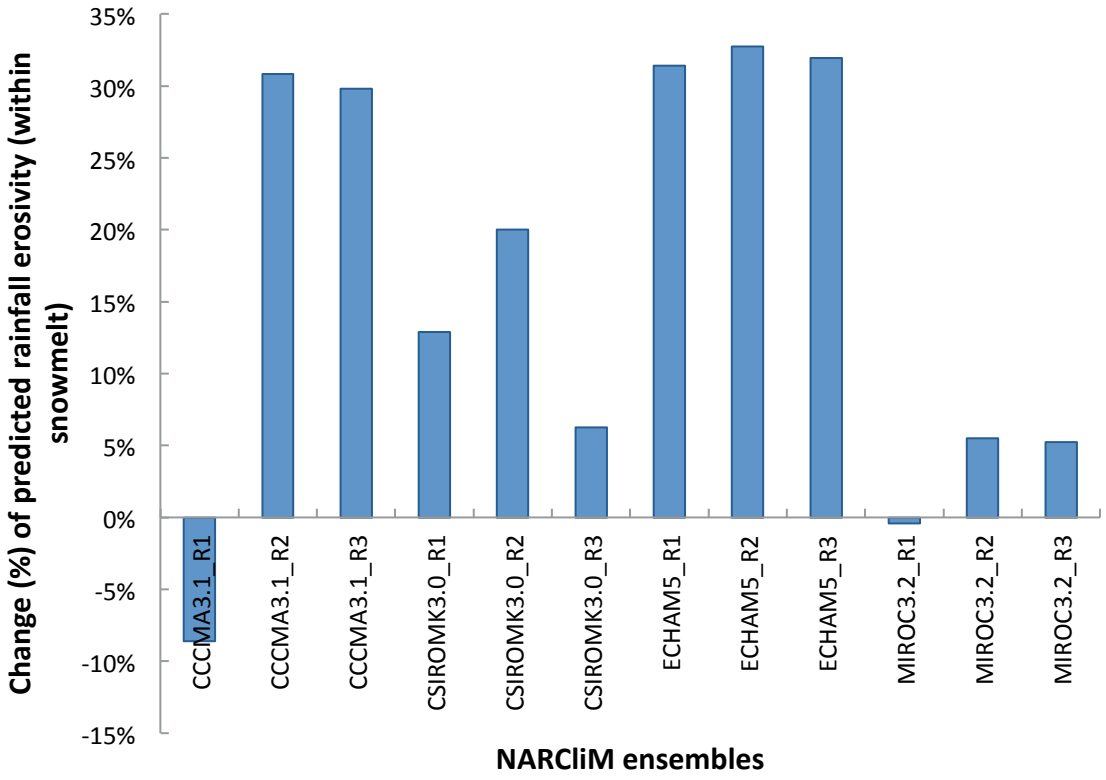

Figure 5-6 12 NARCliM model ensembles and the variations in snow-melting estimations comparing to BoM data.

To minimize the bias, I used the average monthly rainfall and snowmelt runoff erosivity for spring seasons (September, October and November) from all the 12 ensembles in all periods. Average monthly erosivity during thawing season is tending to decrease from baseline period to far future. This is probably due to the projected higher temperature and less snow from previous NARCliM.

Snowmelt and runoff erisivity is more meaningful to be presented by RCMs (SEM: 5.85 for baseline, 2.17 for near future and 0.57 for far future) as they with less standard error of the mean (SEM) than GCMs (SEM: 8.72 for baseline, 11.07 for near future and 23.96 for far future). Agreed with the work of Ji et al., (2016), snowmelt erosivity derived from the RCM R2 are more trustworthy in reproducing precipitation compare to R1 and R3 (Figure. 5-6).

The snow melting mostly occurs in October based on the 7-day observation data from the Snowy Hydro field sites. The trend of the erosivity change is generally decreasing from the baseline period to the far future period. The erosivity with snowmelt in spring in the baseline period is 12.95% higher than that from the previous NARCliM projections without consideration of snowmelting. However, the difference is getting much smaller in the far future (only about 1.63%) due to the projected rise in temperature and decrease in snow depth.

5.4.3 Hillslope erosion risk and the changes in the future

The hillslope erosion is predicted to increase in the future in general with great variation in seasons and locations. The high erosion risk area is predicted to be in ACT and SET in all periods. These include some reserved areas such as Wadbilliga National Park, Monga National Park close to Batemans Bay and wildness areas near Goobarragandra. Figure 5-7 shows the projected hillslope erosion risk across the study area in the baseline period, same patterns exhibit in the future periods.

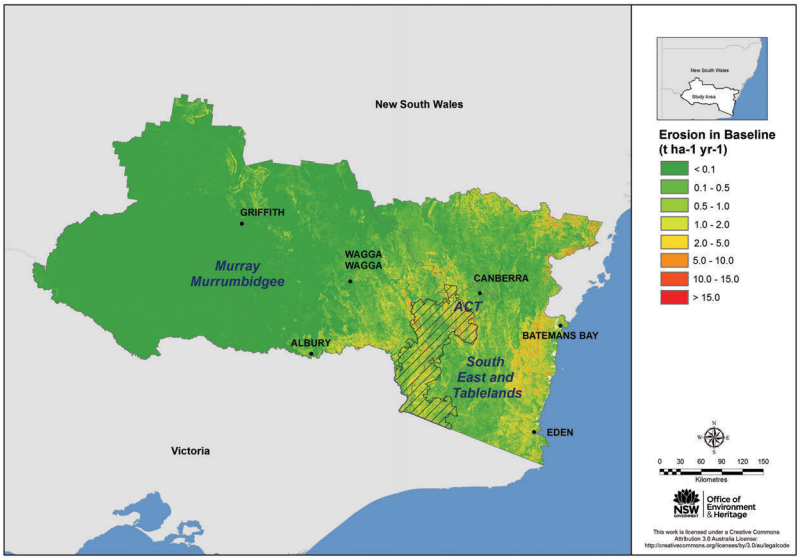

Figure 5-7 Predicted hillslope erosion risk in the baseline period (1990-2009).

Table 5-4 further presents the statistics of the annual erosion rates across the region in the baseline and future periods. The highest risk areas are projected in SET, where the maximum erosion rate reaches 19.95 t ha^{-1} yr^{-1} in the baseline period and slightly decreases in the near future (17.33 t ha^{-1} yr^{-1}) and the far future (19.85 t ha^{-1} yr^{-1}). However, if the mean values are compared, ACT (followed by NSW and ACT Alpine) has the highest mean annual erosionrate reaching 1.36 t ha^{-1} yr^{-1} in the baseline period, 1.40 t ha^{-1} yr^{-1}in the near future and 1.54 t ha^{-1} yr^{-1} in the far future period.

Table 5-4 Mean and maximum annual erosion values (t ha^{-1} yr^{-1}) across the study area in baseline (1990-2009), near future (2020-2039) and far future (2060-2079).

Erosion (t ha^{-1} yr^{-1})	Baseline (1990-2009)		Near Future (2020-2039)		Far Future (2060-2079)	
	MAX	MEAN	MAX	MEAN	MAX	MEAN
MM	14.16	0.16	14.81	0.17	17.08	0.19
SET	19.95	0.79	17.33	0.83	19.85	0.92
ACT	10.54	1.36	10.32	1.40	11.56	1.54
Study Area	19.95	0.37	17.33	0.40	19.85	0.44
Alpine	12.30	1.14	12.89	1.20	13.99	1.30

Table 5-5 summarizes the change (%) of mean annual erosion from baseline to future periods in study area, and Figure 5-8 presents the continuous change of mean annual erosion for the 60-year period. SET is likely to experience greater variation of erosion change in the near future, where mean change is +18.76% in summer and minimum is -23.69% in winter. In the far future, more variation of erosion change is turning to MM region (+69.11% in autumn and +21.70% in spring). Summer is the most vulnerable season with highest change to the future periods compare to the other seasons.

Table 5-5 Mean annual and seasonal changes (%) of erosion values (t ha^{-1} yr^{-1}) across study area in the near future (2020-2039) and the far future (2060-2079).

Erosion Change	Change in Near Future					Change in Far Future				
	MM	SET	ACT	Study Area	Alpine	MM	SET	ACT	Study Area	Alpine
Summer	27.72	18.76	9.24	24.62	24.79	21.01	30.47	5.93	23.81	33.28
Autumn	-3.30	4.66	-11.73	-0.89	-7.81	69.11	40.43	39.57	59.60	48.13
Winter	-9.45	-23.69	-3.60	-13.89	-2.10	35.43	-4.99	26.85	22.48	7.18
Spring	19.53	11.00	13.68	16.74	7.39	21.70	21.48	11.12	21.48	-6.34
ANN	15.74	10.95	4.55	14.07	**7.91**	31.31	27.87	15.56	30.00	**18.16**

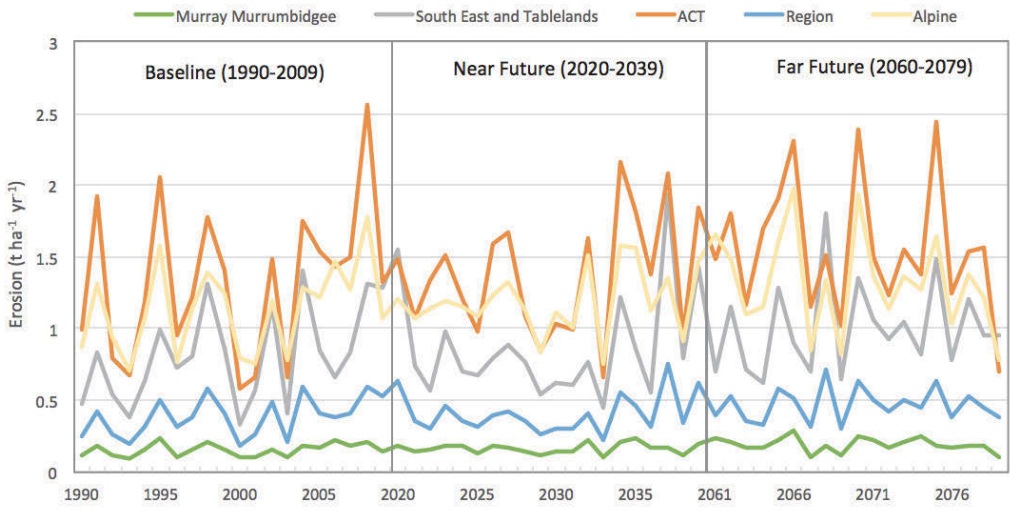

Figure 5-8 Projected hillslope erosion rates and changes in the Alpine region and the surrounding areas in the baseline and future periods.

As estimated from the RUSLE model, ACT has the highest risk of hillslope erosion rather than NSW and ACT Alpine region (Table 5-5). Though the NSW and ACT Alpine area (mountainous) has the highest LS factor, the K-factor and C-factor are relatively low comparing to those from the other part of study area (MM and SET). It is predicted that ACT has higher values in K-factor, C-factor and LS-factor (Figure. 5-9), these factors along with the adjusted rainfall erosivity factor, resulting in the highest erosion in ACT. Despite higher K and C values in MM region, the corresponding hillslope erosion is predicted very low since the area is flat and the LS values are very low.

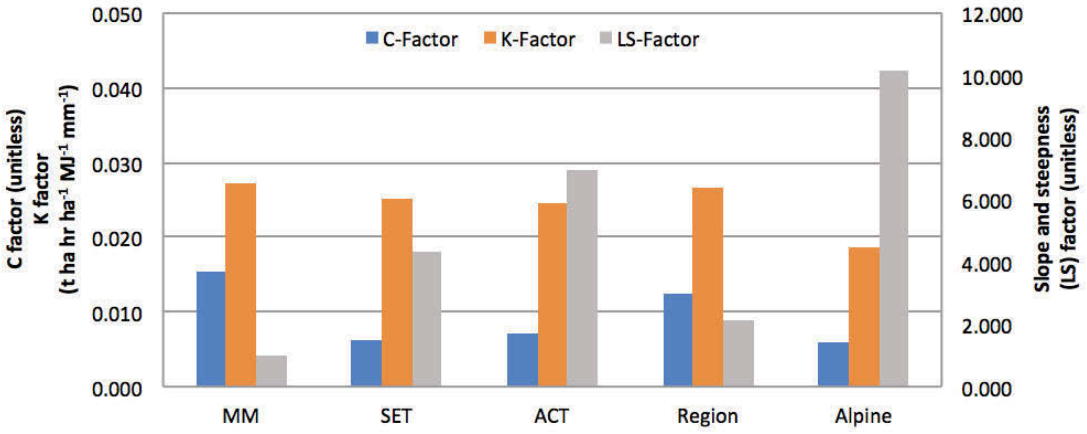

Figure 5-9 Comparison of erosion risk and RUSLE factors (C, K and LS) across the Alpine study area.

5.6 Conclusions

Impact of snowmelt on rainfall erosivity and erosion need to be considered in the NSW and ACT Alpine region in the baseline and near future periods. The snowmelt in spring can increase erosivity by about 9% in the Alpine area. However, with projected temperature

rise and snow cover decreasing, the snowmelt impact on erosivity is less important or even can be ignored in the far future.

The high erosion risk area is projected to be in ACT, followed by the Alpine region and SET. The high erosion risk is due to the combined effects of steep lands and intense rainfall, as well as snow-melting. This highlights the importance of groundcover maintenance and soil management in these regions.

There are significant limitations and bias in input data that influence the accuracy of these outcomes. Daily time step NARCliM GCM/RCM projections (rainfall, snow, temperature) are at a spatial resolution of approximately 10 km which is considered rather coarse and a limiting factor in local ecosystem (erosion) modeling. 12 model ensembles were used to consider snowmelt impact on erosivity. Rainfall erosivity and hillslope erosion are likely to increase about 9.68% and 14.07% in the near future and keep increasing to 24.21% and 30% in the far future on average in the study area.

This research was the first attempt to use snow data and projections to adjust erosivity model and the cover factor in hillslope erosion modeling. The methodology have been developed and applied in the NSW and ACT Alpine region, with potential to be used elsewhere in the world.

Acknowledgement

This research was funded and supported by NSW Office of Environment and Heritage (OEH) Climate Change Fund via a scholarship of $30,000 to support me in the conduct of the Research Project as part of their Course at UTS. It’s part of the project on Climate Change Impacts on NSW's Alpine Region Biodiversity led by OEH. Drs Kathleen Beyer,

Fei Ji, Larissa Brisbane and Anthony Coward from OEH Climate & Atmospheric Science (CAS) supported and managed this project. Professor Jason Evans and Dr Alejandro Di Luca from the Climate Change Research Centre of the University of New South Wales provided the NARCliM rainfall and snow projections. Dr Thomas Chubb from Snowy Hydro helped to provide the field snow data. Associate Professor Peter Kinnell from University of Canberra assisted with rainfall erosivity modelling and technical review. All the above assistance and supports are greatly appreciated.

5.7 References

Almagro, A., Oliveira, T.P.S., Nearing, M.A. & Hagemann, S. 2017. Projected climate change impacts in rainfall erosivity over Brazil. Scientific Reports 7: 8130.

Alexander, L. V., Hope, P., Collins, D., Trewin, B., Lynch, A. & Nicholls, N. 2007. Trends in Australia's climate means and extremes: a global context. Australian Meteorological Magazine, 56, 1-18.

Bormann, K. J., Evans, J. P. & McCabe, M. F. 2014. Constraining snowmelt in a temperature-index model using simulated snow densities. Journal of Hydrology, 517, 652-667.

CSIRO and Bureau of Meteorology 2015, Climate Change in Australia Information for Australia's Natural Resource Management Regions: Technical Report, CSIRO and Bureau of Meteorology, Australia

Evans, J., Ji, F., Lee, C., Smith, P., Argueso, D. & Fita, L. 2014a. Design of a regional climate modelling projection ensemble experiment–NARCliM. Geoscientific Model Development, 7, 621-629.

Evans, J. P., Argueso, D., Olson, R. & Di Luca, A. 2014b. NARCliM extreme precipitation indices report.NARCliM Technical Note 6. Sydney, Australia: Report to the NSW Office of Environment and Heritage, 2014.109 p.

Evans, J. P., Argueso, D., Olson, R. & Di Luca, A. 2016. Bias-corrected regional climate projections of extreme rainfall in south-east Australia. Theoretical and Applied Climatology, 1-14.

Gray, J.M., Bishop, T.F.A. 2017. Climate change impacts on three key soil properties in NSW. Technical Report, NSW Office of Environment and Heritage, Sydney

Gray, J. M., Thomas, F. A., Bishop, T. F. A. & Wilford, J. R. 2016. Lithology and soil relationships for soil modelling and mapping. Catena 147, 429 –440.

Grundy, M. J., Viscarra, R. A., Searle, R. A., Searle, R. D., Wilson, P. L., Chen, C. & Gregory, L. J. 2015. Soil and landscape grid of Australia. Soil Research 53, 835–844. doi:10.1071/SR15191

Guerschman, J. P., Hill, M. J., Renzullo, L. J., Barrett, D. J., Marks, A. S.& Botha, E. J. 2009. Estimating fractional cover of photosynthetic vegetation, nonphotosynthetic

vegetation and bare soil in the Australian tropical savanna region upscaling the EO-1 Hyperion and MODIS sensors. Remote Sensing of Environment 113, 928–945.
Haylock, M. & Nicholls, N. 2000. Trends in extreme rainfall indices for an updated high quality data set for Australia, 1910-1998. International Journal of Climatology, 20, 1533-1541.
Hayhoe, H., Pelletier, R. & Coote, D. 1995. Estimating snowmelt runoff erosion indices for Canada. Journal of Soil and Water Conservation, 50, 174-179.
Ji, F., Evans, J. P., Teng, J., Scorgie, Y., Argueso, D. & Di Luca, A. 2016. Evaluation of long-term precipitation and temperature Weather Research and Forecasting simulations for southeast Australia. Climate Research, 67, 99-115.
Loague, K. M. & Freeze, R. A. 1985. A comparison of rainfall-runoff modeling techniques on small upland catchments. Water Resources Research, 21, 229-248.
Meusburger, K., Leitinger, G., Mabit, L., Mueller, M., Walter, A. & Aleqell, C. 2014. Hillslope erosion by snow gliding–a first quantification attempt in a subalpine area in Switzerland. Hydrology and Earth System Sciences, 18, 3763-3775.
Nash, J. E. & Sutcliffe, J. V. 1970. River flow forecasting through conceptual models part I—A discussion of principles. Journal of Hydrology, 10, 282-290.
Nearing, M.A., Pruski, F. F. & O'Nea, M.R. 2004. Expected climate change impacts on hillslope erosion rates: A review. Journal of Soil and Water Conservation 59(1), 43-50.
OEH, 2013. NSW Office of Environment and Heritage (OEH)
Scientific Rigour Position Statement.
http://www.environment.nsw.gov.au/resources/research/OEHSciRigPosnStmtJul13.pdf.
Ollesch, G., Kistner, I., Meissner, R. & Lindenschmidt, K.-E. 2006. Modelling of snowmelt erosion and sediment yield in a small low-mountain catchment in Germany. Catena, 68, 161-176.
Rango, A. & Martinec, J. 1995. Revisiting the degree-day method for snowmelt computations. JAWRA Journal of the American Water Resources Association, 31, 657-669.
Rawson, A. & Murphy, B. Assessing the impacts of climate change on soils in NSW. Proceedings of the Soil Science Australia and the New Zealand Society of Soil Science Conference, 2012.
Renard, K. G., Foster, G. R., Weesies, G., McCool, D. & Yoder, D. 1997. Predicting hillslope erosion by water: a guide to conservation planning with the Revised Universal Soil Loss Equation (RUSLE), US Government Printing Office Washington, DC.
Risse, L., Nearing, M., Laflen, J. & Nicks, A. 1993. Error assessment in the universal soil loss equation. Soil Science Society of America Journal, 57, 825-833.
Yang, X. 2014. Deriving RUSLE cover factor from time-series fractional vegetation cover for hillslope erosion modelling in New South Wales. Soil Research, 52, 253-261.
Yang, X. 2015. Digital mapping of RUSLE slope length and steepness factor across New South Wales, Australia. Soil Research, 53, 216-225.
Yang, X. & YU, B. 2015. Modelling and mapping rainfall erosivity in New South Wales. Soil Research. 53, 178-189.

Yang, X., Yu, B. & Xie, X. 2015. Predicting Changes of Rainfall Erosivity and Hillslope Erosion Risk Across Greater Sydney Region, Australia. International Journal of Geospatial and Environmental Research, 2, 2.

Yang, X., Yu, B., Zhu, Q. & Liu, D. 2016. Predicting Changes of Rainfall Erosivity and Hillslope Erosion across New South Wales. Australia. Journal of Earth Science Climate Change, 7, 2.

Yang, X., Gray, J., Chapman, C., Zhu, Q., TULAU, M. & MCLNNES-CLARKE, S. 2017. Digital mapping of soil erodibility for water erosion in New South Wales, Australia. Soil Research. (Online earl

Chapter 6: Conclusion

Final conclusions

Various datasets and innovative approaches were applied in this study for examining the impact of extreme weather events impact on rainfall erosivity and erosion from the present to far future, under a changing climate. More frequent and severer bushfires, greater intensiveness of rainfall events, more heat waves (and the effect on snowmelt) were considered in modelling rainfall erosivity and hillslope erosion rates. The overall method and implementation are listed in Figure 6-1.

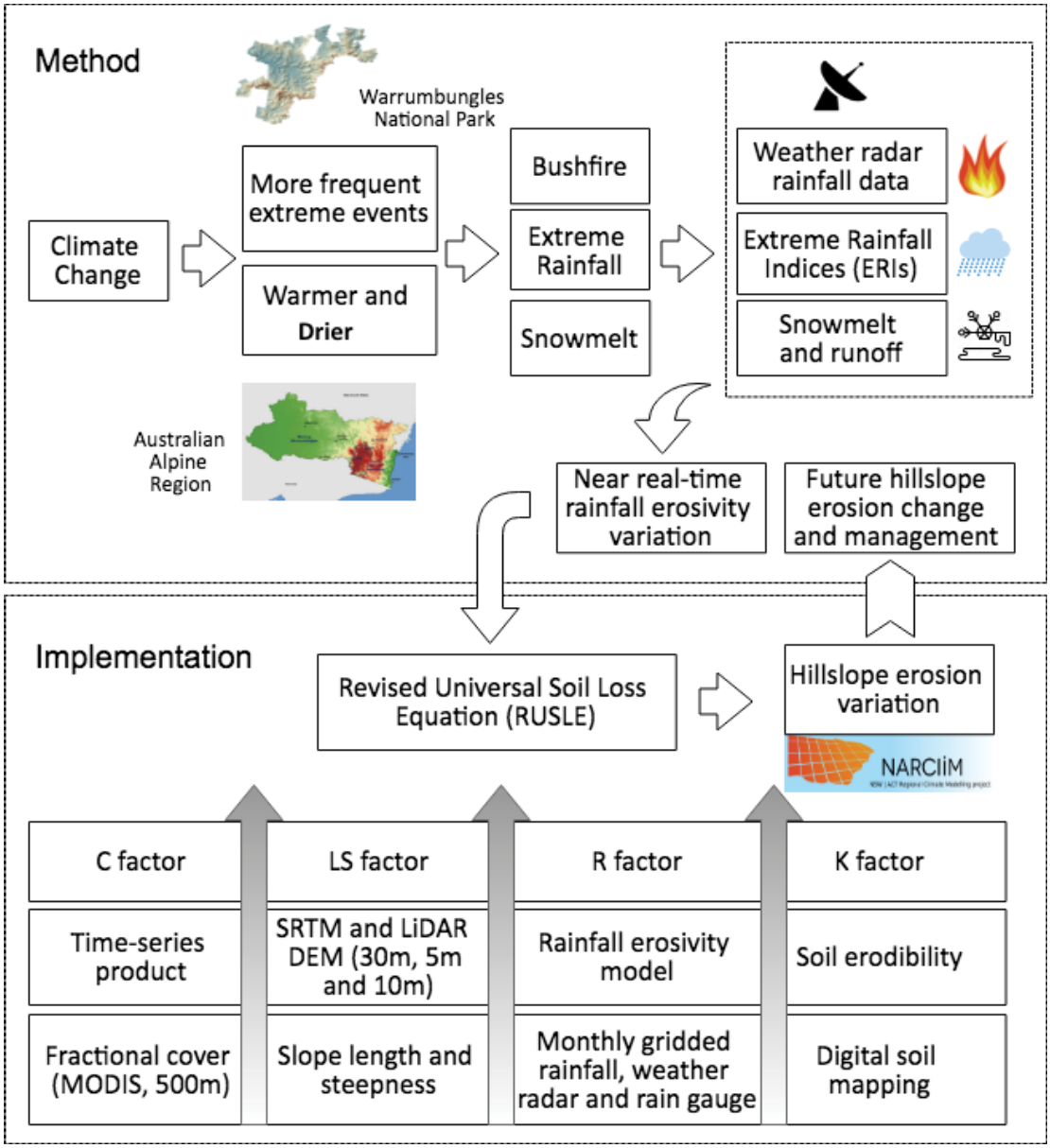

Figure 6-1 Method and implementation of this research

For post-fire erosion, different rainfall data types were investigated over various periods (before and after the bushfire), including pluviograph rainfall, tipping bucket rain gauges and radar-derived rainfall estimates for their potential for estimating EI_{30}. Radar-derived rainfall data has its advantage in high spatial and temporal resolutions. Thus, the exploration of radar rainfall data in estimating EI_{30} is of great importance when rainfall erosivity and post-fire erosion estimation at a storm event or daily time-step is required. I have developed a set methodology to estimate EI_{30}, compared to the actual erosion from soil plots at sub-daily temporal resolutions and provided timely information for park management on erosion control.

The results demonstrated that weather radar underestimated rainfall by a factor of 1.28 (R^2 = 0.75) from July 2015 to Jun 2016 and overestimated rainfall (AF = 0.90, R^2 = 0.74) from July 2016 to Jun 2017, but shows strong correlation with gauged rainfall. EI_{30} for storm events or on a daily basis can be estimated from the radar-based rainfall time-series at high temporal resolutions. The measured soil loss rates at soil plots correspond well with the EI_{30} estimates in the same periods. My results provide evidence to support and promote the use of weather radar technology for estimation of rainfall erosivity for individual storm events. As rainfall erosivity is one of the key factors in causing land degradation at a range of scales, this study reveals the potential in using weather radars for real-time or nearly real-time monitoring and prediction of land degradation around the world. Outcomes from this study have been directly used in hillslope erosion monitoring across the WNP at near-real time (Yang et al., 2018). The methodology and scripts are general, thus applicable for areas where weather radar data available.

An appropriate approach was developed to modelling and mapping event or daily rainfall erosivity and hillslope erosion at near real-time from weather radar data for a burnt national park. The weather radar-based estimates of rainfall erosivity were integrated with other factors into RUSLE, including MODIS derived groundcover (C factor), topographic (LS factor) and soil erodibility (K factor), to predict soil loss from individual storm events after a wildfire. The event-based rainfall erosivity and hillslope erosion maps can provide timely information for climate impact assessment, and a cost-effective means for hillslope erosion hazard identification and rehabilitation.

Maximum EI_{30} was estimated up to 5000 MJ mm ha^{-1} h^{-1} $month^{-1}$ whereas the maximum daily erosion could reach 50 t ha^{-1} yr^{-1} on average across WNP in a single storm event. The modelled average annual rate of hillslope erosion since May 2014 is 1.35 t ha^{-1} yr^{-1} and appears to be declining. On average, a storm event causes soil loss of 4.86 t ha^{-1} yr^{-1}, based on the model with a strong seasonal and spatial variation. Near real-time erosion hotspots were identified after severe storms. Such information is needed in supporting post-fire erosion control and management.

The results also demonstrated that there is great variation (or scale discrepancy) in remote-sensed groundcover from different sensors and spatial resolutions. Although MODIS data have high spectral and temporal resolution, the low spatial resolution limited their applications in groundcover assessment at the scale of a medium-sized national park. This study also emphasized the importance of using appropriately scaled data, which has already become a research focus in remote sensing.

Extreme rainfall indices derived from NARCliM were used to assess and monitor the rainfall erosivity when experiencing more erosive rainfall. The relationship between extreme rainfall indices and rainfall erosivity across the Alpine region was examined. Time series (monthly and annual) rainfall extremes and erosivity risk for the study area

for all 60 years periods have been produced. The spatial and temporal changes (%) of rainfall extremes and the impacts on rainfall erosivity have been quantified based on the study area and its sub-regions.

The results demonstrated that extreme rainfall indices (e.g. Rx5day) can be used to predict high-risk areas and periods of rainfall erosivity, and as indicators for potential hillslope erosion risk. However, the relationships vary among seasons and locations prediction in summer is likely to be more reliable than other seasons with higher correlation (R^2) and coefficient of efficiency (E_c). The results showed that the magnitude of rainfall erosivity increased significantly by climate change (Lee et al., 2018).

Impact of snowmelt on rainfall erosivity was considered in the NSW and ACT Alpine region in the baseline and near future periods. 12 model ensembles were used to consider snowmelt impact on erosivity. The snowmelt in spring can increase erosivity by about 12-19% in the Alpine area. However, with projected temperature rise and snow cover decreasing, the snowmelt impact on erosivity is less important or even can be ignored in the far future. The high erosion risk area is projected to be in ACT, followed by the Alpine region and SET. The high erosion risk is due to the combined effects of steep lands and intense rainfall, as well as snowmelting. This highlights the importance of groundcover maintenance and soil management in these regions. Rainfall erosivity and hillslope erosion (with snowmelt) are likely to increase about 9.68% and 14.07% in the near future and keep increasing to 24.21% and 30% in the far future on average in the study area.

This research assessed the extreme weather events impact on rainfall erosivity and hillslope erosion in southeast Australia. The current outcomes would effectively enhance the capability of government, and provide adaptation and mitigation strategies

in the face of the climate change. This research was the first attempt to use snow data and projections to adjust erosivity model and the cover factor in hillslope erosion modeling. The methodology have been developed and applied in the NSW and ACT Alpine region, with potential to be used elsewhere in the world. In the future, more radar data will be obtained and applied to burnt national parks to continuously monitor hillslope erosion. In the meantime, more field sites and rain gauges are to be established for model validation and improvement. These will provide more useful information for climate change adaptation in future land use planning and management. The methodology and automated processes developed in this study are being applied in other parts of Australia and overseas such as the Loess Plateau in China under a joint project with the State Key Laboratory of Soil Erosion and Dryland Farming on the Loess Plateau. Nonetheless, some limitations in the results still remains, the further research is necessary in the future. The estimation of near real-time rainfall erosivity can be applied to a larger scale, such as state and national scale, to where with the radar weather data. Although the rainfall erosivity has been calibrated from various field rainfall data, the impact of different resolutions data source on estimation results probably be considered, to overcome the underestimation or overestimation bias. More scenarios would be considered such as rainfall on thawing and melting soil, heat wave and snow cover, to examine the possibly change of erosion rates and adapt future changing climate under snowmelt weather.